RTD-TDR-6TDR-63-4185

(UNCLASSIFIED)

RECEIVERS FOR LASER RADARS

TECHNICAL DOCUMENTARY REPORT NO. RTD-TDR-63-4185

10 DECEMBER 1963

AF Avionics Laboratory
Research and Technology Division
Air Force Systems Command
Wright-Patterson Air Force Base, Ohio

Project No. 5191, Task No. 519102

(Prepared under Contract No. AF 33(657)-8769
by Hughes Research Laboratories, Malibu, California.
Author: Robert L. Forward)

NOTICES

When Government drawings, specifications, or other data are used for any purpose other than in connection with a definitely related Government procurement operation, the United States Government thereby incurs no responsibility nor any obligation whatsoever; and the fact that the Government may have formulated furnished, or in any way supplied the said drawings, specifications, or other data, is not to be regarded by implication or otherwise as in any manner licensing the holder or any other person or corporation, or conveying any rights or permission to manufacture, use, or sell any patented invention that may in any way be related thereto.

Qualified requsters may obtain copies of this report from the Defense Documentation Center (DDC), (formerly ASTIA), Cameron Station, Bldg. 5, 5010 Duke Street, Alexandria, Virginia, 22314.

This report has been released to the Office of Technical Services, U.S. Department of Commerce, Washington 25, D. C., for sale to the general public.

Copies of this report should not be returned to the Research and Technology Division, Wright-Patterson Air Force Base, Ohio, unless return is required by security considerations, contractual obligations, or notice on a specific document.

AF-WP-8-OCT 63 1M

HUGHES RESEARCH LABORATORIES
Malibu, California

a division of hughes aircraft company

RECEIVERS FOR LASER RADARS

Project Director — Robert L. Forward
Quantum Physics Department

Authors — W. B. Bridges, W. P. Brown, Jr., I. J. D'Haenens, R. L. Forward, C. R. Giuliano, P. Gottlieb, D. F. Hotz, B. A. Lengyel, T. R. O'Meara, G. S. Picus, C. H. Wilcox

RTD Technical Documentary Report
15 November 1962 through 15 October 1963

Contract AF 33(657)-8769
Project No. 5191, Task No. 519102

RTD-TDR-63-4185

FOREWORD

This report was prepared by the Hughes Research Laboratories, Malibu, California, on Air Force Contract AF 33(657)-8769. The contract was initiated under Task No. 519102 of Project No. 5191, "Receivers for Laser Radars." The work was administered under the direction of AF Avionics Laboratory, Research and Technology Division, Mr. W. C. Schoonover, project engineer.

This report covers the period 15 November 1962 to 15 October 1963.

The experimental and theoretical work presented in this report was contributed by personnel of the Quantum Physics Department, the Electron Dynamics Department, and the Theoretical Studies Department. Mr. I. J. D'Haenens and Dr. C. R. Guiliano were responsible for the ruby laser experiments, Drs. W. B. Bridges and D. F. Hotz were responsible for the gas laser experiments, and Drs. B. A. Lengyel and G. S. Picus contributed the sections on laser detectors. Dr. W. P. Brown, Jr., Dr. P. Gottlieb, Mr. C. H. Wilcox, and Mr. R. L. Forward studied the problems involved in utilizing lasers for radars. The project engineer for the major portion of the contract was Robert L. Forward.

This report is the final report and it concludes the work on contract AF 33(657)-8769.

ABSTRACT

Various problems associated with receivers for laser radars were investigated experimentally and theoretically. The spontaneous emission power of a laser amplifier was calculated theoretically and compared with the experimental results obtained from a ruby laser amplifier. A high gain single pass xenon gas laser amplifier was constructed with a net gain of 48 dB/m at 3.5 μ. The 3.39 μ line of a single pass helium-neon gas amplifier was magnetically tuned and it was found that the gain-bandwidth product of the amplifier varied from 200 Mc to 400 Mc depending upon the polarization and strength of the input signal. A survey of laser detector technology was made. Feasibility studies were made of various coherent optical data processing concepts. Synthetic aperture techniques appear to be only marginally feasible, but there is no fundamental limitation that would prevent the application of pulse compression techniques to optical radar systems. A theoretical investigation of the quantum limitations on laser radar system performance was made. These limitations are not a problem in present systems, but they will have to be considered for future, spaceborne systems where high accuracy is desired.

TABLE OF CONTENTS

SECTION			PAGE
1.	Introduction and Summary		1
	A.	Introduction	1
	B.	Summary	1
2.	Solid-State Laser Amplifiers		5
	A.	Absorption and Scattering Measurements	5
	B.	Spectroscopy	12
	C.	Noise Measurements	15
3.	Gaseous Laser Amplifiers		19
	A.	High Gain Single Pass Xenon Amplifiers	19
	B.	Zeeman Tuned Single Pass Helium-Neon Amplifiers	34
4.	Laser Detector Technology		49
5.	Laser Receiver Systems		53
	A.	Coherent Optical Processing	53
	B.	Quantum Limitations on Optical Receiver Systems	61
6.	Conclusions and Recommendations		73
	References		75
	Appendix I —	Optical Detector Technology	77
	Appendix II —	Spontaneous Emission Power in Laser Amplifiers	109

LIST OF ILLUSTRATIONS

FIGURE		PAGE
1.	Schematic Diagram of Apparatus for Noise Measurements	6
2.	Experimental Arrangement for Noise Measurements	7
3.	Electronic Gain of Amplifier No. 1	9
4.	Electronic Gain of Amplifier No. 2	10
5.	Spectrographic Display of R_1 and R_2 Fluorescence from Amplifier No. 1	13
6.	R_1 and R_2 Fluorescence Spectrum of a 0.05% Ruby Taken Through 1/2 m Jarrell-Ash Monochromator	14
7.	Photograph of Experimental Arrangement	20
8.	Schematic Drawing of Experimental Arrangement	21
9.	Oscillator Laser Tube B-31	23
10.	Single-Pass Gain as a Function of Input Signal for Xenon Pressures Between 0.010 Torr and 0.150 Torr	25
11.	Gain, Discharge Current, and Discharge Power as a Function of Xenon Pressure	26
12.	Typical Variation of Gain with Discharge Current	28
13.	Decrease in Xenon Pressure with Operation	29
14.	Typical Gain, Noise Power Output, and Noise Figure for a Microwave Amplifier	31
15.	Typical Gain and Noise Power Output of a Gas Laser Amplifier	32

FIGURE PAGE

16. The Zeeman Spectrum of the 3.39 μ Transition in Neon 36

17. Experimental Arrangement 38

18. Low Level Gain Bandwidth for σ_R 40

19. High Level Gain Bandwidth for σ_R 41

20. Doppler Broadened Gain Curve and Positions of Axial Cavity Modes Relative to Line Center ν_o 43

21. Relative Gain for Plane Polarized (π) Input. . . 44

22. Relative Gain for Plane Polarized (π) Input Using 3 μ W (High Level) and Less (Low Level) 45

23. Relative Gain for Right Circular Polarization (σ_R) Input Using 3 μ W (High Level) and Less (Low Level). 46

24. Relative Gain for Left Circular Polarization (σ_L) Input Using 3 μ W (High Level) and Less (Low Level). 47

25. Tapped Delay Line Filter with Barker 5 Code . 56

26. Development of Autocorrelation Output of Barker 5 Phase Coded Signal 56

27. A e Optical Delay Line Decoder 59

28. Multiple Reflection Optical Delay Correlator (Barker 5 Phase Code) 60

29. System Model Assumed for Theoretical Analysis 68

30. Detector Model Assumed for Theoretical Analysis 68

31. Spectral Response of Various Photocathodes . . 82

32. Microwave Phototube 89

FIGURE PAGE

33. Physical Configuration of Electron Multiplication System 89

34. Three Modes of Operation of Solid State Photodetectors 93

35. p-i-n Junction Diode 97

36. Constant Current Signal Equivalent Circuit of a Photodiode 99

37. Noise Equivalent Circuit for a Photodiode . . . 103

38. Simplified Energy Level Diagram of Laser 109

39. Linear Amplifier 110

LIST OF TABLES

TABLE		PAGE
1.	Loss Characteristics and Related Constants	11
2.	Operating Characteristics	12
3.	Quantum Efficiencies and Responsivities of Red-Sensitive Photosurfaces	84
4.	Wavelengths of Peak Response and Engstrom's Factors	85
5.	Noise in Photomultiplier Tubes	85
6.	NEP in One-Cycle Band at 6328 Å and 6943 Å for Several Photomultipliers	86
7.	Long Wavelength Cutoff for Various Detector Materials	92
8.	Dynamic Resistance and Detectivities of Candidate Photodiode Materials	100

SECTION 1

INTRODUCTION AND SUMMARY

A. INTRODUCTION

The purpose of this program was to study the various problems arising in the development and use of receivers for laser radars. The areas investigated covered a broad spectrum of laser receiver problems from basic quantum noise considerations to sophisticated coherent data processing techniques.

The experimental work included a study of the noise and amplification properties of a ruby laser preamplifier and a xenon gas laser preamplifier, and an investigation of the operating characteristics of a Zeeman tuned helium-neon gas laser preamplifier.

The theoretical work included a general investigation of the quantum limitations on laser radar system performance, a comprehensive survey of optical detector technology, a definitive study of spontaneous emission from a laser amplifier, and a preliminary investigation of the feasibility of applying coherent data processing concepts such as pulse compression and synthetic aperture techniques to the optical domain.

B. SUMMARY

In the section on solid state laser amplifiers the results of experimental and theoretical work on ruby laser preamplifiers are presented, and calculated and measured values of the noise characteristics are compared. The theoretical work calculated the spontaneous emission power of a laser amplifier as a function of the amplifier configuration and such measurable parameters as gain and inversion. The experimental work involved the construction and investigation of two ruby laser amplifiers. Amplifier No. 1 had Brewster angle end faces and was 2.25 in. long by 0.325 in. in diameter. The electronic gain was 20 dB with a net gain of 5.5 dB; the maximum inversion reached was 0.64, equivalent to 1.28 noise photons per signal mode. This amplifier had excessive scattering loss and was replaced by Amplifier No. 2 (3.0 in. by 0.375 in.) which had perpendicular antireflection coated end faces. In the second amplifier, the electronic gain was only 17.4 dB due to a lower chromium ion concentration, but the net gain was 6.3 dB since the scattering losses

Manuscript released by the author 10 December 1963 for publication as an RTD Technical Documentary Report.

were lower. The maximum inversion reached was 0.675, corresponding to 1.24 noise photons per signal mode. The calculated and observed noise powers of the two amplifiers agree within the limits of the assumptions in the theory and the experimental error.

In the subsection on a high gain single pass xenon amplifier, information is given on the gain, life, and noise performance of a xenon laser amplifier operating at 3.5 μ. A maximum small signal gain of 48 dB/m was observed, with incipient saturation occurring at about 0.4 $\mu W/mm^2$ at the output. Tube life of the order of 100 hours was observed. Experimental results of the study of noise characteristics indicate that the laser amplifier does improve the signal-to-noise ratio of a receiver system if used before a detector; however, quantitative measurements of the noise were not made.

The subsection on Zeeman tuned single pass helium-neon amplifiers describes the gain measurements taken at 3.39 μ during the magnetic tuning of a helium-neon amplifier. It was found that the gain bandwidth product of the amplifier varied from 200 Mc to 400 Mc depending upon the polarization state and power level of the input signal.

The material presented in Appendix I is summarized in the section on laser detector technology. It is concluded that the traveling-wave phototube and the solid state photodiode are the best devices available to date for detectors of microwave modulated light. The phototube is better for wavelengths less than 7000Å because of its greater bandwidth and the photodiode is better for wavelengths greater than 1.1 μ because of its quantum efficiency. Between 0.7 and 1.1 μ, the choice depends upon system requirements.

In the subsection on synthetic apertures at optical wavelengths a study of the feasibility of applying synthetic aperture concepts to laser radars is described. There was no investigation of methods to carry out this processing, but instead it was assumed that the processor existed. The problem was then investigated from the standpoint of physical feasibility in terms of the target characteristics, the probable environment, and the effects of the very short wavelength of light compared to microwave wavelengths. The synthetic aperture technique does not appear feasible in the atmosphere or in space at long ranges with high closing rates. It is marginally feasible in space at short ranges and low velocities.

The subsection on optical radar pulse compression systems outlines findings indicating that there is no fundamental limitation that would prevent the application of pulse compression techniques to optical radar systems. Because of the present capabilities of laser modulators and demodulators, it was felt that phase or polarization coded systems were preferable to chirp techniques. Preliminary configurations were designed for an active optical fiber delay line and a multiple reflection delay line.

In the subsection on signal-to-noise ratios of laser receiver systems, calculations of the signal-to-noise ratios of an optical signal are reviewed. These calculations were made after attenuation in a transmission medium and after amplification by four different systems: (1) a photodetector, (2) a single mode laser amplifier, (3) a single mode optical heterodyne, and (4) a laser preamplifier followed by an optical heterodyne.

It was found that an amplifier must be used before the signal becomes too weak (when the average number of received photons approaches unity) or information will be irretrievably lost. If the number of received signal photons is appreciably larger than unity, any of the amplifiers can be used, provided they do not degrade the signal too much. The degradation factor for the laser amplifier is related to the inversion; the degradation factor for the optical heterodyne or photodetector is the quantum efficiency.

The subsection on position prediction accuracy of Doppler radar describes a theoretical study of the fundamental quantum limits to the measurement of range and range rate. It was determined that the measurement of range and range rate are not independent because of quantum mechanical uncertainty relationships. It was also found that there are optimum values for the range and range rate accuracies and the pulse repetition rate that are related to the target velocity, the frequency and average number of the received photons, and the desired accuracy of future position prediction. These considerations are not relevant to present systems, but they will have to be considered for future, spaceborne systems where high accuracy is desired. For instance, if the target velocity is 10 km/sec, the average number of received photons is four, and the desired future position accuracy is $\pm$ 1/10 m, there is an optimum value for the accuracy of the Doppler shift measurement of $\pm$ 16 kc/sec.

SECTION 2

SOLID STATE LASER AMPLIFIERS

One of the factors governing the feasibility of a laser preamplifier for use in a laser radar is the noise behavior in such a system. The noise considered here arises from the spontaneous emission due to fluorescence in the system. If the spontaneous emission were constant or varying in time in some known fashion, the final detector could be biased so as to subtract it out. The fluctuations in the fluorescent noise, however, cannot be biased out. These fluctuations depend upon the spontaneous noise power from the amplifier and it is this quantity which has been examined.

Theoretical calculations of the fluorescent emission power of a laser amplifier were made; they were presented in the Appendix to Interim Engineering Report No. 2 (Ref. 1) and the ASD Laser Receiver Meeting Summary (Ref. 2). A slightly revised version is included here as Appendix II. Experiments have been carried out and compared with the theory. Two different ruby amplifiers were studied in detail and the calculated and observed noise powers agree within the limits of the assumptions made and the experimental error. The bandwidth properties of both signal source and amplifiers have been examined and compared.

A. ABSORPTION AND SCATTERING MEASUREMENTS

The experimental apparatus was set up according to the arrangement shown in Figs. 1 and 2. It consisted of a signal source, beam splitter, polarizer, amplifier, and detector. The signal source used is a ruby laser with the C-axis oriented at 90° to the propagation axis. The signal was stopped down with two apertures so that the spot entering the amplifier was about one-third the size of the input aperture. This corresponds to a beam angle of about 5 mrad ($\sim 10^{-5}$ sr). The beam splitter and photodiode provide a means for sampling the light before amplification in the ruby amplifier. The polarizing prism was used immediately before the amplifier to insure that only signals of the desired polarization were allowed to enter the amplifier. The polarizing prism was necessary because it was found that some depolarization takes place in the beam splitter even though the laser was oriented to produce the desired polarization for the amplifier.

Gain measurements were made on two different amplifiers. Amplifier No. 1 was a rod 2.25 in. long by 0.325 in. in diameter with Brewster angle ends and Amplifier No. 2 was 3.0 in. by 0.375 in. with

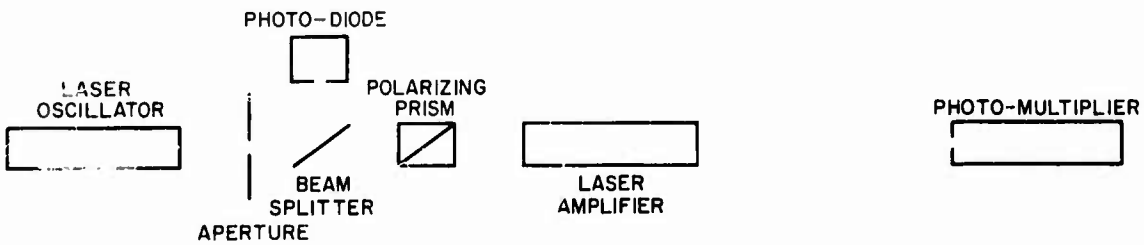

Fig. 1. Schematic Diagram of Apparatus for Noise Measurements.

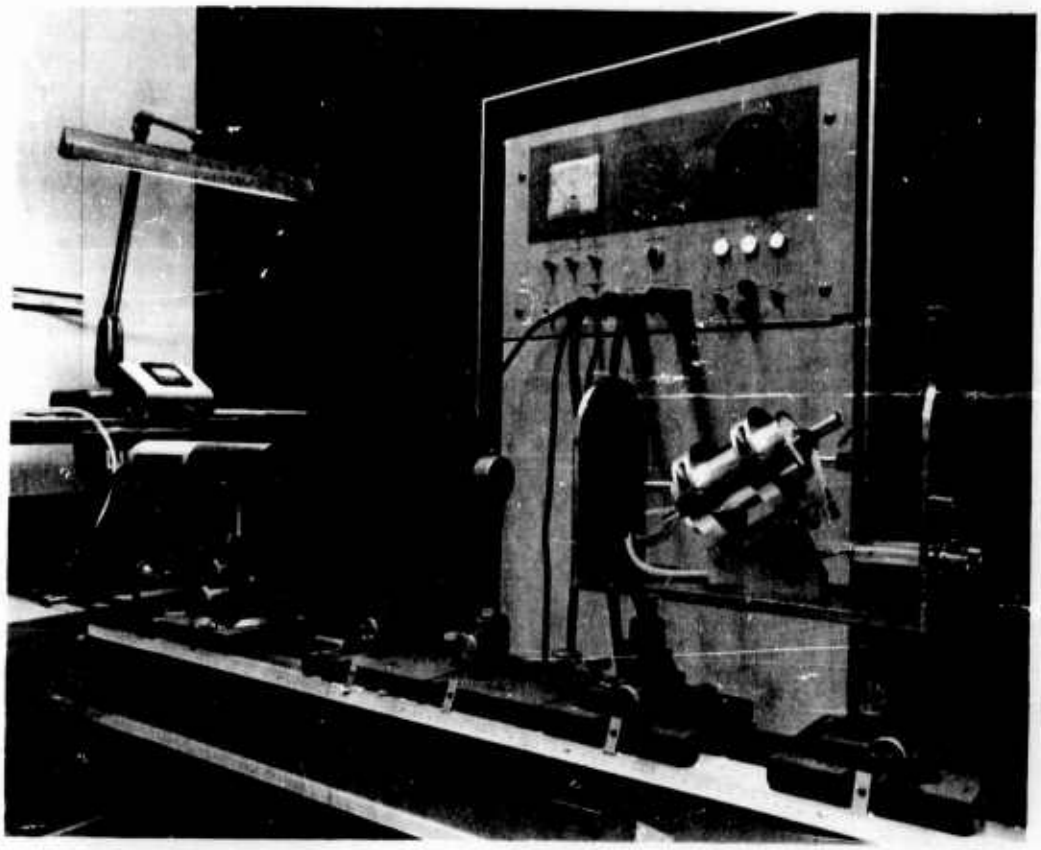

Fig. 2. Experimental Arrangement for Noise Measurements.

perpendicular antireflection coated end faces. Net gains of 5.5 dB and 6.3 dB, respectively, were achieved. Figures 3 and 4 show plots of electronic gain as a function of pumping time at a constant pumping rate. (The pump power supply utilized a pulse shaping network with an essentially square-wave output. Each capacitive section contributes 400 J in 150 μsec pumping time. Hence, a pumping rate of 2.67 MW was obtained.)

The actual gain measurements were carried out in the following manner. Delay circuits on the amplifier, oscillator, and oscilloscope were arranged so that the signal pulse was fired into the amplifier at the end of the pumping period of the amplifier. The input and output signals were viewed at that time on a dual-beam oscilloscope with a sweep rate of 5 μsec/cm. Thus the gain was measured for the individual laser spikes. The difference in insertion loss for the two amplifiers is partly due to a concentration difference but is also caused by large scattering losses in Amplifier No. 1. A computation of the scattering loss can be accomplished by a measurement of the dead loss measurements for both polarizations and by the use of the following equation:

$$L = (1 - R)^2 e^{-(\alpha + \delta)\ell} \tag{1}$$

where R is the reflectivity at the end faces, α and δ are absorption and scattering cross sections, respectively, and ℓ is the length of the rod.

We may rewrite (1) in exponential form, obtaining

$$L_{dB} = -10 \log (1 - R)^2 + \alpha_{dB}\ell + \delta_{dB}\ell \tag{2}$$

where L_{dB} is the single pass loss through the amplifier in decibels, $\alpha_{dB} = -\frac{10}{2.3}\alpha$ and $\delta_{dB} = -\frac{10}{2.3}\delta$. The assumption is made that δ is the same for σ and π polarizations (i.e., light polarized perpendicular and parallel to the optic axis, respectively). For Amplifier No. 1, $R_\sigma = 0$ (Brewster's angle for σ polarization), whereas $R_\pi = 0.25$. For Amplifier No. 2 both scattering and reflection losses are assumed to be the same for both polarizations and are lumped together in the δ-term. We also use the fact that $\alpha^\pi = \alpha^\sigma/10$.

The measured losses in both amplifiers for the two polarizations are substituted into (2) to yield the results listed in Table 1.

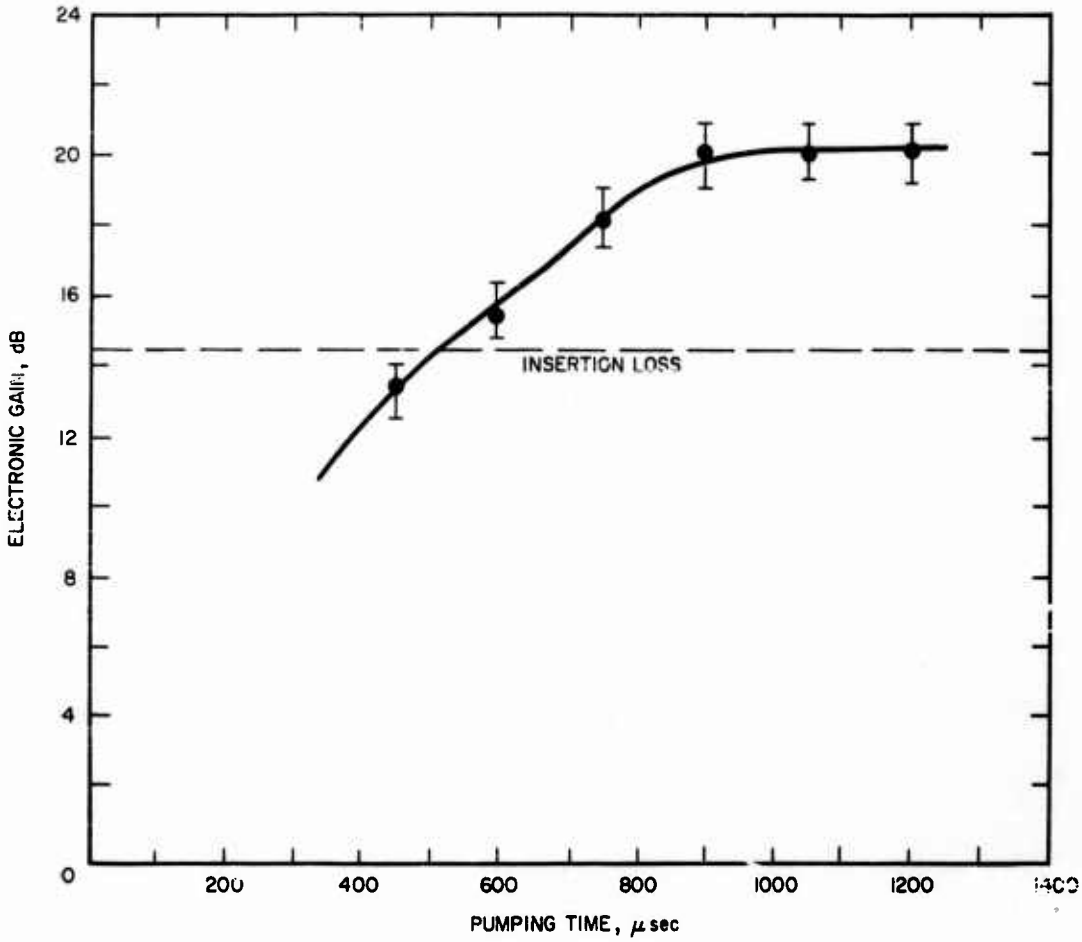

Fig. 3. Electronic Gain of Amplifier No. 1.

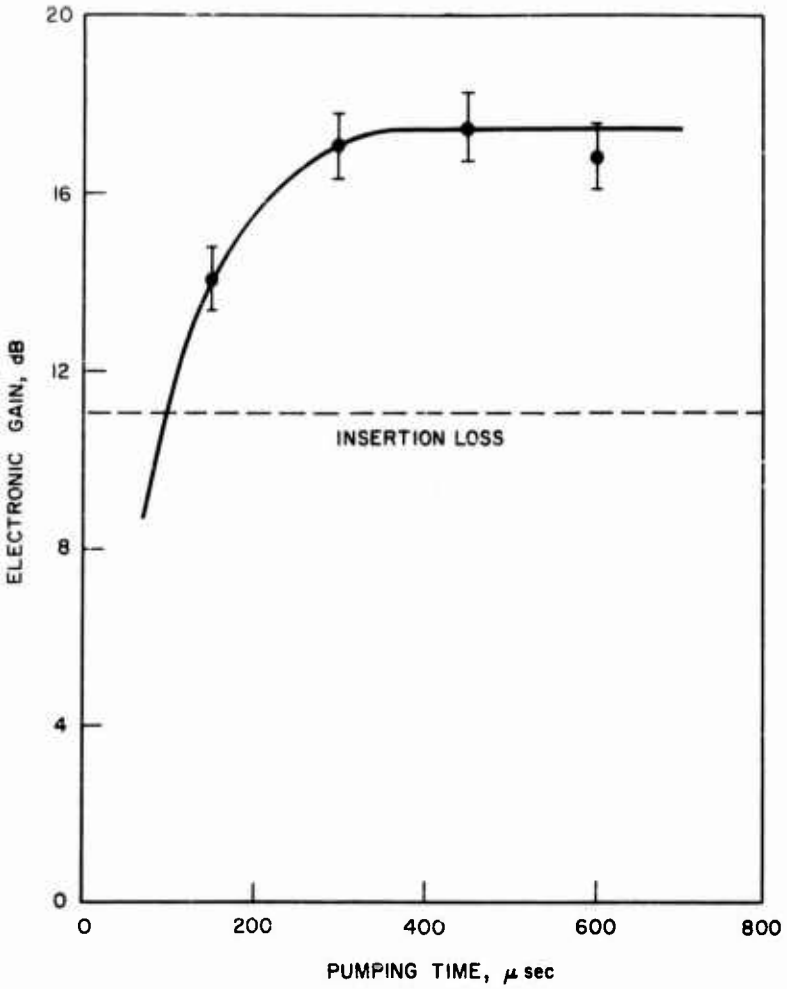

Fig. 4. Electronic Gain of Amplifier No. 2.

TABLE 1

LOSS CHARACTERISTICS AND RELATED CONSTANTS

	Amplifier No. 1 2.25 in. x 0.325 in. Brewster angle end faces	Amplifier No. 2 3.0 in. x 0.375 in. Perpendicular anti-reflection end faces
Measured loss of σ polarized light (L_σ)	14.5 dB	11.1 dB
Measured loss of π polarized light (L_π)	6.0 dB	1.8 dB
Calculated absorption constant (α^σ)	2.13 dB/cm	1.36 dB/cm
Calculated scattering constant (δ)	0.40 dB/cm	0.098 dB/cm
Cr^{+3} concentration calculated from α^σ	0.087%	0.055%

Evaluation of absorption and scattering enables us to determine the inversion reached at the point of maximum gain in the amplifier.

$$G_{dB} = 10 \log (1 - R)^2 + (I\alpha_{dB} - \delta_{dB})\ell \qquad (3)$$

where G_{dB} is the measured net gain in decibels and

$$I = \frac{N_2 - N_1}{N_2 + N_1} \quad . \qquad (4)$$

The maximum net gain G_{dB}^{max} and inversion are given in Table 2.

TABLE 2

OPERATING CHARACTERISTICS

		Amplifier No. 1	Amplifier No. 2
Gain	(G_{dB}^{max})	5.5	6.3
Inversion	(I)	0.64	0.675
Noise photons	(N)	1.28	1.24

In Table 2,

$$N = \frac{N_2}{N_2 - \frac{g_2}{g_1} N_1} \tag{5}$$

is the number of noise photons per signal mode. This quantity occurs in the expression for the spontaneous noise power to be discussed below.

B. SPECTROSCOPY

Comparisons of the oscillator and amplifier bandwidths were made spectroscopically using a 3.4 m Jarrell-Ash spectrograph. Some of the spectrographic plates are reproduced in Fig. 5. The total spread of the oscillator bandwidth is about 2.5×10^{10} cps. (The individual modes of the oscillator which occur within its bandwidth are approximately 0.1×10^{10} cps wide when resolvable and are separated by 0.2×10^{10} cps.) On the other hand, the amplifier bandwidth at half gain is approximately ten times larger, about 25×10^{10} cps. The fluorescence of a 0.05% ruby was also observed spectrophotometrically, using a 1/2 m Jarrell-Ash monochromator. Both σ and π fluorescence were measured for the R_1 and R_2 lines. These are displayed in Fig. 6. The relative intensities of R_1/R_2 fluorescence for the σ and π polarizations are

$$\left(\frac{R_1}{R_2}\right)_\sigma = 1.65 \quad ; \quad \left(\frac{R_1}{R_2}\right)_\pi = 0.697 \quad .$$

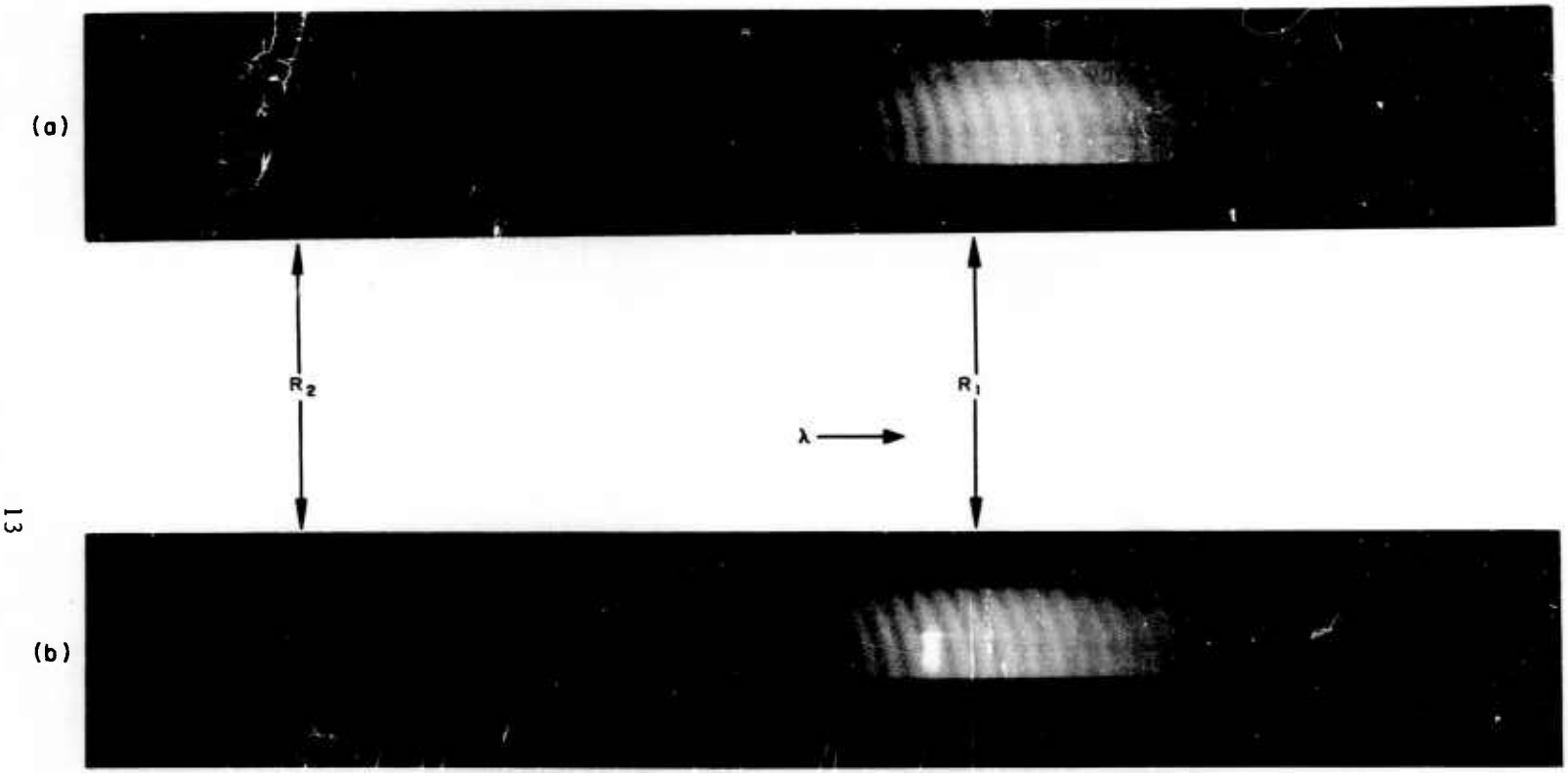

Fig. 5. Spectrographic Display of R_1 and R_2 Fluorescence from Amplifier No. 1.

(a) Fluorescence alone
(b) Fluorescence with amplified laser signal superimposed

(Note: The regular fringes across the fluorescence bands are due to interference effects arising from a focusing lens in the system. The shift of the center of the R_1 fluorescence peak to a longer wavelength relative to the laser signal is caused by heating of the amplifier during pumping.)

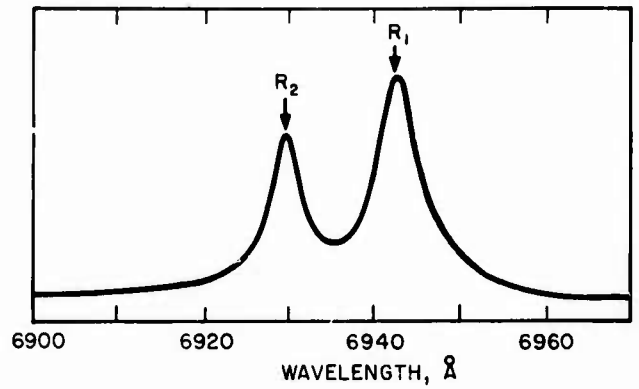

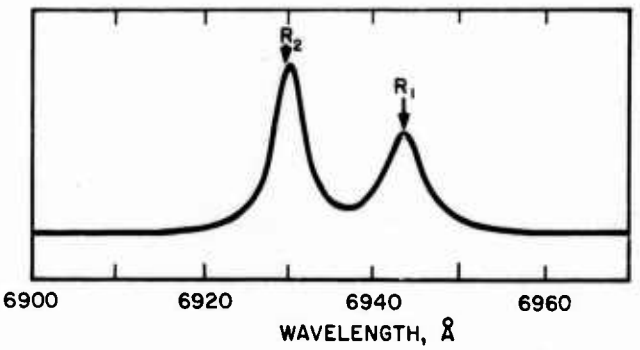

Fig. 6. R_1 and R_2 Fluorescence Spectrum of a 0.05% Ruby Taken Through 1/2 m Jarrell-Ash monochromator (a) Fluorescence for σ-polarization (b) Fluorescence for π-polarization.

C. NOISE MEASUREMENTS

The spontaneous emission power from the amplifiers was measured and compared with the theoretical estimate in a treatment previously disclosed (Appendix II). Calibration of the photomultiplier tube was accomplished by observing the known output of a helium-neon gas laser at 6328 Å and using the reported response curve of the S-10 photosurface to obtain the response at 6943 Å. The bandwidth of the interference filter on the photomultiplier tube is such that both R_1 and R_2 fluorescence were observed. Since we are interested only in R_1 noise, we subtract out the R_2 fluorescence using the known emission spectrum (see Fig. 6). Only the fluorescence corresponding to the high gain polarization (σ - polarization) is desired for the comparison between theory and experiment. This was observed by placing the polarizing prism between the amplifier and the detector.

The predicted spontaneous emission power (Appendix II) for a Lorentzian shaped line is given by

$$\frac{P_{tot}}{h\nu} = \left(\frac{N_2}{N_2 - \frac{g_2}{g_1} N_1}\right) \frac{2\nu^2 A}{C^2} (g - 1) \left(\frac{\log g}{\log \frac{g}{2}} - 1\right)^{1/2} \Delta\nu_{1/2} \qquad (6)$$

photon/sec sr

where

N_1, N_2 ≡ respective population densities

g_1, g_2 ≡ respective degeneracy factors

$\Delta\nu_{1/2}$ ≡ linewidth at one-half gain

g ≡ $e^{\alpha l}$ = amplifier gain

A ≡ cross-sectional area of amplifier.

Substituting the pertinent quantities into (4) for Amplifiers No. 1 and 2 and using detector solid angles of 2.14×10^{-4} sr and 1.25×10^{-4} sr, respectively, we obtain 4.14×10^{16} photon/sec for Amplifier No. 1 and 3.52×10^{16} photon/sec for Amplifier No. 2. These numbers correspond to the total number of fluorescence photons per second in the solid angle of the detector which occur in the σ polarization of the R_1-line.

The total emission power received for σ-polarization in Amplifiers No. 1 and 2 is 6.8×10^{16} photon/sec for No. 1 and 7.0×10^{16} photon/sec for No. 2. Multiplying these numbers by 0.623, the ratio of R_1 fluorescence to $R_1 + R_2$ fluorescence obtained from Fig. 6, one obtains:

	Amplifier No. 1	Amplifier No. 2
Measured	4.24×10^{16}	4.36×10^{16}
Calculated	4.14×10^{16}	3.52×10^{16}

The agreement is well within the limits of the approximations made and the experimental errors.

The feasibility of laser preamplifiers really depends upon fluctuations in the spontaneous emission since these fluctuations constitute the true noise in the sense of signal detectability. Our study has been limited to a determination of the total spontaneous emission power and to a comparison with the theoretical prediction. The fluctuations in the noise power which govern signal detectability have not been investigated experimentally.

We can state some conditions, however, which can be imposed on the system in order to minimize the noise. First, the aperture of the detector should be limited so as to subtend a solid angle no larger than the signal beam. This eliminates the detection of fluorescence lying outside of the actual signal beam. Thus it is necessary to observe only noise photons which cannot be spatially filtered from the signal photons. Second, a frequency filter should be used. Because the oscillator bandwidth is much smaller than that of the amplifier, only a small fraction of noise is of the same frequency as that of the signal. A simple calculation based on the assumption of a Lorentzian line shape gives the fraction of spontaneous emission whose frequency lies in the signal frequency region.

$$g(\nu) = \frac{1/\pi\Delta\nu_{1/2}}{(\Delta\nu_{1/2})^2 + (\nu_o - \nu)^2} \tag{7}$$

is the equation for a rentzian line with a width at half-height of $\Delta\nu_{1/2}$ and a central frequenc y ν_o. The function is normalized so that

$$\int_{-\infty}^{\infty} g(\nu)\,d\nu = 1 \quad . \tag{8}$$

The fraction of noise in the fluorescence spectrum corresponding to the laser frequency is given by

$$\frac{\Delta\nu_L\, g(\nu_o)}{\int_{-\infty}^{\infty} g(\nu)\, d\nu} = \Delta\nu_L \frac{1}{\pi\Delta\nu_{1/2}} \tag{9}$$

where $\Delta\nu_L$ is the bandwidth of the laser oscillator. Substitution of values in the above equation gives

$$\Delta\nu_L \frac{1}{\pi\Delta\nu_{1/2}} \cong \frac{2.5 \times 10^{10}}{25 \times 10^{10}(\pi)} = \frac{1}{10\pi} \approx 0.032 \tag{10}$$

or about 3%. Thus about 97% of the fluorescence could be filtered out without interfering with the signal.

With the above constraints of spatial and frequency filtering using apertures, post-amplifier filtering and, of course, polarization discrimination, it is possible to investigate the problems of detectability more fully.

C. R. Giuliano

SECTION 3

GASEOUS LASER AMPLIFIERS

Gas lasers have a number of characteristics such as continuous single-mode operation, good frequency stability, and low power requirements which make them very suitable for use in laser receiver systems. These characteristics obviously make gas lasers almost ideal for use as local oscillators in optical superheterodyne systems. Their value as laser preamplifiers is less obvious due to the low gains per unit length and the narrow amplification bandwidths of most transitions. The studies carried out under this contract concentrated on these two problem areas in an effort to define more quantitatively the potential value of gas lasers as single pass preamplifiers. The section on high gain single pass xenon amplifiers reports the results of the investigation of the high gain transition of xenon in the infrared, and the section on Zeeman tuned single pass helium-neon amplifiers reports the result of investigations of the effect of magnetic tuning on the amplification characteristics.

A. HIGH GAIN SINGLE PASS XENON AMPLIFIERS

High optical gain at 3.508 μ has previously (Ref. 3) been observed in a xenon-helium discharge. The reported figure of over 50 dB/m is sufficiently high to make this laser transition ($5d[7/2]^0_3 \rightarrow 6p[5/2]_2$) an interesting candidate for a single pass optical receiver preamplifier. Consequently, work was initiated on xenon-helium and pure xenon laser discharge tubes.

1. Gain Measurement

Preliminary measurements of single pass gain in xenon were given in the Appendix of Interim Engineering Report No. 3 (Ref. 4) and have been published elsewhere (Ref. 5). From the variation of gain with input signal power given in that report, it was evident that some gain saturation was present, even at the lowest signal levels used in those measurements. In order to repeat the measurement with lower signal levels it was necessary to use a more sensitive detector than the thermopile which would also discriminate the amplified signal from the light originating in the amplifier itself. A phase-locked detection system satisfying these requirements was assembled; the entire experimental arrangement is shown in Figs. 7 and 8. The various components in this system are described below.

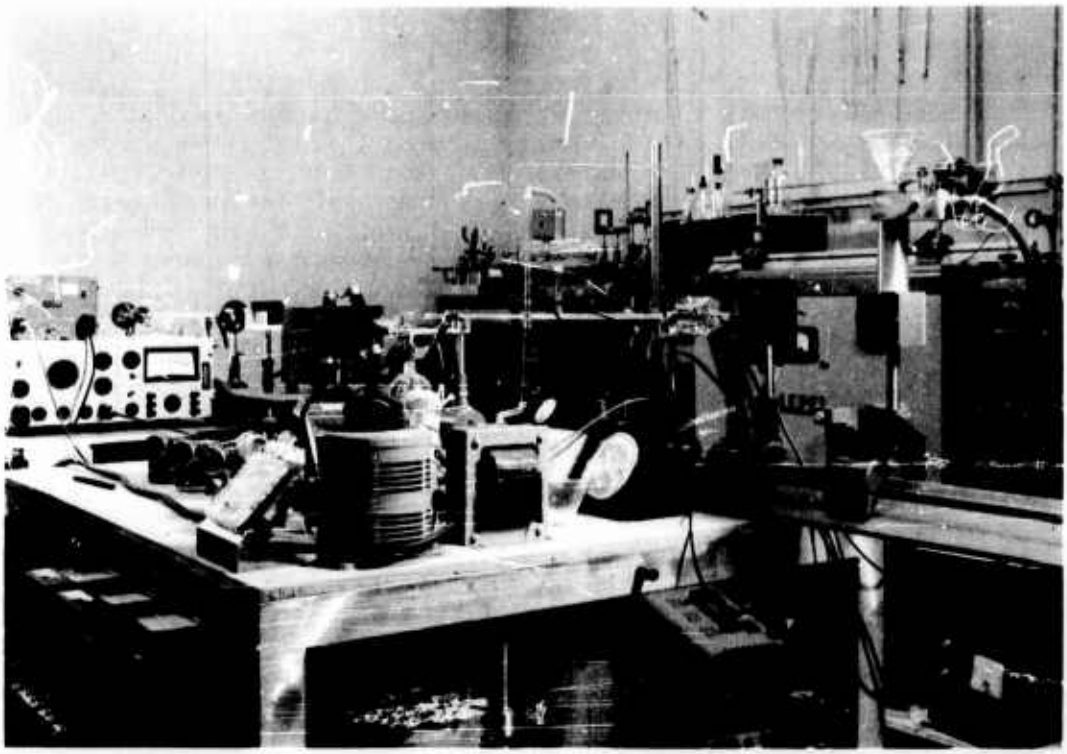

Fig. 7. Photograph of Experimental Arrangement.

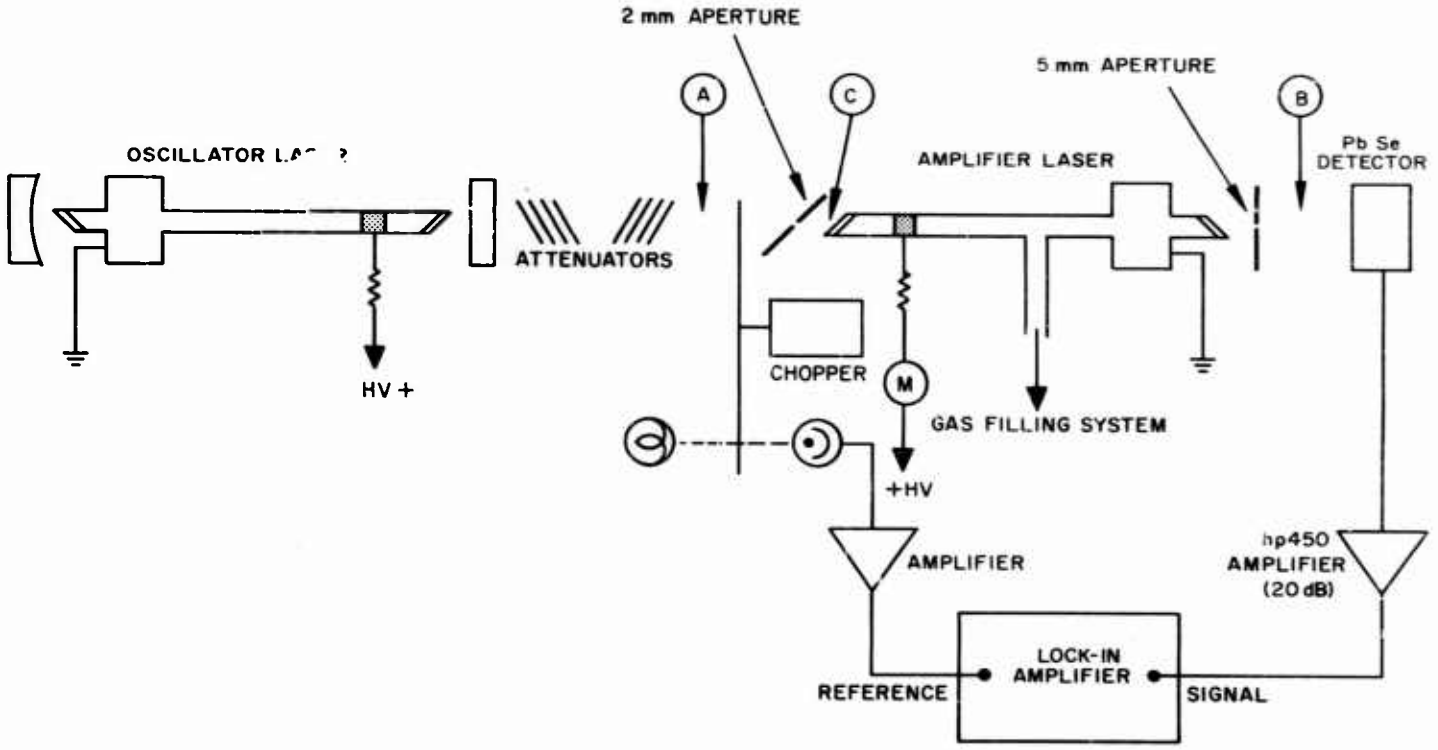

Fig. 8. Schematic Drawing of Experimental Arrangement.

The laser used as a signal source is shown more clearly in Fig. 9. This tube used a hot cathode dc discharge with the discharge dimensions 5 mm in diameter by 60 cm long. The windows were made of 0.060 in. Homosil quartz and were attached to the discharge tube with a vacuum epoxy (Varian "Torr Seal"). A pure xenon fill of 0.100 Torr initially was used in this tube; the tube volume was increased by adding a bottle on a side arm. (Refer to subsection 2, "Tube Life.") The oscillator cavity used a 100 cm radius gold-coated mirror (opaque) and an uncoated quartz flat (approximately 4% reflectivity) spaced 90 cm apart, giving a longitudinal mode spacing of about 170 Mc. Since the 3.508 μ line is about 150 Mc wide, single mode operation was quite probably achieved but measurements were not made due to the lack of a suitable (170 Mc output) detector at this wavelength.

A number of glass filters (Corning 7-56) were used as attenuators. These were tilted slightly to prevent reflected light from returning to either the oscillator or amplifier laser. The attenuators were calibrated at 3.508 μ wavelength with an Eppley thermopile inserted at position A (Fig. 8). Attenuation ranged from 5.2 to 5.8 dB per filter.

A three-vane chopper was used to modulate the signal at approximately 90 cps. A light source and photocell were included inside the chopper housing to provide a reference signal to the lock-in amplifier (Princeton Applied Research Model JB-4).

A special aperture, 2 mm in diameter, was used to limit the beam size and thus prevented multiple paths through the amplifier by reflection from the inner wall. An elliptical hole was made in an evaporated silver coating on a quartz flat; this shape was chosen so that it would appear as a round hole when tilted at the Brewster angle. This type of aperture has minimum loss in transmission, minimum scattering in the direction of incidence, and no reflection in the direction of incidence (Ref. 6). Using such a stop there is no chance that spontaneous emission from the input end of the amplifier will be fed back into the amplifier.

The amplifier laser was identical in all respects to the oscillator laser described above, except that it was sealed on to a vacuum pump station and gas filling manifold. As a test of over-all tube quality and cleanliness this tube was initially filled with a normal helium-neon mixture and run at 6328 Å; it produced 20 mW, indicating excellent quality windows and alignment.

The detector used was a lead selenide cell (obtained from Hughes Santa Barbara Research Center) operated at 77°K; it had a minimum detectable signal of the order of 10^{-9} W at 3.508 μ when used with the lock-in amplifier. A Hewlett-Packard hp 450 amplifier was ahead of the lock-in amplifier. A 5 mm diameter aperture was used

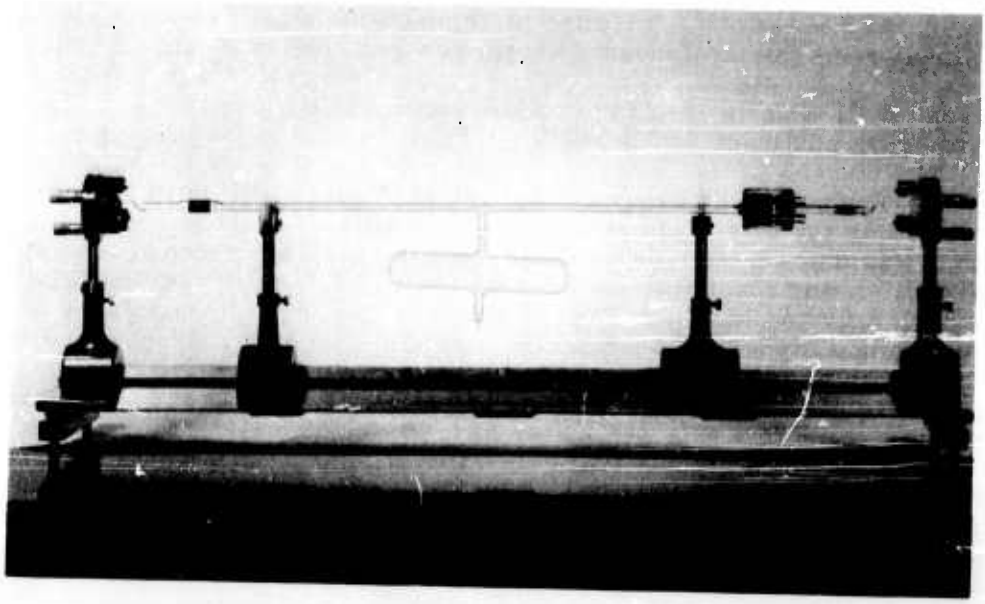

Fig. 9. Oscillator Laser Tube B-31.

between the amplifier output and the detector cell to shield the detector from the hot cathode in the amplifier laser. The over-all detection system was calibrated by comparison with the power measured by an Eppley thermopile placed at position B (Fig. 8), with the laser amplifier and chopper turned off. A number of points on the curve were obtained by inserting the previously calibrated attenuators.

Alignment and transmission through the amplifier were checked by measuring the unattenuated signal power at points B and C (Fig. 8) with the thermopile. The measured transmission loss was 0.87; this agrees well with the loss for two Brewster angle quartz windows calculated from published data (0.88).

The amplifier gain was measured by taking the ratio of power incident on the lead selenide cell with the amplifier discharge on to power incident on the lead selenide with the discharge turned off. No correction was made for the fact that the incident power is measured through only one window. Figure 10 gives the amplifier gain as a function of input signal level for xenon pressures from 0.150 Torr to 0.010 Torr, with the discharge current optimized at each pressure. The maximum gain observed was 29 dB at a xenon pressure of 0.015 Torr, corresponding to a gain per meter of (100 cm/60 cm) 29 dB = 48 dB/m. It is evident from Fig. 10 that gain saturation occurs at very low levels. A line of output power equal to 5 μW can be drawn through the points of incipient gain saturation and a line of output power equal to 60 μW through the points where the gain is reduced by 3 dB, indicating that saturation is independent of pressure. The beam size, measured at the output end of the amplifier, was approximately 4 mm in diameter. This agrees closely with the size predicted by simple diffraction from the 2 mm input aperture. With this spot size, the power densities are estimated to be approximately 0.4 $\mu W/mm^2$ for incipient saturation and 4 $\mu W/mm^2$ for 3 dB saturation.

Operation of the amplifier was quite unstable with xenon fills below 0.010 Torr. Rapid gas cleanup occurred at the high discharge current densities necessary to achieve maximum gain. The dotted portion of the 0.010 Torr curve in Fig. 10 is probably due to gas pressure decreasing below 0.010 Torr during the end of this run of measurements. An attempt was made to attain constant pressure operation by leaking xenon into the system during the measurement; the valve and gauge on the gas filling manifold were sufficiently far from the location of the cleanup (presumed to be caused by sputtering at the cathode) that this method proved unreliable. Although curves are not shown in Fig. 10 for pressures less than 0.010 Torr, the gain was observed to drop off rapidly below this pressure. Figure 11 shows the variation of unsaturated gain with xenon pressure. Also shown are the discharge current and power at the optimum gain point. The discharge power increases less rapidly than the current since the voltage drop decreases

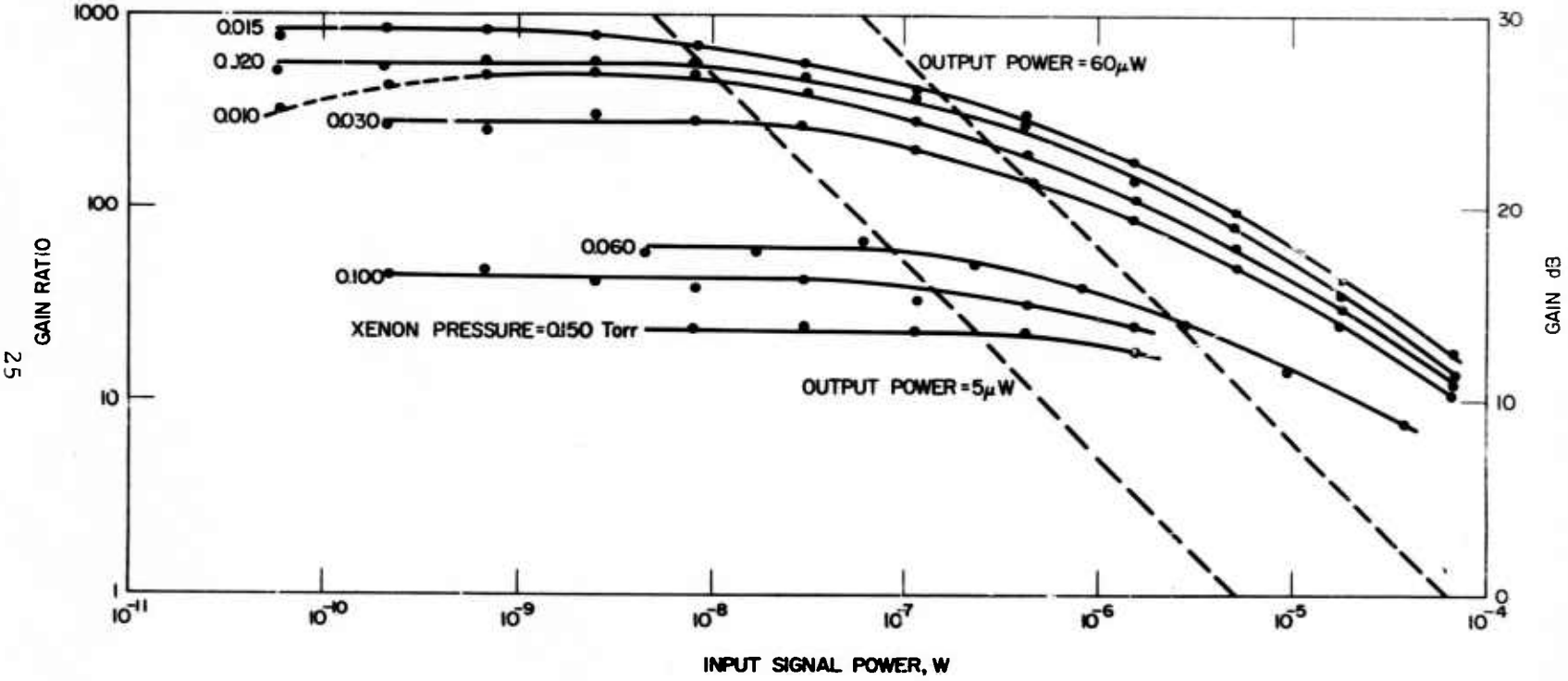

Fig. 10. Single-pass Gain as a Function of Input Signal for Xenon Pressures Between 0.010 Torr and 0.150 Torr.

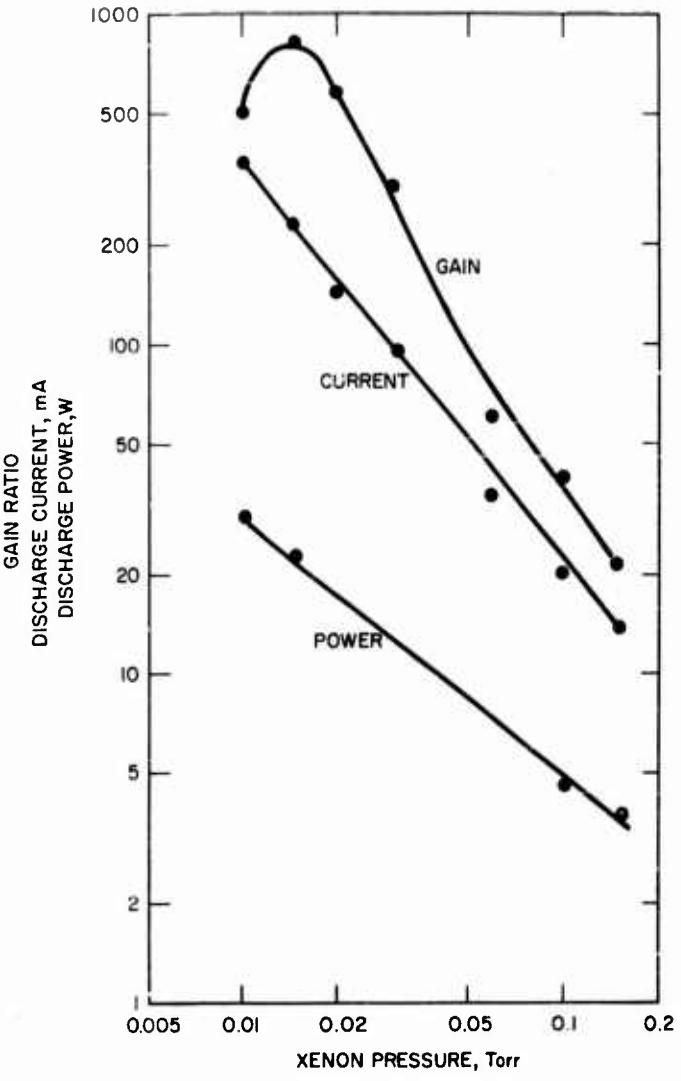

Fig. 11. Gain, Discharge Current, and Discharge Power as a Function of Xenon Pressure.

from over 200 V at 0.150 Torr to about 100 V at 0.010 Torr. Figure 12 gives the typical variation of gain with discharge current for a fixed xenon pressure and different input signal levels. Because of the limited time available, rf excitation of the amplifier was not attempted although the preliminary measurements (Refs. 4 and 5) indicated that 5 or 10 dB more gain per meter might be obtained.

2. Tube Life

The tubes used in this experiment were identical in structure to the helium-neon tubes used for general experimental work in this laboratory. Experience with the helium-neon tubes indicates that life should be more than 1000 hours, with no observed gas cleanup over that interval. Some premature failures have been caused by impurity gas evolution from the cathode, coupled with insufficient gettering. In contrast, the two sealed off xenon tubes operated to date exhibited serious gas cleanup. Figure 13 gives the measured xenon pressure as a function of operating time for the oscillator laser used in the present experiment. (The pressure was deduced from previously measured discharge V-I curves.) This tube was run with increasing discharge current as the xenon pressure decreased in order to keep the tube at its maximum output power. This probably accounts for the increasing cleanup rate between 40 and 80 hours of operation. This tube is still operative (in fact, it has more output power than at tipoff), but the total projected life is less than 100 hours, or less than 20 hours more. The tube volume, including the added bottle (see Fig. 9), is approximately 270 cm^3. Pressure versus operating time records were not kept on the sealed off xenon tube used in earlier experiments (B-25), but its life was approximately 20 hours; it had a volume of 130 cm^3 and an initial xenon fill of 0.050 Torr pressure. Assuming the same average cleanup rate in atoms per second as that observed in tube B-31, the predicted life would be approximately 24 hours — in good agreement with the observed life of 20 hours.

The cleanup mechanism is presumed to be the "burying" of xenon under a sputtered layer of cathode material. Hot cathode helium-neon tubes exhibit little or any sputtering after 100 hours of operation. Apparently the heavier xenon atoms with energies corresponding to the normal hot cathode potential fall are much more effective in sputtering than either neon or helium. (When operated as cold cathode tubes, with a much higher cathode fall, both xenon and helium-neon tubes exhibit a great deal of cathode sputtering, and rapid gas cleanup.) No life experiments have been made with sealed off, rf excited xenon lasers.

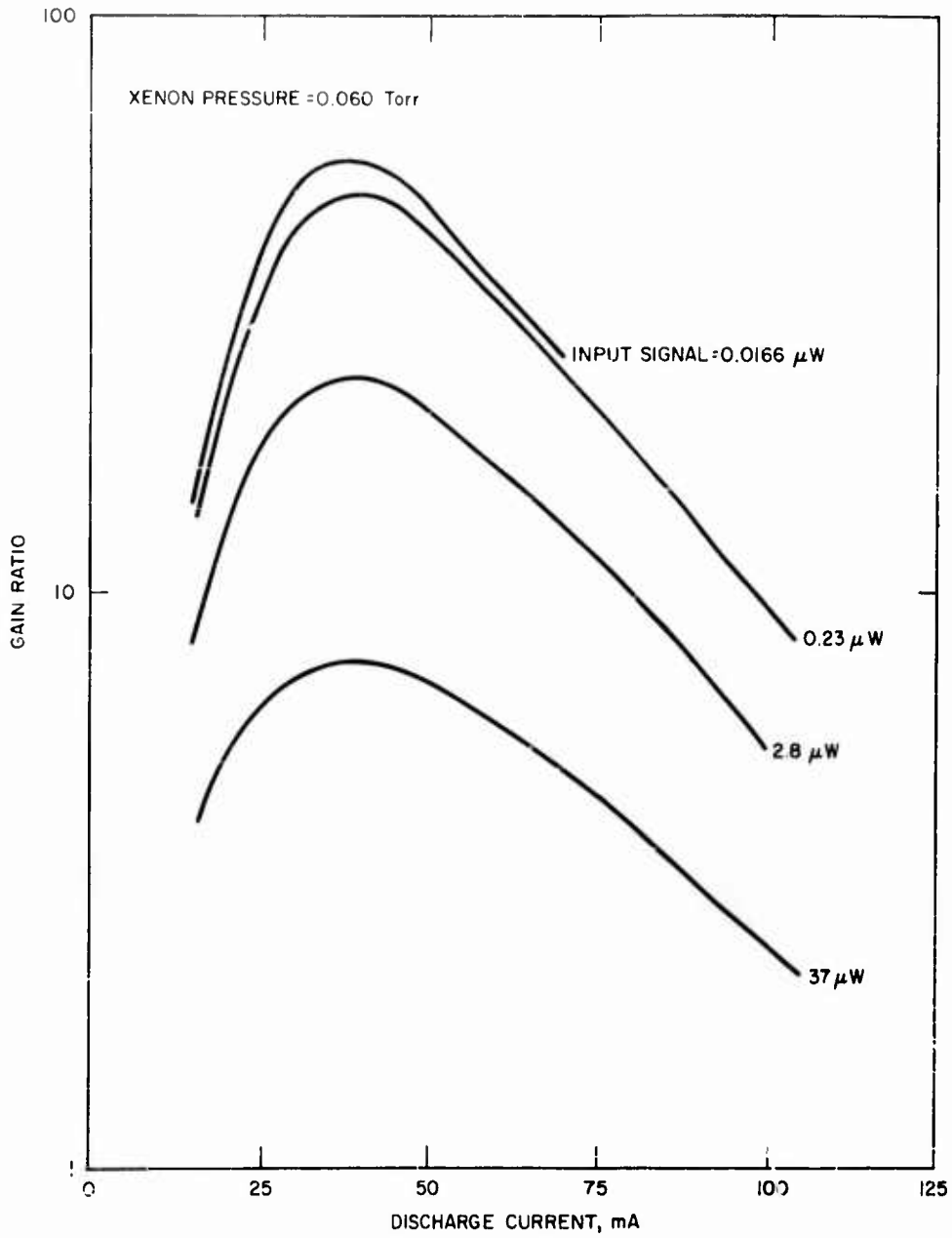

Fig. 12. Typical Variation of Gain with Discharge Current.

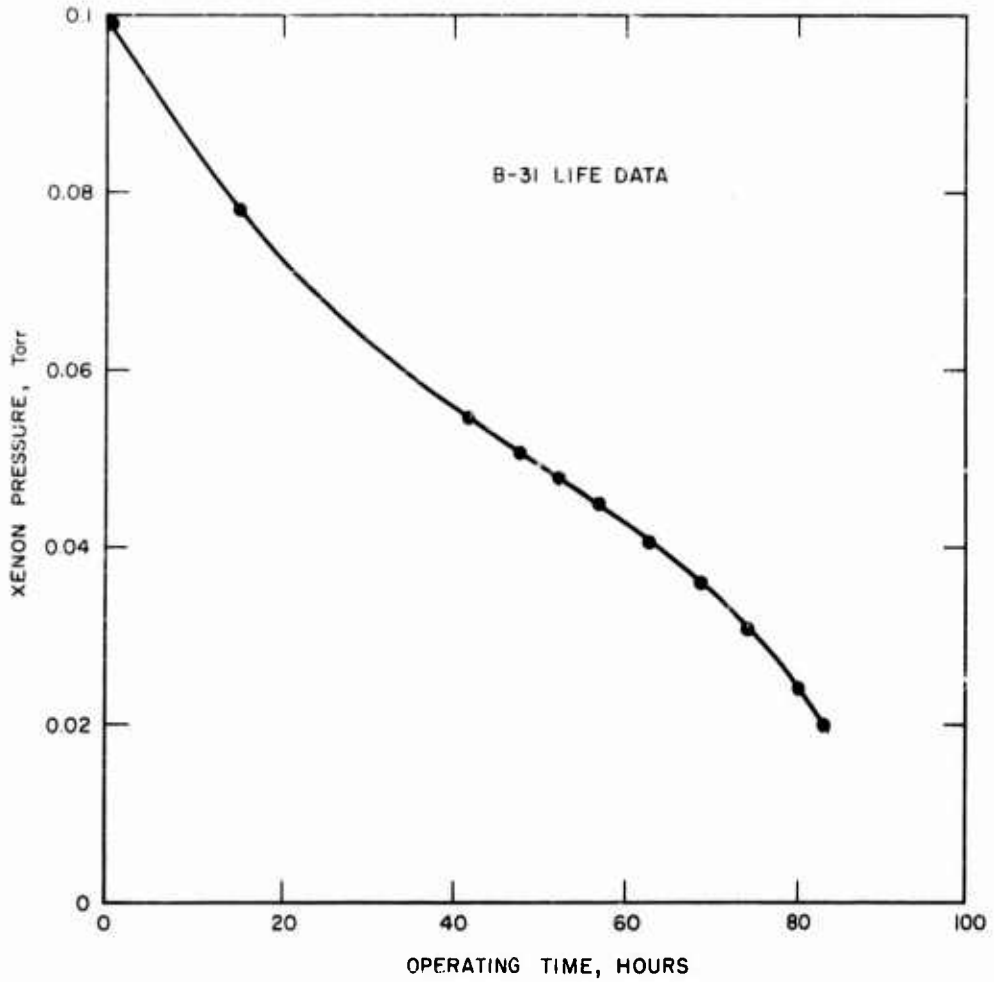

Fig. 13. Decrease in Xenon Pressure with Operation.

3. Noise

We review briefly the concepts involved in the characterization of noise performance at microwave frequencies. Figure 14 shows the gain G(f), output noise power spectral density $P_n(f)$, and noise figure F(f) as functions of frequency f for a typical microwave amplifier (e.g., a traveling-wave tube). The useful bandwidth of the amplifier is B_A; B_D is the bandwidth of the receiver in front of which the amplifier is used. In almost all cases $B_D < B_A$, and often $B_D \ll B_A$. For the definition and measurement of noise figure, it is usually assumed that $B_D \ll B_A$. Even the cases where $B_D > B_A$ (as, for example, a traveling-wave tube followed by an untuned crystal detector) present very little difficulty. This is because the typical microwave amplifier produces a negligible amount of noise outside the amplifier passband since the production of noise is so intimately tied to the gain mechanism. If noise were present outside the pass band, it would be a simple matter to build a practical, low-loss, passive filter to eliminate this contribution completely.

The noise figure F is defined by

$$F = \frac{(S/N)_{in}}{(S/N)_{out}} = \frac{S/kTB_D}{GS/GkTB_D + P_n} = \frac{GkTB_D + P_n}{GkTB_D} = 1 + \frac{P_n}{GkTB_D} \tag{11}$$

where S is the signal power, T = 290°K, and P_n is the total noise power detected.

$$P_n(f_o) = \int^{\infty} p_n(f) \times \text{response of detector}\,(f, f_o)\, df \tag{12}$$

where f_o is the center of the detector response curve. In microwave amplifiers it is always possible to use a bandwidth B_D that is small enough so that $p_n(f)$ is approximately constant over that band, thus making $P_n(f_o) = p_n(f_o)\, B_D$, and F independent of the detector bandwidth. It is this consideration that makes noise figure so widely useful as a measure of amplifier noise behavior.

By contrast, consider the corresponding characteristics of the laser amplifier, shown schematically in Fig. 15. The useful amplifier

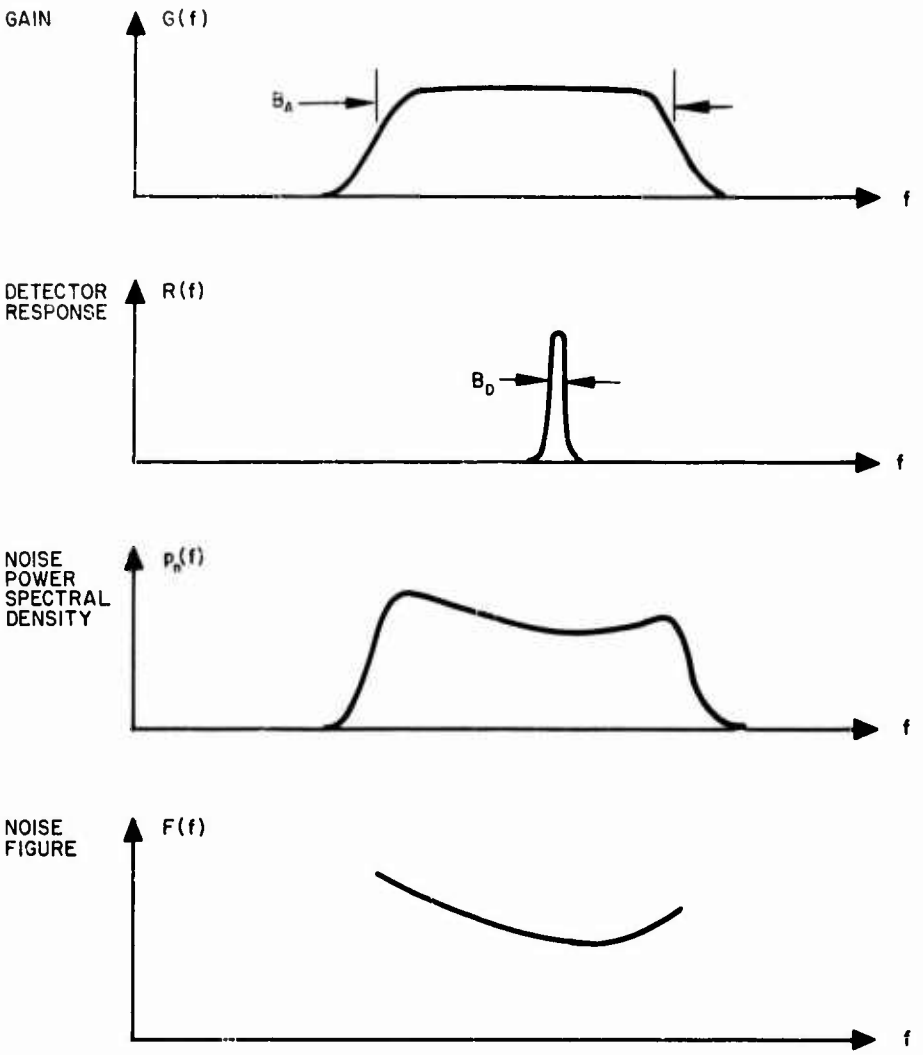

Fig. 14. Typical Gain, Noise Power Output, and Noise Figure for a Microwave Amplifier (i.e., Traveling-Wave Tube) Also Shown is the Response of a Typical Microwave Detector (i.e., a Superheterodyne Receiver).

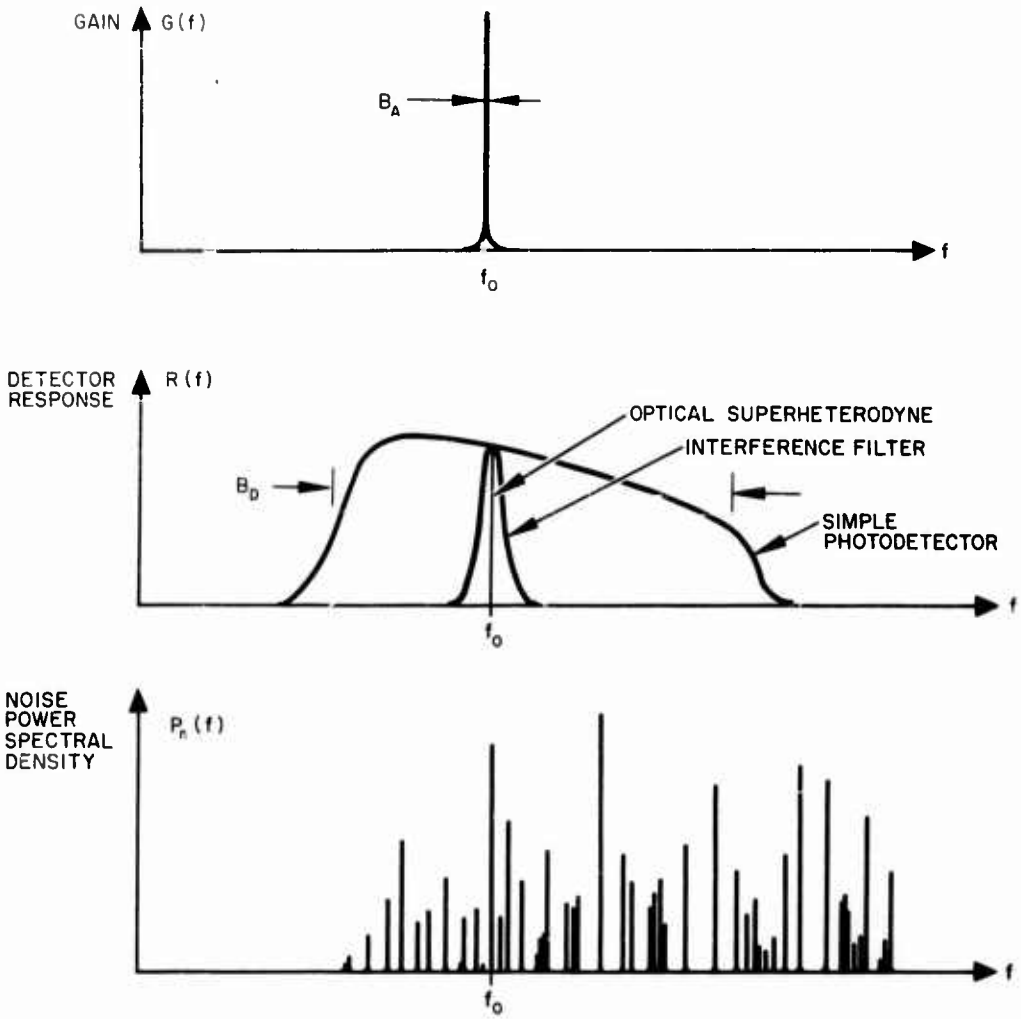

Fig. 15. Typical Gain and Noise Power Output of a Gas Laser Amplifier. Also Shown is the Response of Typical Optical Detectors.

bandwidth may be of the order of 100 Mc (approximately 150 Mc for the 3.5 μ xenon transition), while the detector bandwidths may range as high as 10^8 Mc for a simple photodetector down to a few megacycles or less for the optical superheterodyne configuration. Bandwidths between these extremes may be obtained with passive filters. It may be possible to approach $B_D < B_A$ for some laser lines with a grating filter (monochomator); but it is not likely, however, in the infrared, where the high-gain laser lines occur. It should be possible to achieve $B_D < B_A$ with a passive optical cavity filter ahead of the detector with a sacrifice in transmission and with the addition of a blocking filter to suppress unwanted modes. The most promising receiver configuration, however, is the optical superheterodyne for which B_D can be made comparable to B_A or much less than B_A. The discussion of microwave amplifiers also would apply in close analogy to an optical amplifier used before a superheterodyne receiver.

Noise figure as defined by Eq. (11) would be a useful measure of amplifier performance, provided, of course, that the problem of spatial filtering has already been solved for the optical amplifier by reducing both signal and noise to a single propagating mode. On the other hand, we may note that it is necessary to use the optical superheterodyne to measure the noise figure, and that the technique of optical heterodyning is still quite new. It is equally clear that the noise figure will not tell the whole story for receivers other than the optical superheterodyne.

Unlike the microwave amplifier, the laser has very strong noise contributions outside the amplifier passband that are completely unrelated to the gain mechanism, i.e., spontaneous emission on other transitions. To use the amplifier with a simple detector it is necessary to know $p_n(f)$ over the range of detector sensitivity (or filter passband when a filter is used between amplifier and detector). The relative measurement of $p_n(f)$ could be made with a high-resolution spectrometer, although measurement of the absolute level in watts per cps may present some difficulty. Another way to evaluate the laser amplifier for use with broad-band detectors would be to make absolute power measurements with a sequence of filters of bandwidth B_F; the resulting power $P_n(B_F)$

$$P_n(B_F) = \int_{f_o - B_F}^{f_o + B_F} p_n(f)\, df \qquad (13)$$

would then tell how narrow the filter bandwidth must be to obtain a given signal-to-noise ratio. The disadvantages in this method of specifying the laser noise are obvious: $P_n(B_F)$ depends on the shape and symmetry of the measuring filters and furthermore, P_n will be a discontinous

function of B_F since $p_n(f)$ is a line spectrum. At this time no single method of specifying noise performance for laser amplifiers is as satisfactory for all possible applications as noise figure for microwave amplifiers.

4. Noise Measurements

Because of the limited time available, it was not possible to make the type of measurements described above. Attempts to improvise filters to improve signal-to-noise ratio proved unsuccessful because of equipment difficulties. The noise performance of the xenon gas laser preamplifier, within the limitations of experiments undertaken, is as follows: With the particular lead selenide detector and electronic amplifiers used, and with no spectral or spatial filtering other than the simple apertures shown in Fig. 8, signal levels of less than 5×10^{-11} W could be measured reasonably accurately. With the amplifier discharge turned off but with everything else the same, signals of the order of 10^{-9} W were the smallest that could be reasonably measured.

The comparison is admittedly very subjective, since the "measurability" of the signals was judged by eye from a fluctuating meter. It is also true that the lead selenide detector may not have been operating at optimum temperature or with optimum electronics, but it was quite clear that the laser amplifier did not degrade the signal-to-noise ratio, but improved it on the order of 10 dB. This occurred despite the fact that the detector was receiving spontaneous emission from the amplifier over the range of about 0.2 μ to 4.5 μ. It is hoped that further measurements will yield a satisfactory description of the xenon amplifier noise behavior.

W. B. Bridges

B. ZEEMAN TUNED SINGLE PASS HELIUM-NEON AMPLIFIERS

The near infrared transitions in the noble gas lasers, e.g., the 3.39 μ transition in neon and the 3.50 μ transition in xenon, are characterized by high gain and narrow gain bandwidths. If one were to consider their use as a preamplifier for an optical Doppler radar, a relative velocity of only about 10^4 cm/sec (about one-tenth the velocity of sound) would shift the return signal to the half power point because of the 300 Mc bandwidth. Such a narrow-band preamplifier would necessarily be of limited use unless it were possible to tune the narrow amplification bandwidth over a wide frequency range. A tuning mechanism is

available in the Zeeman effect which permits shifting the gain bandwidth of the amplifying transition linearly over wide frequency ranges at modest expenditures of power.

Assuming that the signal to be amplified originates from a narrow-band, coherent source such as a laser, there may be unexpected effects when one attempts to tune a high gain amplifying transition across such a narrow signal. Therefore it was considered worthwhile to investigate the optical amplification of very narrow-band, coherent input signals. A first requirement would be the accurate determination of the gain bandwidth of the amplifying transition and the work reported below on the determination of the bandwidth for the 3.39 μ transition in the helium-neon laser represents our progress toward this goal.

The technique used for this measurement employs a fixed frequency single mode oscillator and a tunable single pass amplifier. The transition in neon used in both oscillator and amplifier is $5\,s'\,[\,1/2\,]_1 \rightarrow 4\,p'\,[\,3/2\,]_2$ (in Racah notation). The plane polarized output of the oscillator is converted to either right circular (σ_R) or left circular (σ_L) polarization using a quarter-wave plate. The amplifier, when placed in an axial magnetic field parallel to the oscillator input beam, amplifies either σ_R or σ_L according to the theory of the Zeeman effect. Variations in the axial magnetic field then change the frequency of the σ_R or σ_L amplifying transitions relative to the line center and input frequency ν_o, and hence will tune the amplification bandwidth across the relatively narrow oscillator output.

A description of the Zeeman effect for the transition is sketched in Fig. 16(a); the information is taken from Ref. 7. Figure 16 (b) is the usual diagram enabling a simple calculation of the splitting frequencies. Examination of Fig. 16(b) allows us to sketch Fig. 16(c) which indicates in the usual manner the allowed transitions and the frequency splittings relative to the line center (Ref. 8). The horizontal axis indicates a frequency scale with π components drawn on top and σ components below. The three π components are plane polarized parallel to the field and the six σ components are plane polarized perpendicular to the field when observed normal to the field. When viewed along the magnetic field, the σ components are circularly polarized. When the light observed propagates in a direction antiparallel to the magnetic field direction, σ_R in emission corresponds to frequencies above ν_o, and σ_L corresponds to frequencies below ν_o. Conversely, when the field sense is reversed (parallel to the light propagation direction), σ_R in emission corresponds to frequencies below ν_o and σ_L to frequencies above ν_o (Ref. 9). There are no π components radiated spontaneously along the field.

The experimental setup sketched in Fig. 17 indicates the elements necessary to measure amplifier bandwidths. The oscillator

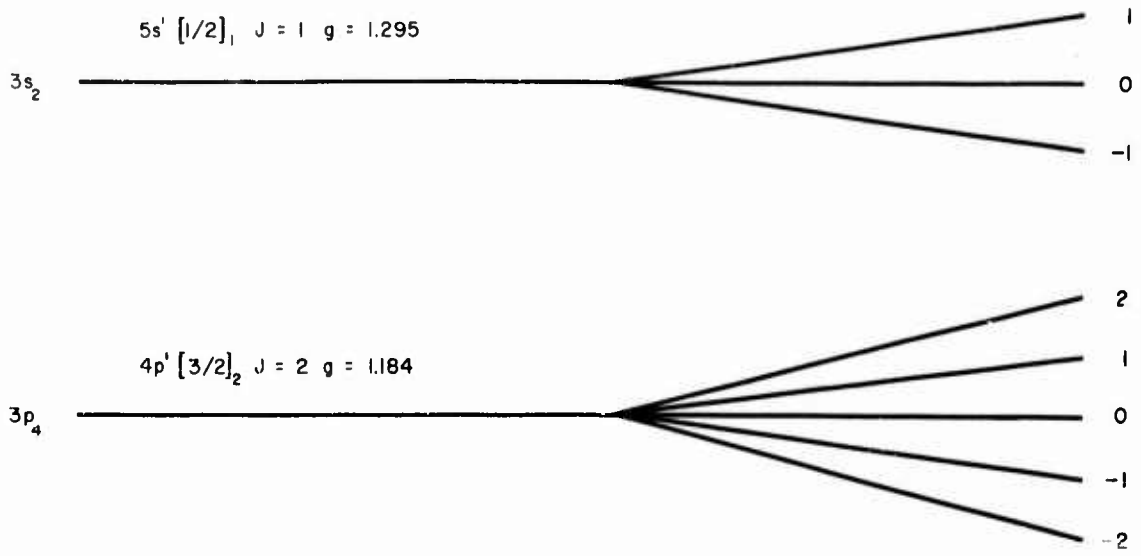

(a) The 3.39 μ transition in neon

g_i = 1.295	$(mg)_i$ =	1.295	0	-1.295	
	m_i =	+1	0	-1	
		σ_L π σ_R	σ_L π σ_R	σ_L π σ_R	
	m_f = 2	1	0	-1	-2
g_f = 1.184	$(mg)_f$ = 2.368	1.184	0	-1.184	-2.368

(b) Splitting frequencies of the allowed transitions.

Fig. 16. The Zeeman Spectrum of the 3.39 μ transition in Neon.

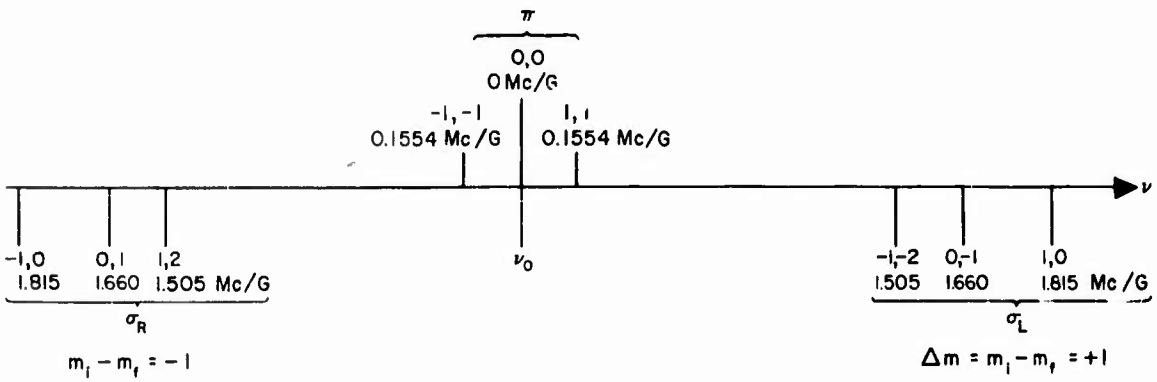

(c) Zeeman spectrum and splitting frequencies for the 3.39 μ transition.

Fig. 16 (Continued)

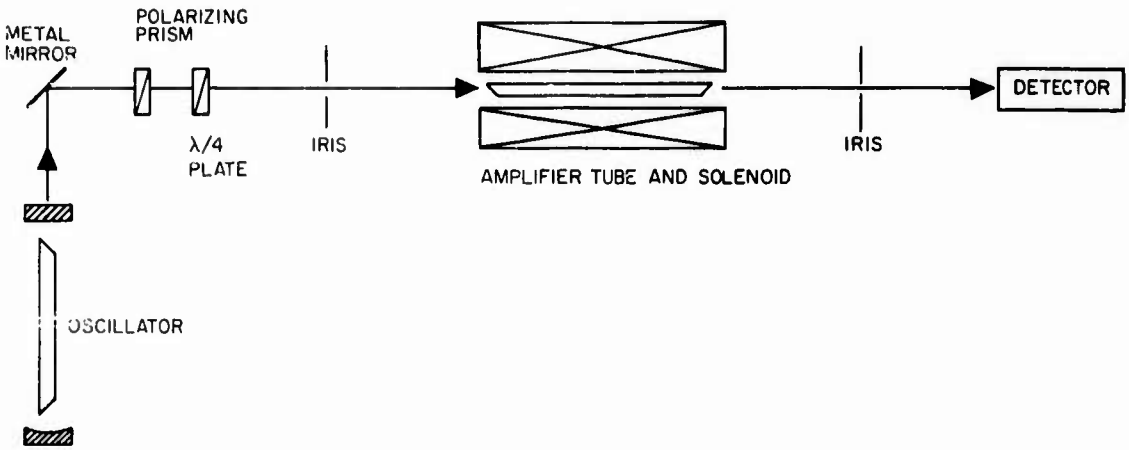

Fig. 17. Experimental Arrangement.

cavity was 43 cm long, establishing a cavity mode spacing (Δ_c) of 350 Mc. The cavity was formed by an aluminum coated spherical mirror of 1 m radius and a Fresnel reflecting quartz flat. The tube was a hot cathode dc discharge tube having 3 mm bore with 25 cm active length, and normally was operated at 16 mA dc discharge current. The plane polarized output was oriented in the vertical in order that the external metal mirror did not mix the beam polarization state on reflection. The oscillator axis was fixed at 90° to the amplifier axis in order to minimize effects due to the leakage field of the solenoid. The Glan polarizing prism was used as a simple attenuator. The quarter-wave plate was a quartz Soleil compensator adjusted to the proper thickness and rotated 45° to the beam plane of polarization. The amplifier tube had a 5 mm bore and a 60 cm active length. It normally was operated at about 35 mA dc discharge current. The fore and aft irises were tilted slightly with respect to the beam axis and were approximately 5 mm in diameter. A calibrated thermopile was the detector, with 118 μV corresponding to 1 mW/cm^2.

For the measurements the quarter-wave compensator was set to pass right circularly polarized light (σ_R) and the amplifier output was recorded as a function of solenoid current I. Figure 18 represents an average of several measurements for σ_R gain bandwidth versus solenoid current I for low level input signals of the order of 10 μW. The ordinate represents amplifier output relative to the output at zero axial field. The determination of the bandwidth at half maximum points is inaccurate since the average of several measurements is 240 ± 20 Mc. The peak gain (gain at line center) is not a very accurately measured parameter in our arrangement, probably because of slow drifts. Our highest value obtained was 25 dB/m at these input levels.

Raising the input power by a factor of 10 to levels of 100 μW drops the peak gain to about 18 dB/m and broadens the line to an average of 270 ± 40 Mc (Fig. 19). There is evidence here of gain saturation in the amplifier and an interesting asymmetry appears. The gain peaks to one side of zero field; for σ_R the peak usually falls on the negative current side, and on the positive current side for σ_L (this is not always the case, however).

A word about the single mode oscillator is in order as a possible explanation for this phenomenon. Since we know that the line width (Ref. 10) is somewhere on the order of 300 Mc, we have utilized a cavity short enough (43 cm) that the axial modes are spaced 350 Mc apart. With this spacing, use of a 1 m radius spherical mirror and a flat mirror implies that the cavity is very nearly in the half confocal or hemispherical mode which is known to lower cavity Q for transverse modes and hence suppress them relative to the axial modes. Second, the cavity spacing generates a separation between axial modes of 350 Mc ($\Delta_c = c/2d$). Our approximate knowledge of the Doppler broadened

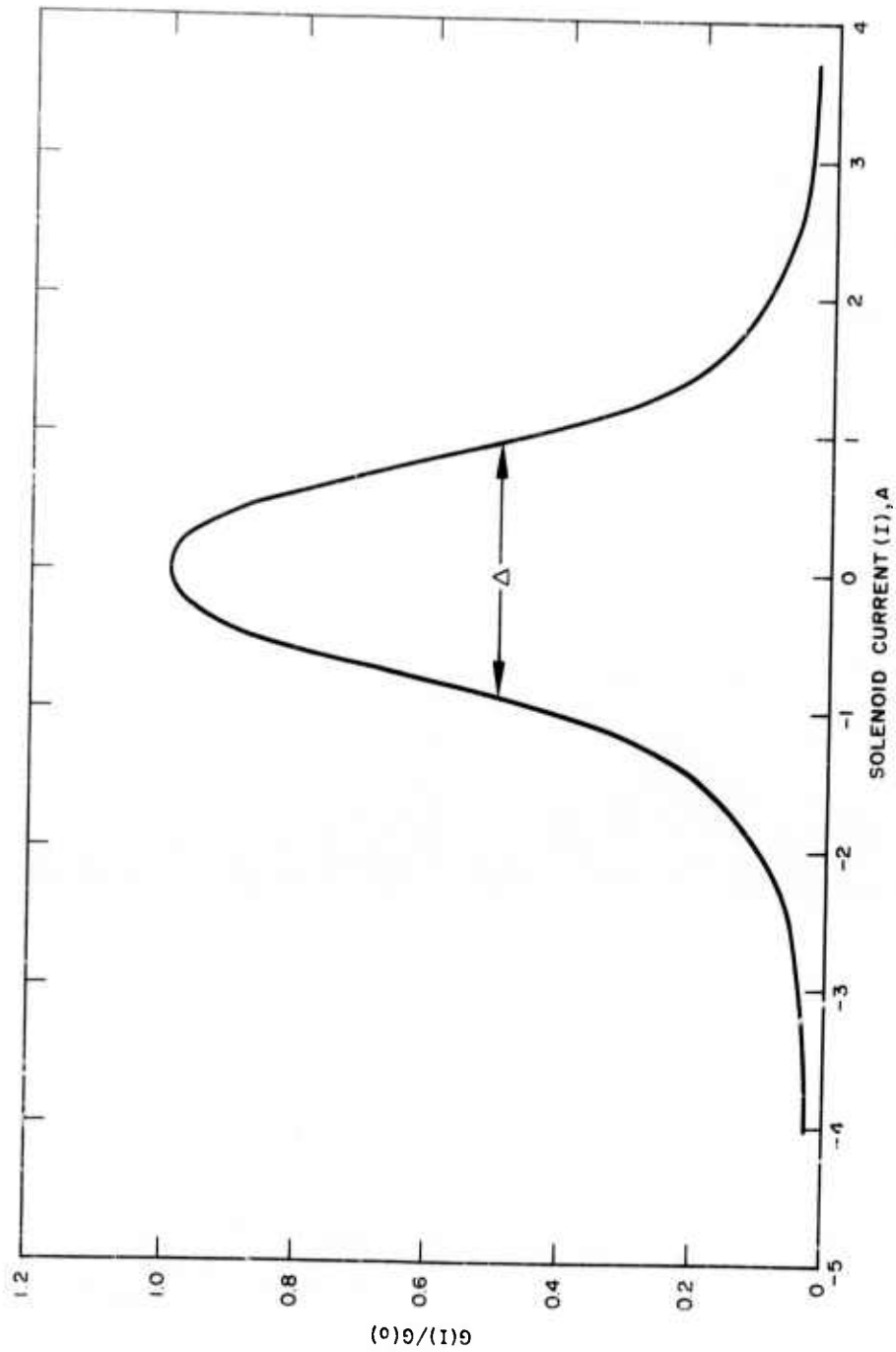

Fig. 18. Low Level Gain Bandwidth for σ_R.

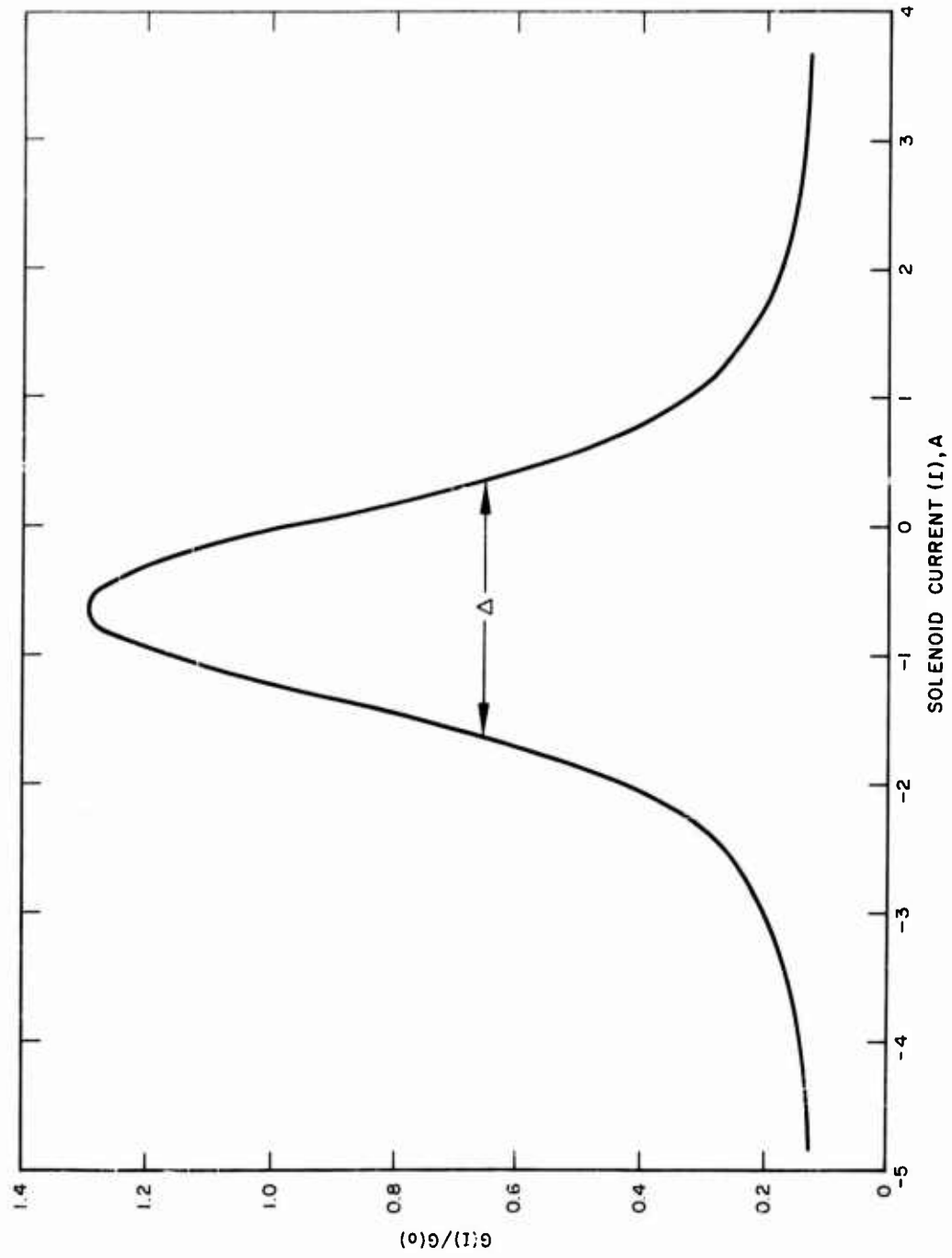

Fig. 19. High Level Gain Bandwidth for σ_R.

gain bandwidth assured us that the laser was oscillating in only one axial mode, a necessary condition for this experiment. If we neglect any cavity pulling effects and indicate the actual laser output frequency by ν_c (Fig. 20) we can see that an offset of ν_c from the line center ν_o could contribute to the observed asymmetry as follows: If ν_c does not coincide with ν_o, the difference in output is small but multiplied by the amplifier. In the particular situation illustrated in Fig. 20, shifting the Doppler line for σ_R in the amplifier to the left ($H > 0$) would cause the amplifier output to peak away from $H = 0$ at an output exceeding that for $H = 0$. However, the fact that this asymmetric behavior was not observed for low level input signals indicates that amplifier saturation may be a determining factor. The fact that the asymmetry sometimes appeared on the opposite side of the line center could be explained by the position of ν_c with respect to ν_o; we usually attempted to maximize the oscillator output by adjustment of the cavity before a measurement run. All these observations were made using σ_R input but no essential differences were observed using σ_L input.

A sequence of runs was made using plane polarized input to the amplifier. The gain curves were approximately gaussian and symmetric (Fig. 21) — about $H = 0$ for input power ranging from 10 μW to 300 μW. Here, however, the bandwidth appeared to narrow with increasing input power; this behavior is just the opposite to that of the σ components. We have no explanation for this effect.

An input signal much below 10 μW became lost in the noise of the thermopile detector. Therefore, in order to study the effects of input signal levels of 10 μW and less an indium antimonide detector was substituted for the thermopile. The oscillator discharge was sine wave modulated at 1 kc, enabling a phase sensitive detection scheme to be used to discriminate against amplifier noise. Relative gain as a function of solenoid current (the solenoid constant was 77 G/A) was measured for a high level input of about 3 μW and a low level input in the noise level of the calibrated thermopile. Three different polarization states were employed in the input beam; π (Fig. 22), σ_R (Fig. 23), and σ_L (Fig. 24). For these six runs we are certain that the cavity spacing, and hence a possible difference between the oscillator frequency ν_c and the line center ν_o, was constant for all these gain curves. In addition, the shift off center in opposite directions for σ_R and σ_L, and the symmetry of the double peaked gain curve for π, confirm that $\nu_c \pm \nu_o$ was constant during these observations. We also note that for π input the gain curve narrows for increasing input power, whereas increasing input level produces a broadening for σ_R and σ_L gain. This effect was previously noted using a calibrated thermopile as a detector although the double peaked gain curve was not observed at higher levels of input power.

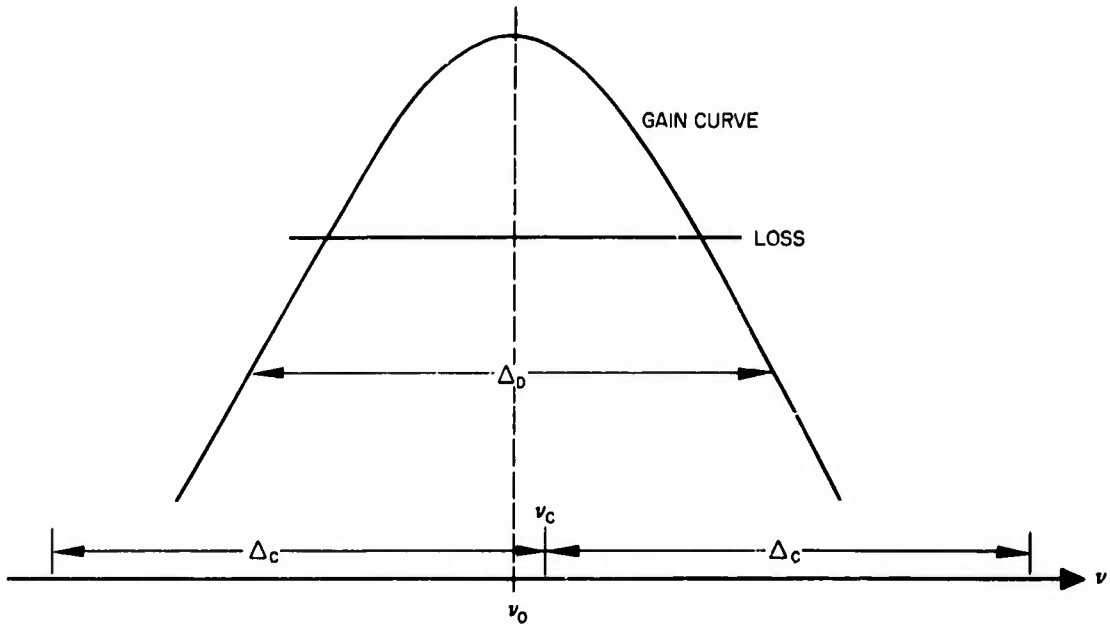

Fig. 20. Doppler Broadened Gain Curve and Positions of Axial Cavity Modes Relative to Line Center ν_o.

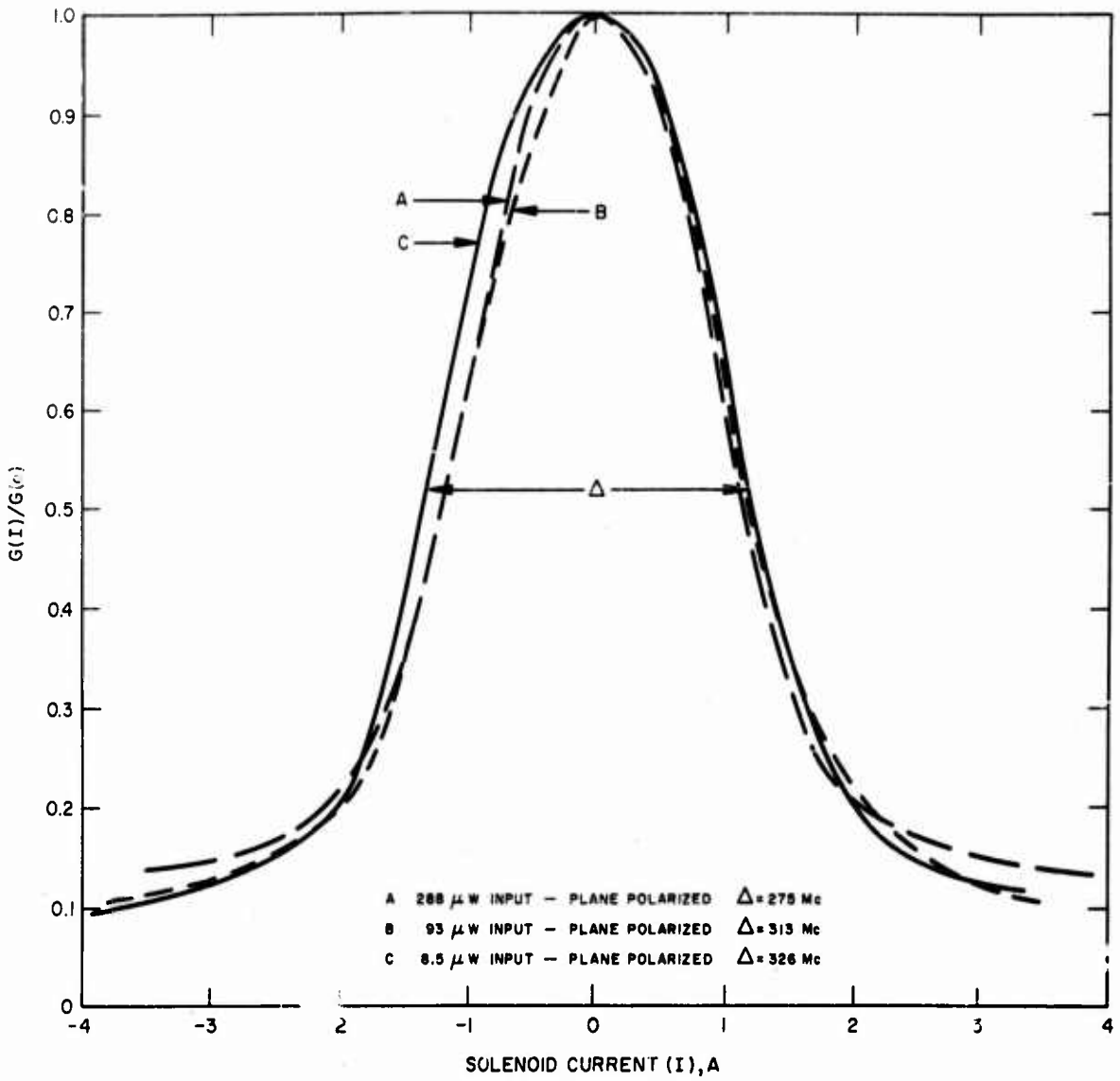

Fig. 21. Relative Gain for Plane Polarized (π) Input.

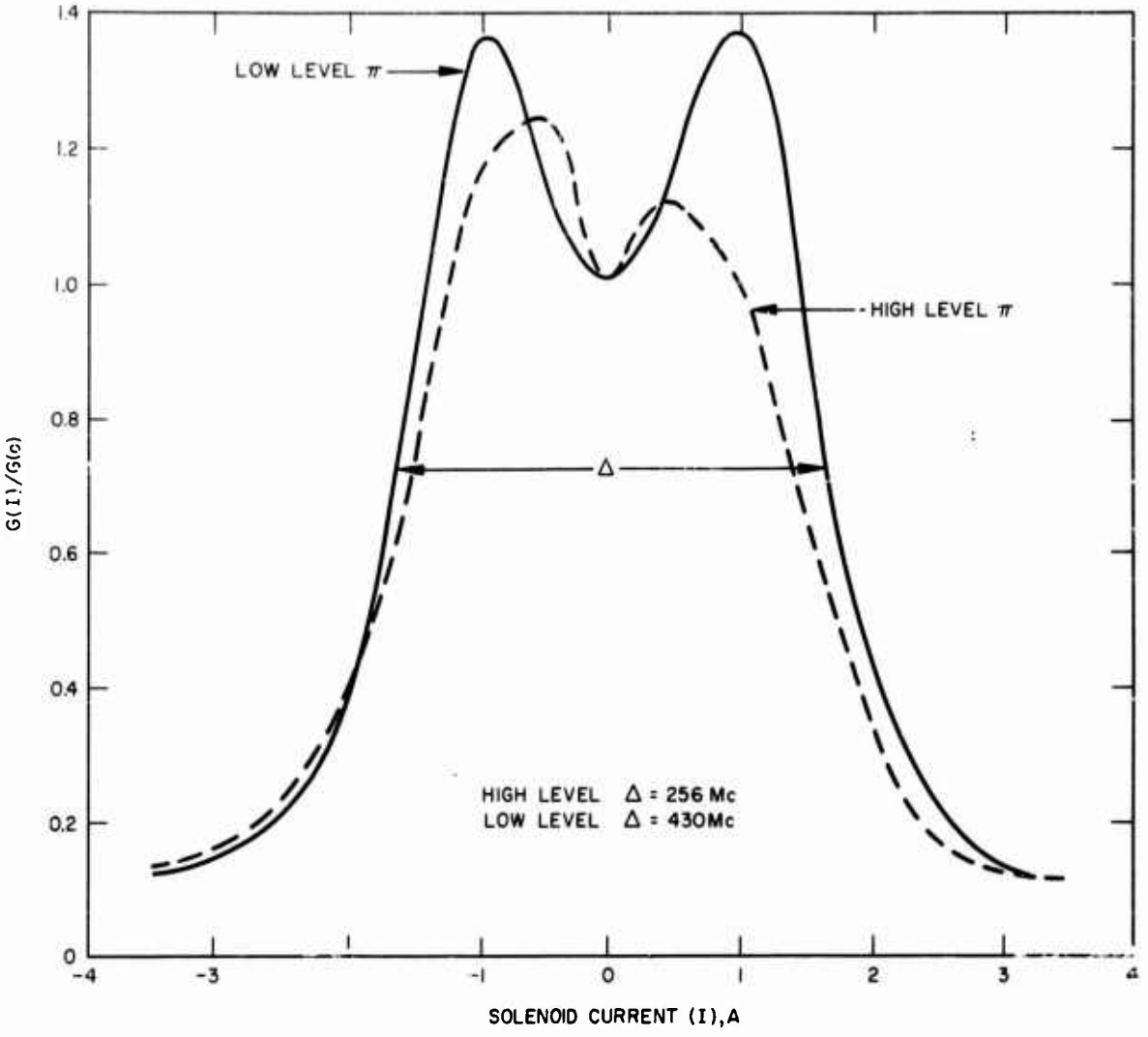

Fig. 22. Relative Gain for Plane Polarized (π) Input using 3 μW (High Level) and Less (Low Level).

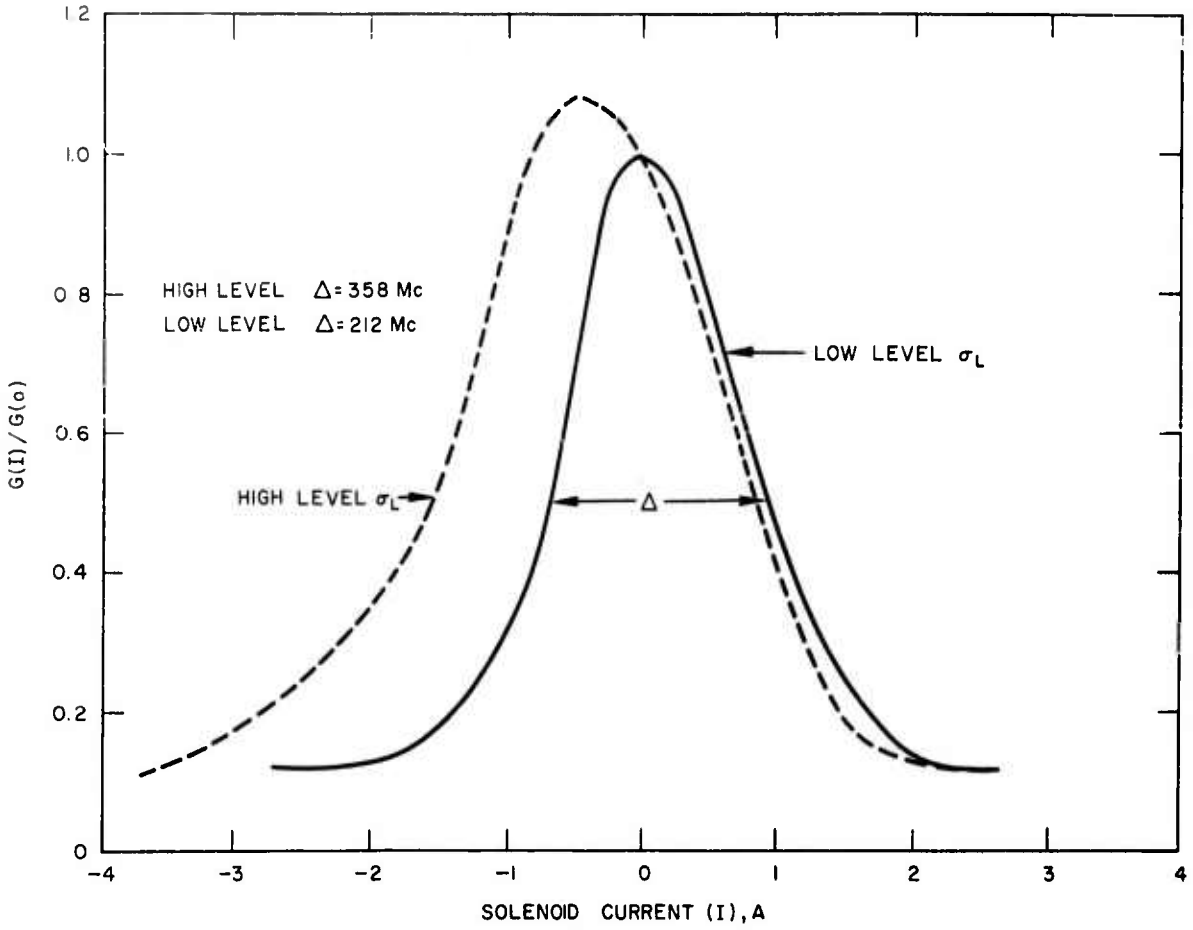

Fig. 23. Relative Gain for Right Circular Polarization (σ_R) Input Using 3 μW (High Level) and Less (Low Level).

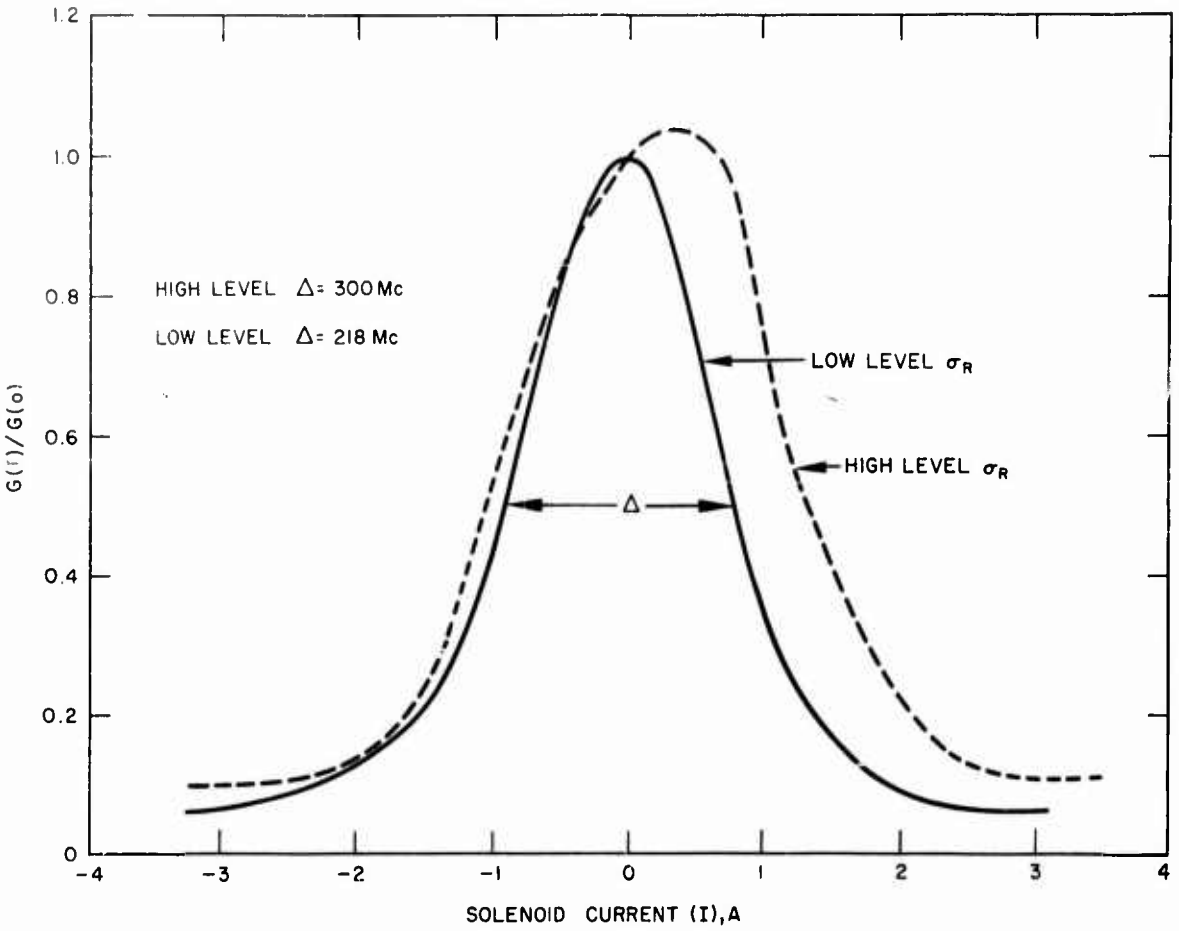

Fig. 24. Relati Gain for Left Circular Polarization (σ_L) Input Using 3 μW (i gh Level) and Less (Low Level).

It is tempting to try to explain the doubled peaked gain curve for low level π input as being caused by the effect of the axial magnetic field on the energy and particle balance mechanisms required to maintain the dc discharge (Ref. 11). Partial pressures and discharge current density for the amplifier tube were optimized for maximum gain by operating the amplifier as a laser on the laser processing station when the tube was built. If the axial magnetic field causes the current density to be altered, it also would cause the gain to be reduced from the maximum. This is not consistent with the observed increase in gain for fields of about 80 G. The particle balance mechanism in the discharge involves ambipolar diffusion to the laser tube wall. The axial magnetic field would affect this slightly, and its largest effect would be to increase the low energy component of the electron energy distribution at the expense of the higher energy electrons. This effect, if any, would be a decrease in the gain. The effects of the magnetic field seem to have very little effect on the gain and for this reason we have neglected it in our discussion. Accordingly, we have assumed that the Doppler width for σ_R, σ_L, and π are identical.

From these preliminary measurements we can conclude that the gain bandwidth may range from 200 Mc to 400 Mc in halfwidth depending on the polarization state and power level of the input signal. It would not be surprising if the observed variations in the gain bandwidth were related in some way to the spectral purity and coherence properties (Ref. 12) of the input as well as gain saturation in the 3.39 μ transition.

D. F. Hotz

SECTION 4

LASER DETECTOR TECHNOLOGY

This section summarizes the detailed discussion of various detectors for modulated laser light included as Appendix I.

Laser sources which are sufficiently well developed to be considered as transmitters in communications or radar systems fall into the wavelength range from 0.4 to 4 μ (4000 to 40,000 Å). This decade of the electromagnetic spectrum is further subdivided into three regions when we consider the types of detectors capable of sufficiently fast response to demodulate at microwave frequencies. In the first region, from 4000 Å to 7000 Å, photoemissive detectors are the most efficient. Photoemitting surfaces with peak quantum efficiencies up to 0.2 are available and these can be incorporated into structures (e.g., the traveling-wave phototube) with response well into the kilomegacycle range. The second range, from 7000 to 11,000 Å (1.1 μ), can be covered with phototubes with an AgOCs cathode (S-1 photosurface); however, the peak available quantum efficiency is only 0.0005. It is worthwhile to consider using solid-state photodiodes which display quantum efficiencies of the order of 0.5 for many applications in this intermediate region of wavelengths. In the third range of wavelengths, greater than 1.1 μ, only the solid-state diode can be used, since by proper choice of materials these devices can be fabricated to display response at wavelengths up to 5.5 μ.

The various types of detectors can be compared in more precise terms if they are regarded as transducers of photon current to electrical current. It is then possible to evaluate their optical performance in terms of a quantum efficiency η and their electrical performance in terms of an equivalent output resistance R_{eq} as follows:

Suppose the average power incident on the detector power in a stream of photons of frequency ν is P_o and that this stream is modulated at some microwave frequency ω to a depth given by the modulation index m. The instantaneous incident power is then

$$P(t) = P_o + mP_o \cos \omega t . \qquad (14)$$

The incident photon flux is $P(t)/h\nu$ and if η represents an over-all quantum efficiency (i.e., the probability that an incident photon produces

a measurable charge carrier in the detector), the magnitude of the current at the modulation frequency is given by:

$$i(\omega) = \frac{e\eta m P_o}{h\nu} \quad . \tag{15}$$

The detector and the circuit in which it is incorporated can be represented by an infinite impedance signal generator of magnitude $i(\omega)$ in parallel with a resistance R_{eq}. The average power delivered to the detector load will be

$$1/2\ i(\omega)^2\ R_{eq} = 1/2 \left(\frac{emP_o}{h\nu}\right)^2 \eta^2\ R_{eq} \quad . \tag{16}$$

The theoretical and electrical parameters for determining the amount of signal power a detector is capable of delivering can be summed up in the quantity $\eta^2\ R_{eq}$; this can be used as a figure of merit for comparing different devices. A complete specification of detector performance also requires descriptions of transit time limitations on the frequency response (where they exist) and some indication of the noise power delivered by the device and its frequency spectrum. These aspects of the potential laser demodulator detectors are summarized in the next paragraph. For a more detailed discussion and references, see Appendix I.

Photoemitting surfaces with quantum efficiencies greater than 0.01 are available in the wavelength range from 0.4 to 0.65 μ. The S-20 surface, for example, has a quantum efficiency of 0.45 at 6328 Å and 0.028 at 6934 Å. Photomultipliers are valuable because their high internal gain raises both signal and shot noise to a level well above receiver noise but transit time dispersion in such phototubes cuts off the frequency response above 100-200 Mc. A version of the phototube which overcomes this transit time limitation is the traveling-wave phototube, in which the microwave modulated electron stream from the photocathode is coupled to a traveling-wave helix. Microwave power gains up to 40 dB have been reported with such structures and responses up to 10 Gc have been observed. R_{eq} for the traveling-wave phototube (a function of the helix length) is in the range from 10^5 to $10^6\Omega$. Because of the traveling-wave structure, bandwidth ratios of 3:1 or 4:1 should be attainable. If high quantum efficiency photocathodes are used, values of 1000Ω or better for the figure of merit $\eta^2 R_{eq}$ should be achieved. Because the tubes reported to date have not utilized optimum photosurfaces for the ruby or helium-neon lasers with which they were tested, only

values of the order of one ohm have so far been reported. Microwave noise properties of traveling wave phototubes have not yet been reported in the literature.

The wavelength response of all phototubes can be extended to 1.1 μ by use of an S-1 photosurface. The quantum efficiency is then limited to about 0.002 and $\eta^2 R_{eq}$ for traveling-wave phototubes with such surfaces will be of the order of 4Ω or less.

Another point that should be mentioned is that the sensitive area of such phototubes can be made quite large — several square centimeters if necessary — thus providing an element of flexibility in optical design.

The dynamic crossed-field photomultiplier is another approach for overcoming the frequency response limitation of the photomultiplier without sacrificing gain. This device requires a microwave driving frequency and provides a bandwidth equal to one-half this frequency. Its mode of operation is such that it collects only the electrons emitted during approximately one-sixth of each cycle. Thus, its available signal power is also reduced by about this amount. It is therefore not possible for this device to attain the performance capability of the traveling-wave phototube.

In the solid-state photodiodes the transit time frequency response limitation is overcome by fabricating very thin p-n or p-i-n structures close to the sample surface. The capacitance of such structures can then be reduced to tolerable limits by reducing the photosensitive junction area. For diodes reported in the literature to date, both the transit time and RC limitation to frequency response have fallen in the range of 1 to 10 Gc. R_{eq} for these diodes in this frequency range is only of the order of 10Ω, so that quantum efficiencies of at least 0.3 are required to give values of $\eta^2 R_{eq} > 1\Omega$. Since every photon absorbed by such a detector can produce a free carrier, the over-all quantum efficiency will be limited by external effects such as reflection losses and masking effects due to contact configuration. Quantum efficiencies of the order of 0.3 to 0.5 have been reported. Because the diode, per se, does not have internal gain, its shot noise is generally swamped by thermal noise in its equivalent series resistance and receiver noise. The effect of receiver noise can be somewhat reduced by resonating the diode capacity with an inductance at the desired operating frequency. The relative bandwidth is then limited to approximately 10% at frequencies of several gigacycles where Q factors of the order of 10 can be attained.

Low capacities of only a few picofarads can be attained only in very small devices — typically in those with areas of 10^{-2} cm^2. The problems of efficiently collecting and focusing the signal radiation are significantly increased because of this small sensitive area.

A very significant recent development has been the incorporation of internal gain at the microwave signal frequency by operation of photodiodes in parametric amplifier circuits. In the work reported by Sawyer (Ref. 13) a gain of 25 dB was attained with a corresponding 20-fold decrease in the minimum detectable signal. Initial operation was at a modulation frequency of 22.5 Mc.

The traveling-wave phototube and the solid-state photodiode are at this time the most prominant candidates for detectors of microwave modulated laser radiation. For wavelengths shorter than 6500 or 7000 Å, the phototube appears to have the advantage because of its internal gain and wider bandwidth. Only the diodes can be used beyond 1.1 μ because photoemissive surfaces do not have long wavelength response. Between 0.7 and 1.1 μ, the various detectors available must be closely compared and evaluated with respect to specific system requirements to permit selection of the optimum detector.

G. S. Picus

SECTION 5

LASER RECEIVER SYSTEMS

Although the primary emphasis of this contract has been on the development and study of laser preamplifiers and detectors for use in laser radars, other aspects of the laser radar receiver problem have also been investigated. These additional studies investigated coherent data processing techniques and quantum limitations on optical radar performance.

A. COHERENT OPTICAL PROCESSING

Now that laser optical radars are an actuality, it is tempting to inquire as to which of the many microwave radar coherent data processing principles and techniques might be applied to the optical domain. It is reasonable to suppose that most of the well-known techniques were devised either to overcome limitations of the microwave domain or to exploit possible unique advantages. Thus, while many principles will not retain significant merit when translated a factor of 10^4 in frequency, many others may well possess equal or increased advantages.

1. Synthetic Apertures at Optical Wavelengths

In microwave radar, poor angular resolution has always been a serious limitation because the largest physical antennas are not more than a few hundred wavelengths across. The synthetic aperture technique was invented to provide improved angular resolution under a certain set of restricted, though useful, circumstances.

The fundamental principle is that of taking a dish or array of reasonable size ℓ and translating it along a line normal to its axis of radiation symmetry, this is usually done by the motion of the carrying vehicle. Individual pulses are transmitted, received, stored, and combined coherently to produce an array of greater effective length L. There is no intention here of reviewing the theory of synthetic aperture systems, for this is given in many places. References 14 to 16 contain some of the recent unclassified material in this field.

It is probably not obvious that improved angular resolution would be of as much interest in laser optical systems as in microwave systems, because of the great increase in frequency. Yet resolution

at long ranges may be insufficient, and apertures of many feet may be feasible by coherent storage, but not with a lens or mirror system.

The problems of creating synthetic apertures was treated in the Interim Engineering Report No. 2 of this contract. The material was classified Confidential. In order to keep this Final Report unclassified, only the general conclusions will be presented, and the reader should refer to the Interim Report for a more detailed discussion.

The preliminary examination given in Interim Engineering Report No. 2 pointed out a number of areas where further work is required. Generally, though, applications involving the vehicle and/or transmission path in the atmosphere are unlikely to have much merit. Applications in space involving relatively short ranges and low velocities may be useful, but under these conditions the improvement may be less needed. Applications in space involving long ranges, high powers, and high closing rates appear very formidable technically. For all applications, target motion – scintillations due to rotation and vibration – will be a serious problem, especially on uncooperative targets. Even under the best of circumstances, accuracy is improved only in one angular dimension, and range rate and angle may not both be improved unambiguously.

C.H. Wilcox
W.P. Brown, Jr.
R.L. Forward

2. Optical Radar Pulse Compression Systems

Pulse compression techniques in radar systems evolved from the desire to decrease the effective pulse length of the transmitted signal to obtain higher range resolution of the radar system without degrading the sensitivity by decreasing the energy per pulse. Conceptually, the easiest way to obtain higher resolution is to redesign the transmitter so that it transmits the same amount of energy in a shorter duration pulse. The other techniques described below become necessary only when we are prevented from increasing the energy per pulse by peak power limited transmitter components.

All of the pulse compression systems are essentially techniques for coding the transmitted signal in some way so that the energy leaving the antenna at different times can be recognized in the receiver and processed accordingly, thus allowing the returns from two close targets to be separated out. One common technique is to change the frequency of

the transmitted signal during the pulse. Since the time of transmittal is uniquely related to the frequency, the pulse compression is easily accomplished by dispersive elements upon return. Another more sophisticated technique is to code the transmitted signal with binary phase, frequency or amplitude modulation in the form of special codes. These codes have the particular property that their autocorrelation function has a very strong central peak and weak sidelobes.

a. Phase Coded Systems

Although frequency modulated (chirp) pulse compression systems are conceptually more simple than coded systems, it is felt that present light modulation techniques make the coded systems easier to implement in the optical region.

By way of illustration, we suggest an optical radar pulse compression system which might be built along the following lines. The transmitter source is a laser which must be phase-stable (or stabilized) for a time equal to the duration of the transmitted pulse. This light output is then binary phase coded by a phase modulator which is similar to the traveling-wave phase modulator built by C. J. Peters of Sylvania (Ref. 17). Since these modulators operate in the X-band region (10^{10} cps) it is possible that we can compress the laser pulse down to less than a nanosecond, which is equivalent to a range resolution of a few centimeters. Any suitable phase code may be used. For example, the Barker code is generally optimum for less than 14 digits. Other codes are available for up to 100 digits. The Barker 5 code is used as an illustration in Figs. 25 and 26.

On return, the pulse is sent through a suitable tapped delay line (Fig. 25) where the reciprocal of the transmitted code is reproduced in the phase delays on the taps. If we carefully note the amplitude of the coherently combined output of the taps as the signal passes through the delay line, we see that the contributions from the various taps nearly cancel each other out except for the interval when the phase code on the signal is matched by the phase code on the delay line taps. The various steps can be followed in Fig. 26.

b. Delay Line Storage

Wideband delay line storage, or more generally, wideband storage, is fundamental to pulse compression systems of all types, including matched filter systems (Ref. 18). Among the various devices used for this function are (1) lumped-parameter electrical delay networks, (2) acoustic delay in quartz, (3) acoustic delay in steel, (4) coaxial cable, (5) waveguides in both dispersive and nondispersive modes, (6) rotating magnetic drums, and (7) shift register.

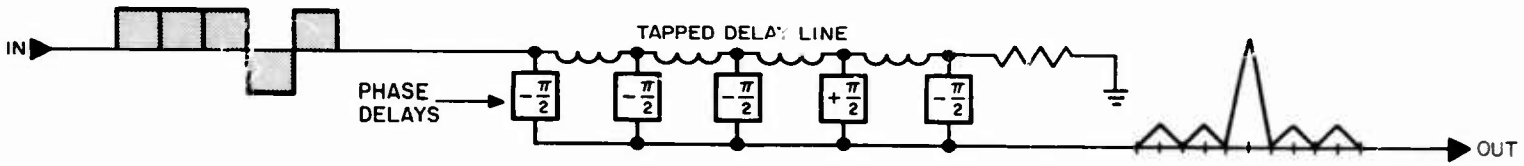

Fig. 25. Tapped Delay Line Filter with Barker 5 Code.

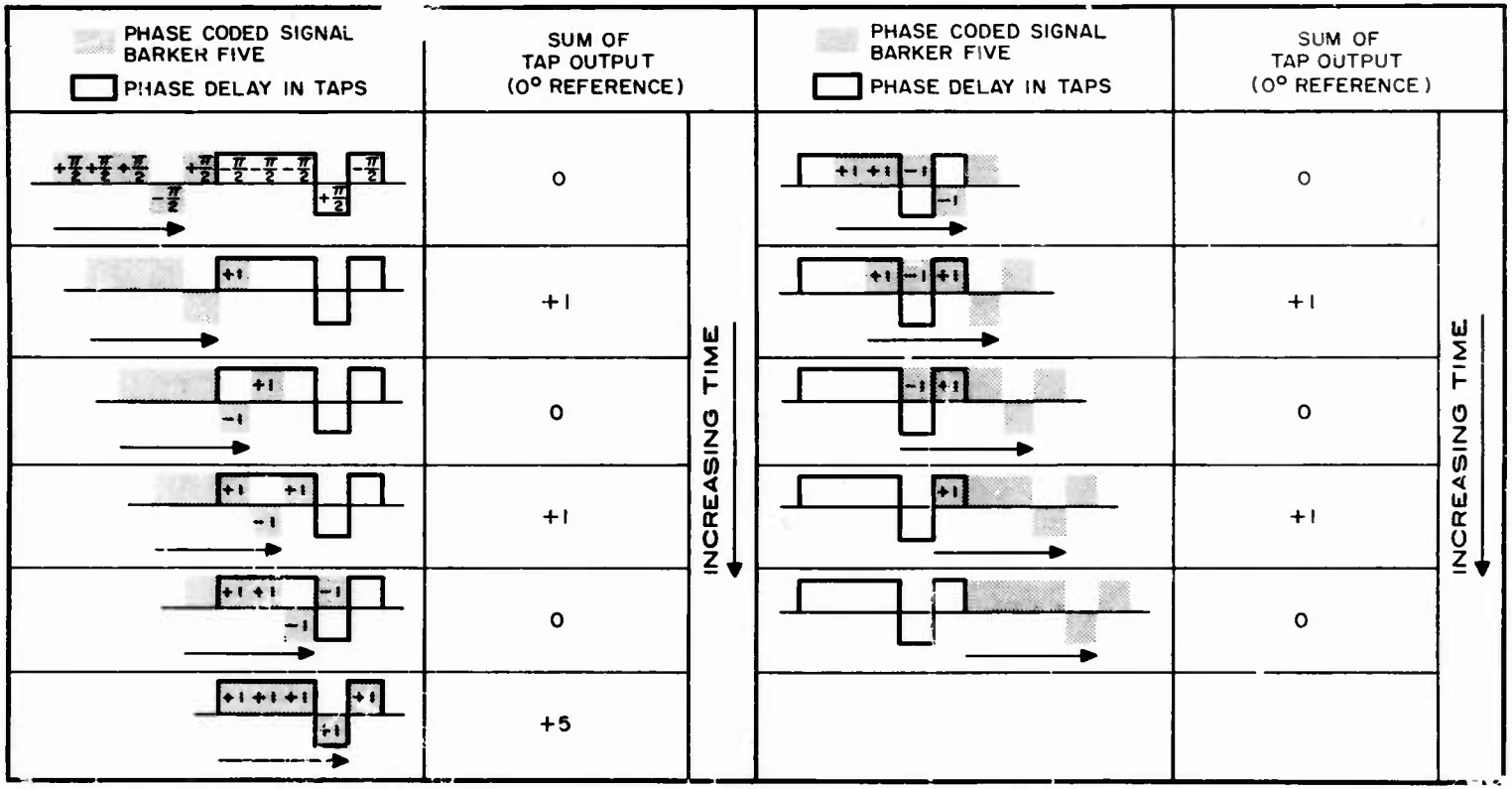

Fig. 26. Development of Autocorrelation Output of Barker 5 Phase Coded Signal.

There are two ways to handle the storage and delay of coherent optical radar returns in convenient-sized packages. One method is to heterodyne the optical signals down to the microwave or rf region and use the storage devices developed in this region. The other is to develop optical devices capable of storing, delaying, and coherently combining the various components of the received optical signals without conversion.

The heterodyne system is considered to be a feasible method of obtaining pulse compression with pulses presently available from lasers. The millisecond pulse lengths of a standard ruby laser could be compressed by lumped-parameter electric delay lines with megacycle bandwidths. This technique could improve the range resolution from hundreds of kilometers to a few kilometers. With the present low power levels this improvement is academic, since much better range resolution has been obtained by modifying the ruby transmitter to operate in the giant pulse mode with pulse lengths on the order of 10^{-8} sec or a range resolution of a few meters. Even the giant pulse is capable of being compressed several orders of magnitude by heterodyning to microwave frequencies and using wideband microwave waveguide delay lines.

Although these heterodyne techniques will require considerable effort in the development of microwave components that will maintain the necessary phase stability, the problem seems straightforward. In the rest of this section we concentrate on optical delay techniques which are the only feasible methods for obtaining range resolutions below 1 cm.

c. The Active Optical Delay Line

One of the possible methods of implementing a delay line for pulse compression of an optical radar pulse is to use an active optical "waveguide" made of glass fibers. In order to obtain a relatively large delay in a reasonably small space it is proposed to make the cross section quite small, of the order of 4 mils or less. Ordinarily, the attenuation would be high at these optical frequencies — of the order of . B/m. However, by making the glass rod a laser "amplifier" as well as a delay line, we can use the energy available from inverted populations to overcome the attenuation.

Only quite recently continuous laser action was obtained from a barium crown glass rod by Young at American Optical (Ref. 19). The rod was 4 mils in diameter with a 40-mil cladding of soda-lime-silicate glass which allowed refraction ray-axis angles up to 10° to be totally reflected. Young's rod was only 1-3/16 in. long — far shorter than needed for delay systems. However, Kcester (Ref. 20) reports amplification in a fiber 12 μ in diameter and 5 m long. Further

advances are to be expected; this art is still in its infancy. A typical design configuration for an active optical delay line decoder is shown in Fig. 27.

The received signal might first be amplified by a laser preamplifier — although it is by no means certain that this will be required. The signal then enters the active delay line decoder. The number of taps on the spiral would generally be equal to the number of digits in the code. The distance between taps (in the figure, the circumferential length of a turn) would be chosen to give an optical delay time equal to the duration of the compressed pulse (which, of course, is also the length of any one phase bit in the transmitted code). At the bottom of each turn is a glass rod junction which taps off a small portion, perhaps 5%, of the light traversing the main spiral. It would be best (but not essential) that this junction be made nonreciprocal so that a larger portion of the incident light could be extracted. This could be done by using lead oxide glass for the tap. A magnetic bias field as shown in Fig. 27 would activate the Faraday rotation effect in the lead oxide, making the junction nonreciprocal. These "tap off" signals must be added coherently, with appropriate phase steps being added according to the transmitted code. This requires some adjustment. In effect, one must simultaneously adjust many interferometers, which is no trivial problem — particularly if there is any type of interaction between adjustments. Although this adjustment (in one form or another) is necessary in any matched filter, the dimensions of a wavelength are exceptionally short here, which complicates the problem. An electro-optical phase shifter is suggested in Fig. 27 as a suitable means of obtaining the required phase shift, from any one tap point to the output, according to the decoding requirements, and for making the necessary adjustments. Any of several electro-optical schemes is feasible; for example, a dielectric may be used whose incremental dielectric constant is proportional to a static electric bias field.

d. Multiple Reflection Delay Line

The fiber optic type of delay line mentioned above is ideal for compact storage of a pulse many kilometers long. If the laser pulse to be compressed is already fairly short, however, multiple reflection from parallel mirrors becomes a suitable delay mechanism. For example, the pulse duration of the giant pulse laser is on the order of 10^{-8} sec, which requires a storage length of only 3 m. The techniques of grinding and aligning parallel surfaces in the optical region are well known from similar work with Fabry-Perot interferometers. One particular method of using this technique is shown in Fig. 28. The receiver laser pulse, assumed to be 5×10^{-9} sec and phase-modulated with a Barker 5 code, is formed into a narrow collimated beam and bounced back and forth between the two coaxial cylindrical mirrors. The outer mirror is highly reflecting,

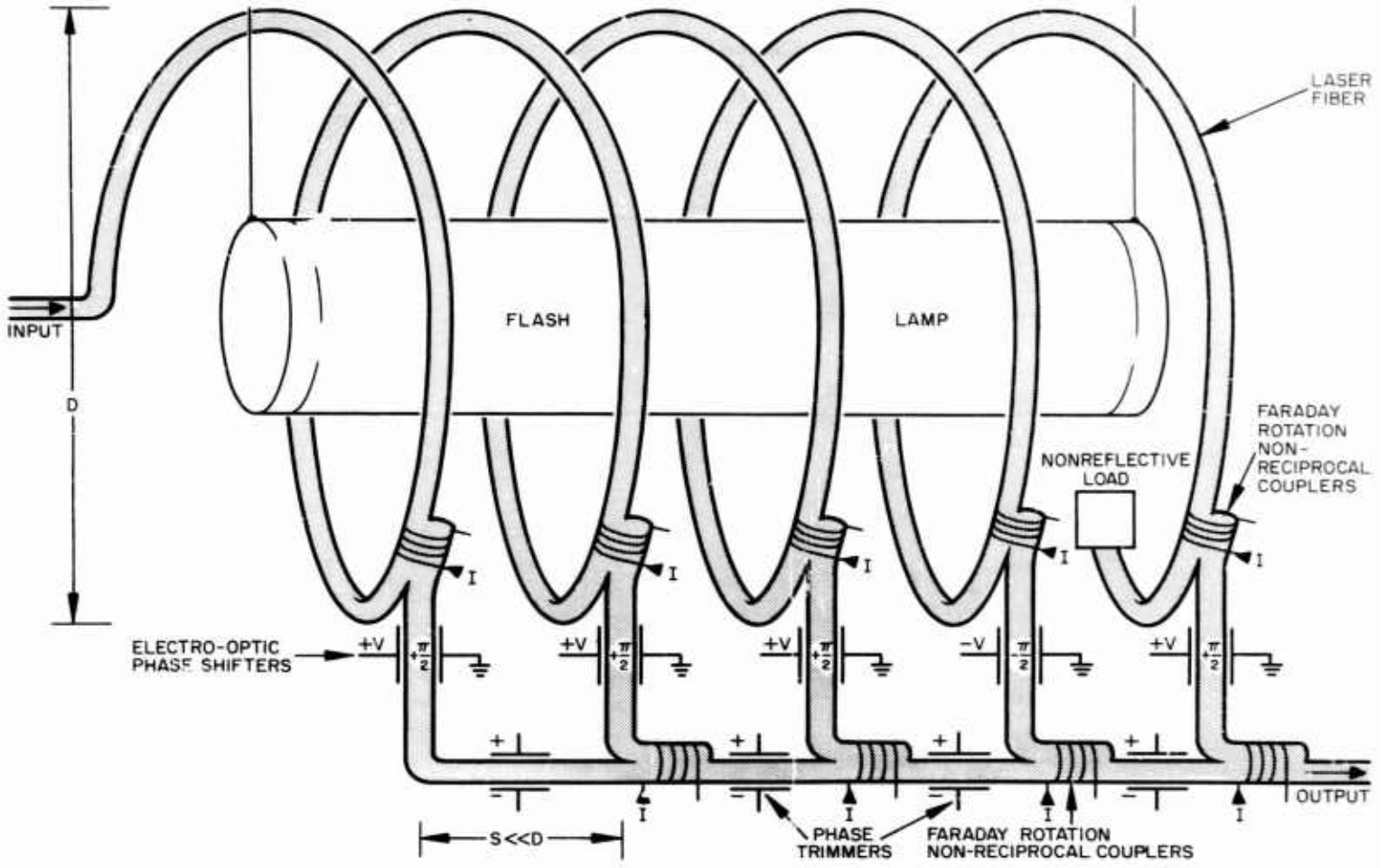

Fig. 27. Active Optical Delay Line Decoder.

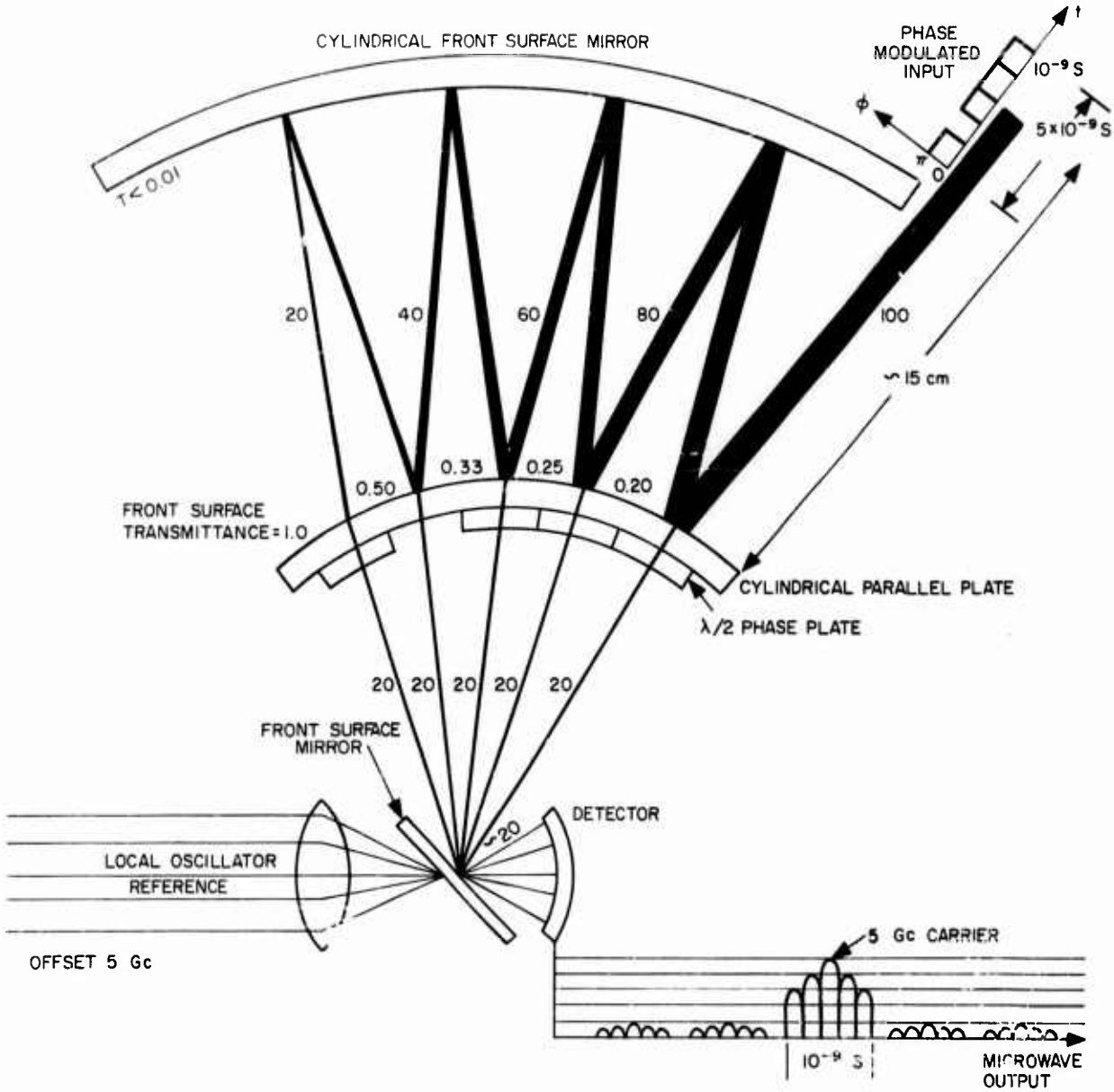

Fig. 28. Multiple Reflection Optical Delay Correlator (Barker 5 Phase Coder).

and the inner mirror has a varying transmittance which taps off a sample of each pulse. The other side of the inner cylinder contains thin film dielectric phase shifters laid in the inverse Barker 5 code. The five sampled outputs are mixed with a phase-stable, offset local oscillation laser at five different points on a detector. Since the local oscillator and the laser pulse are assumed to be phase stable, the microwave difference frequency generated at each point on the detector will also be phase stable. If the detector is much smaller than a microwave wavelength, the electrical outputs from the five detection points will add coherently, giving an output corresponding to the auto-correlation function of the Barker 5 code. This particular configuration has the disadvantage that the signal energy is not concentrated into the compressed pulse, but this is overcome by the conversion gain obtained by the mixing with the local oscillator.

e. Summary

There is no fundamental limitation that would prevent the application of pulse compression techniques to optical radar systems. The necessary data processing can be done either directly at optical frequencies or at microwave frequencies after heterodyning. The need for such complicated techniques is debatable since present giant pulse lasers have a range resolution capability of a few meters. However, it is interesting to note that present optical elements can give azimuth and elevation resolution of centimeters at kilometer distances; this report indicates that range resolution down to a few centimeters is also feasible. With this kind of resolution, three dimensional pictures of nearly photographic quality could be obtained by radar techniques over kilometer ranges.

T. R. O'Meara

Robert L. Forward

B. QUANTUM LIMITATIONS ON OPTICAL RECEIVER SYSTEMS

Because of the large amount of energy packed into each optical photon and the decrease in energy emitted from a thermal source according to the Planck radiation law, thermal sources almost always will contribute a negligible amount of noise to the narrow band laser systems. Although thermal noise is no longer a problem it has been replaced by another type of noise which is quantum mechanical in origin. No matter what devices are considered, or how the calculations are done, it is always present. It appears even when there are no devices at all, just the signal alone. There is no escaping it

since it is inseparable from one of the most powerful and all-inclusive concepts in quantum mechanics — the uncertainty principle.

This new type of noise (which may be called fluctuation noise, statistical noise, quantum noise, photon noise, etc.) is inherent in the signal due to the limitations imposed on the preparation of the photons by quantum mechanics. It is an unusual noise since it causes dropout only and does not create false alarms. In the optical region it is very important and a much greater problem than thermal noise.

1. Signal-to-Noise Ratios of Laser Receiver Systems

In Interim Engineering Report No. 1 an analysis was presented which calculated the signal-to-noise ratios of an optical signal after attenuation in a transmission medium and after amplification by four different laser receiver systems. These systems were a photodetector, a single mode laser amplifier, a single mode optical heterodyne, and a laser preamplifier followed by an optical heterodyne. This work was later included as Appendix C of the ASD Laser Receiver Meeting Summary Report (Ref. 21). The analysis concludes that an amplifier must be used before the signal becomes too weak (when the average number of received photons approaches unity) or information will be irretrievably lost even if there are no sources of external noise. If the system parameters indicate this will happen, a laser amplifier should be used in front of the transmitter (assuming the power handling capabilities are available).

If the number of received signal photons is appreciably larger than unity (or the number of background photons), any of the amplifiers can be used provided they do not degrade the signal too much. The degradation factor for the laser amplifier is related to the inversion; the degradation factor for the optical heterodyne and detector is the quantum efficiency. Analysis shows that they are mathematically equivalent in their effect on the signal-to-noise ratio. The signal degradation calculated for the various situations is summarized below.

a. Effects of Quantum Noise on an Optical Signal

Assume that a narrow-band modulated laser signal comes from some point in space. The signal could be a pulse from a laser in a communications system or a return from a laser illuminated target in a radar system. The problem is to see the burst of light corresponding to that bit and any others that may follow. Because of the quantum nature of light, each burst of laser energy consists of a finite, integral number of photons. If the bursts are very intense, they will have millions of photons and the average signal power can be accurately controlled. However, let us assume that

by the time our bursts have reached the receiver they contain an average of only a few photons. Then the number of photons in the bursts will follow a Poisson distribution which has a statistical variation in the number of photons given by the square root of the average number of photons. The square root of 9 is 3 and of 1 is 1. With these large fluctuations in the number of photons, it is easy to see that quite often a burst designed to indicate a bit will not contain enough photons to qualify. And since our receiver has lost part of the original information, we have a finite signal-to-noise ratio, even though we have not yet introduced any noise into the discussion! If the burst has an average of $\bar{n}$ photons, then the average energy is $\bar{n}h\nu$; if the burst is $2\Delta t = 1/B$ long, then the average signal power is

$$S_s = \bar{n}\, h\nu\, B \quad . \tag{17}$$

Since the fluctuations in the number of signal photons vary as the square root of the average number of photons, the strength of the signal will vary around the mean by about $\bar{n}^{1/2}$. In reality, a Poisson distribution for small numbers of photons not only has a considerable "skew" and higher order moments, but also does not assume negative values. To properly discuss the effect of the fluctuations on the information contained in the signal would require considerable time. Therefore, for a first estimate we will assume that the rms value of the fluctuations in the number of photons can be interpreted as a source of "noise," with the average noise power given by

$$N_s = \left(\overline{\delta n^2}\right)^{1/2} h\nu\, B = \bar{n}^{1/2}\, h\nu\, B \quad . \tag{18}$$

That is, the signal-to-noise ratio is

$$\left.\frac{S}{N}\right|_s \approx \bar{n}^{1/2} \quad . \tag{19}$$

As the number of photons in the signal increases, the fluctuation noise increases. But since it varies with the square root, the signal-to-noise ratio increases with the number of photons in the signal. Thus, for a large number of photons this fluctuation noise is no longer a problem. The important factor is that the signal-to-noise ratio decreases considerably when the number of photons per burst, pulse, or bit approaches unity.

b. Effect of Transmission Loss on an Optical Signal

Even assuming it would be possible to guarantee that a given number of photons will be transmitted per pulse, if a transmission loss exists between the source of the photons and the receiver, it is found that because the loss mechanism is quantum mechanical in nature and picks the photons off the signal in a random fashion, only a moderate amount of attenuation is necessary to give a Poisson distribution for the number of photons per pulse. This result applies not only to the case where photons are lost to an attenuating medium but also to the case of $1/r^2$ loss in free space where the photons are lost out of the receiver's acceptance cone.

Assume a transmission of an average of $\bar{n}_T$ photons with a variance of δn_T^2. After an attenuation of $L < 1$, the average number of photons received and its variance is given by (Ref. 22)

$$\bar{n}_R = L\bar{n}_T \tag{20}$$

$$\overline{\delta n_R^2} = L(1 - L)\bar{n}_T + L^2\overline{\delta n_T^2} \tag{21}$$

$$\approx L\bar{n}_T = \bar{n}_R \qquad L \ll 1 \ .$$

Thus, despite the nature of the distribution of the transmitted photons, the received photons have a Poisson distribution after attenuation, and the signal-to-noise ratio of the received signal is simply

$$\left.\frac{S}{N}\right|_R = \bar{n}_R^{1/2} \ . \tag{22}$$

This result reveals an important difference between signal-to-noise calculations in the microwave region and in the optical region. In the microwave region a cold (0°K) attenuator affects signal and noise in the same way so that the signal-to-noise ratio at the output of the cold attenuator is the same as that at the input. In the optical region, however, a cold attenuator causes an increase in the relative fluctuation of the signal, and information is irretrievably lost, so that the signal-to-noise ratio at the output of a cold optical attenuator is less than that at the input.

c. Analysis of a Photodetector

The properties of a photodetector are well known. A good photodetector will have negligible dark current and if a good optical system is used to cut down sky background, then its only limitation is its quantum efficiency. The photomultiplier process introduces some noise due to the fluctuations in the amplification, but this is usually less than 15% of the fluctuation noise.

If the received signal at the input to the photodetector is represented by an average of $\bar{n}_R$ received photons, then the signal-to-noise ratio can be shown to be

$$\left.\frac{S}{N}\right|_D = (\epsilon \bar{n}_R)^{1/2} = \epsilon^{1/2} \left.\frac{S}{N}\right|_R . \tag{23}$$

We find that the signal-to-noise ratio at the input of the receiver has been degraded by the square root of the quantum efficiency of the photocathode.

d. Analysis of a Laser Preamplifier

The properties of a laser amplifier have received a considerable amount of study. The work of Shimoda, Takahasi, and Townes (Ref. 23) was used as a reference. The signal-to-noise power ratio at the output of a single mode high gain laser preamplifier and a Poisson distribution of received photons is given by

$$\left.\frac{S}{N}\right|_L = \frac{\bar{n}_R}{\left[2Kn_R + K^2\right]^{1/2}} \tag{24}$$

where $K = n_2/n_1 - n_1$ depends upon the population inversion of the laser. In the limit where the number of received photons is larger than the number of spontaneous photons ($n_R >> K$), the fluctuations of the signal are much larger than the fluctuations of the spontaneous emission and we have

$$\left.\frac{S}{N}\right|_L = \left[\frac{\bar{n}_R}{2K}\right]^{1/2} . \tag{25}$$

Thus even a high gain laser needs good inversion or it will degrade the signal-to-noise ratio.

e. Analysis of an Optical Heterodyne

An optical heterodyne was analyzed using the terminology of Oliver (Ref. 24) and Gordon (Ref. 25), but with a different concept of noise. The signal-to-noise power ratio at the output of a single mode optical heterodyne can be shown to be:

$$\left.\frac{S}{N}\right|_H = \frac{\epsilon\bar{n}_R}{\left[2\epsilon\bar{n}_R + 1\right]^{1/2}} = \frac{\bar{n}_R}{\left[2\frac{\bar{n}_R}{\epsilon} + \frac{1}{\epsilon^2}\right]^{1/2}} \tag{26}$$

which is completely analogous to the case of the laser for high gain. In the limit where the number of received photons is large we have

$$\left.\frac{S}{N}\right|_H = \left[\frac{\epsilon\bar{n}_R}{2}\right]^{1/2} . \tag{27}$$

f. Analysis of a Laser Preamplifier Followed by an Optical Heterodyne

An analysis was then made of a system which uses a laser preamplifier in front of an optical heterodyne in an attempt to make up for the poor quantum efficiency of the heterodyne mixer. In this case it was found that the signal-to-noise ratio at the output is given by

$$\left.\frac{S}{N}\right|_{LH} = \frac{\bar{n}_R}{\left[\left(2K + K^2\right) + \frac{1}{G}\left(\frac{2}{\epsilon} - 1\right)\bar{n}_R + \frac{1}{G^2\epsilon^2}\right]^{1/2}} . \tag{28}$$

In the limit of high laser gain this reduces to the signal-to-noise ratio at the output of the laser, independent of the quantum efficiency ϵ of the photomixer

$$\left.\frac{S}{N}\right|_{LH} = \frac{\bar{n}_R}{\left(2K\bar{n}_R + K^2\right)^{1/2}} \approx \left(\frac{\bar{n}_R}{2K}\right)^{1/2} = \left.\frac{S}{N}\right|_L . \tag{29}$$

Thus a laser preamplifier with good inversion can be profitably used before an optical heterodyne with a relatively poor quantum efficiency in the photocathode.

R. L. Forward

2. Position Prediction Accuracy of Doppler Radar

The problem of frequency determination for a weak signal is intimately connected with the general problem of minimum noise limitations in quantum mechanical communications systems. However, the information required from the signal in a Doppler radar is much less than that required from a general communications system. We can thus forgo the usual analysis and focus attention on a simple model. Although practical systems will have a different construction and operation, this model will provide a simple theoretical basis for the calculation of the minimum amount of information required by the receiver. For this analysis, we use the simple model shown in Fig. 29.

The essential unit of this model is the detector which consists of many narrow band absorption stages. Each stage absorbs photons above a certain energy, and they are arranged as shown in Fig. 30. The photons will travel through the detector until they reach the stage with a small enough gap to absorb them. The stage will absorb all the photons and subsequently fluoresce or otherwise announce the arrival. However, there is a limit to the precision with which the arrival time of a photon at a given stage may be specified

$$\Delta t = \frac{1}{\Delta\omega} \quad . \tag{30}$$

We have assumed that Δt is much larger than the length of the transmitted pulse T. Since we are trying to measure the Doppler shift to an accuracy of $\Delta\nu$ with a single, indivisible amount of energy, then any conceivable fit that will obtain this accuracy of frequency measurement will also smear out the short transmitted pulse over the time Δt. (For typical system values, $T \approx 10^{-8}$ sec, $\Delta\omega \approx 10^{6}$ rad/sec, $\Delta t \approx 10^{-6}$ sec.) If there are N photons in a pulse, and all have the same energy and arrival time, we can fit the output of the absorbing stage to a Poisson distribution to determine the actual arrival time to within

$$\Delta t = \frac{1}{(\Delta\omega)\sqrt{N}} \quad . \tag{31}$$

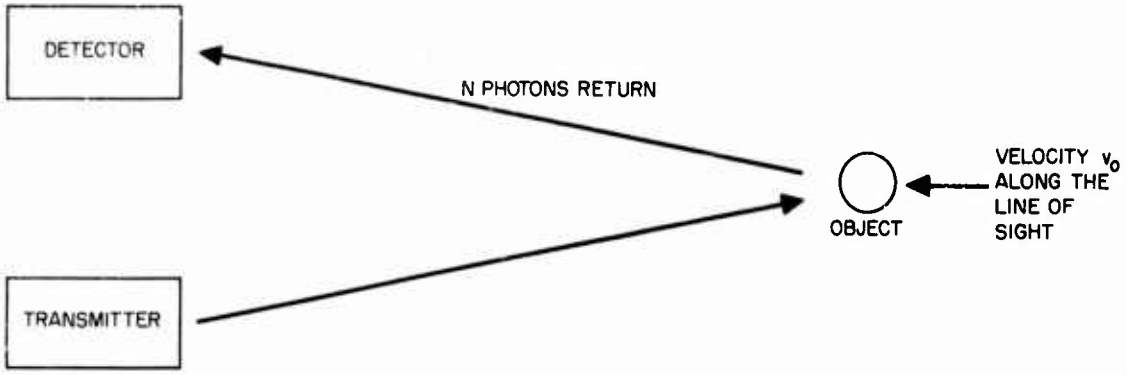

Fig. 29. System Model Assumed for Theoretical Analysis.

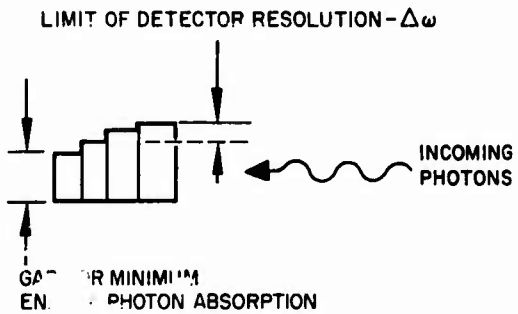

Fig. 30. Detector Model Assumed for Theoretical Analysis.

Thus, if we have enough incoming photons, we can measure range and range rate to any desired accuracy, but if we are dealing with a small number of photons, the measurement of range and range rate are not independent. These and the following results should apply to more sophisticated receiver systems which have amplification prior to range and range rate measurement because the available information content of the received pulse is determined by the number of received photons, not the number of amplified photons. However, this point needs quantitative verification.

For a given pulse we can measure the velocity to

$$\Delta v = \left(\frac{\Delta\omega}{\omega_o}\right) c \tag{32}$$

where c = velocity of light and the uncertainty in the position at which this velocity was measured to

$$\Delta x_o = v_o \Delta t \ . \tag{33}$$

Since a Doppler radar is usually used to obtain information for the prediction of the future position of the target, we will assume that the uncertainty in the future position is the quantity of interest. After a time τ (which could be the repetition rate of the radar) the rms uncertainty in position will be

$$U = \left[(\Delta x_o)^2 + \tau^2 (\Delta v)^2\right]^{1/2} . \tag{34}$$

The number of photons per pulse is distributed about some mean $\overline{N}$ with probability $P(N)$, and there is a nonzero probability that no photons will arrive in a given pulse period τ. In this unfortunate case the position is only known from the previous measurement, and after two pulse periods has evolved to

$$U^1 = \left[(\Delta x_o)^2 + 4\tau^2 (\Delta v)^2\right]^{1/2} . \tag{35}$$

There is also a nonzero probability $P^2(0)$ that two consecutive pulses will have no photons, and so on. The probability that a pulse will contain photons is $1 - P(0)$. Hence, the actual uncertainty is

$$U = \left\{ \tau^2 (\Delta v)^2 \left[1 - P(0) + \sum_{n=2}^{\infty} n^2 P^{n-1}(0) \right] + (\Delta x_o) \right\}^{1/2} . \quad (36)$$

The summation term in this expression gives the uncertainty caused by skipping n - 1 consecutive pulses as n goes from 2 to ∞. We now substitute

$$(\Delta x_o)^2 = v_o^2 (\Delta t)^2 = \frac{v_o^2}{(\Delta \omega)^2} \sum_{n=1}^{\infty} \frac{P(n)}{n} \quad (37)$$

and express Δv in terms of $\Delta \omega$ to get

$$U = \left\{ \tau^2 \left(\frac{\Delta \omega}{\omega_o} \right)^2 c^2 \left[1 - P(0) + \sum_{n=2}^{\infty} n^2 P^{n-1}(0) \right] + \frac{v_o^2}{(\Delta \omega)^2} \sum_{n=1}^{\infty} \frac{P(n)}{n} \right\}^{1/2} \quad (38)$$

Let

$$A = 1 - P(0) + \sum_{n=2}^{\infty} n^2 P^{n-1}(0) \quad (39)$$

and

$$B = \sum_{n=1}^{\infty} \frac{P(n)}{n} = \left(\frac{\bar{I}}{N} \right) . \quad (40)$$

Then we can minimize U with respect to $(\Delta \omega)^2$. The minimum of U will occur at

$$(\Delta \omega)^2 = \frac{v_o \omega_o}{\tau c} \sqrt{\frac{B}{A}} \quad (41)$$

or

$$(\Delta t)^2 = \frac{\tau c}{v_o \omega_o} \sqrt{AB} \quad (42)$$

and the corresponding minimum in position uncertainty is

$$U_{min} = \sqrt{\frac{2v_o \tau_c}{\omega_o} \sqrt{AB}} \quad . \tag{43}$$

For a Poisson distribution

$$P(N) = \frac{(\overline{N})^N e^{-\overline{N}}}{N!} \tag{44}$$

and

$$P(0) = e^{-\overline{N}} \quad . \tag{45}$$

As long as $\overline{N}$ is not much less than one, A will be of order unity. B will always be no larger than order unity. In an ideal situation, where the average number of received photons $\overline{N}$ is greater than four and where the fluctuations are due only to the statistics of the photons and not to the fluctuations of the target return, we can replace A by unity and B by $1/\overline{N}$.

$$(\Delta\omega)^2 = \frac{v_o \omega_o}{\tau_c \overline{N}^{1/2}} \tag{46}$$

$$(\Delta t)^2 = \frac{\tau_c}{v_o \omega_o \overline{N}^{1/2}} \tag{47}$$

$$U_{min} = \left[\frac{2v_o \tau_c}{\omega_o \overline{N}^{1/2}}\right]^{1/2} = \frac{v_o}{\Delta\omega} \left[\frac{4}{\overline{N}}\right]^{1/4} = v_o \Delta t \left[\frac{4}{\overline{N}}\right]^{1/4} \quad . \tag{48}$$

These equations indicate that in a quantum limited system, there are optimum values for the range and range rate accuracies and the pulse repetition rate. These values are related to the target velocity, the frequency and average number of the received photons, and the desired accuracy of future position prediction. It is obvious that for present-day tactical situations, these considerations are not of practical importance, but in future, spaceborne systems where high accuracy is desired, they will have to be considered.

For instance, if the target velocity is 10 km/sec, the average number of received photons is four and the desired future position accuracy is ± 1/10 m, the optimum value for the accuracy of the Doppler shift measurement is ± 10^5 rad/sec = ± 16 kc/sec.

P. Gottlieb

SECTION 6

CONCLUSIONS AND RECOMMENDATIONS

Solid state ruby amplifiers have a good inversion ratio, reasonably high gain, and the spontaneous emission power output predicted by theory. The present ruby lasers amplify over a wide frequency range, have a fairly wide acceptance angle, and are capable of pulsed operation only. The theory indicates that they should make good preamplifiers for a laser receiver system provided the preamplifier characteristics in angle, frequency, and time are matched to the expected signal characteristics. It is recommended that further work be done in developing frequency and spatial filtering techniques.

Gas laser amplifiers have very high gains in the infrared, are magnetically tunable, and have comparatively narrow frequency bandwidths. Experimental results indicate that a gas laser amplifier improves the signal-to-noise ratio of a receiver system if used before a detector. It is recommended that quantitative measurements of the noise, gain bandwidth, and inversion characteristics of high gain tunable gas lasers be made.

The traveling-wave phototube is the better detector for wavelengths less than 7000 Å because of its greater bandwidth, the photodiode is better for wavelengths greater than 1.1 μ because of its quantum efficiency. It is recommended that research and development on fast photovoltaic and photoconductive detectors packaged in wideband microwave circuits be supported.

Optical synthetic aperture techniques do not appear feasible in the atmosphere or in space at long ranges with high closing rates. They are marginally feasible in space at short ranges and low velocities.

No fundamental limitation was found that would prevent the application of pulse compression techniques to optical radar systems. Phase or polarization coded systems are preferable to chirp techniques because of the present capabilities of laser modulators and demodulators. It is recommended that further theoretical and experimental work be done on the feasibility of applying coherent processing concepts to the optical region.

The laser preamplifier and the optical heterodyne receiver— the two methods of coherent detection— have the same fundamental limitations on their noise performance. They both have internally generated noise, signal degradation factors, and require good optical systems to limit their operation to a minimum number of spatial modes.

The measurements of range and range rate in an optical Doppler radar system are not independent because of quantum mechanical limitations. There are optimum values for the range and range rate accuracies and the pulse repetition rate that are related to the target velocity, the frequency and average number of received photons, and the desired accuracy of future position prediction. Further refinements in this area, although of great theoretical importance, probably would not be of practical significance.

REFERENCES

1. I. J. D'Haenens, Appendix to Interim Engineering Report No. 2 (CONFIDENTIAL) "Receivers for Laser Radars (U)" Contract AF 33(657)-8769 (14 May 1963).

2. I. J. D'Haenens, in "Summary of ASD Meeting on Receiver Technology for Detecting Signals Produced by Lasers (U)" ASD-TDR-63-721 (CONFIDENTIAL), R. L. Forward, Ed. (25 September 1963), pp. 5-11.

3. R. A. Paananen and D. L. Bobroff, Appl. Phys. Letters 2, 99-100 (1963).

4. W. B. Bridges, Appendix to Interim Engineering Report No. 3, "Receivers for Laser Radars," Contract AF 33(657)-8769 (14 August 1963).

5. W. B. Bridges, Appl. Phys. Letters 3, 45-46 (1963).

6. E. I. Gordon, private communication.

7. C. E. Moore, Atomic Energy Levels (U. S. Government Printing Office, Washington, D. C., 1949), Vol. 1.

8. H. E. White, Introduction to Atomic Spectra (McGraw-Hill, New York, 1934).

9. F. A. Jenkins and H. E. White, Fundamentals of Physical Optics (McGraw-Hill, New York, 1937).

10. T. Bridges, private communication.

11. R. Buser, J. Kainz, and J. Sullivan, Appl. Opt. 2, 861-862 (L) (1963).

12. R. H. [illegible]ke, Phys. Rev. 93, 99-110 (1954).

13. D. E. Sawyer, Proc. IEEE 51, 1238 (1963).

14. C. W. Sherwin, J. P. Ruina, and R. D. Rawcliffe, IRE Trans. MIL-6, 111-119 (April 1962).

15. L. J. Cutrona and G. O. Hall, IRE Trans. MIL-6, 119-121 (April 1962).

16. R. C. Heimiller, IRE Trans. MIL-6, 122-129 (April 1962).

17. C. J. Peters, Proc. IEEE 51, 147-153 (1963).

18. G. L. Turin, Trans. IRE IT-6, 311-329 (June 1960).

19. G. C. Young, Appl. Phys. Letters 2, 151 (1963).

20. C. J. Koester, Proc. 1963 Pacific Computer Conference (IEEE) CIT, Pasadena, California, March 15-16, 1963, pp. 54-62.

21. R. L. Forward, in "Summary of ASD Meeting on Receiver Technology for Detecting Signals Produced by Lasers (U)," ASD-TDR-63-721 (CONFIDENTIAL), R. L. Forward, Ed., (25 September 1963), pp. 47-67.

22. H. A. Haus and J. A. Mullen, NEREM Record, 90-91 (6 November 1962).

23. K. Shimoda, H. Takahasi, and C. H. Townes, J. Phys. Soc. Japan 12, 686-700 (1957).

24. B. M. Oliver, Proc. IRE 49, 1960-1961(L) (1961); H. A. Haus and C. H. Townes, Proc. IRE 50, 1544-1545 (L) (1962); B. M. Oliver, Proc. IRE 50, 1545-1546 (L) (1962).

25. J. P. Gordon, Proc. IRE 50, 1898-1908 (1962).

APPENDIX I

OPTICAL DETECTOR TECHNOLOGY

1. INTRODUCTION

The function of the photodetector is to provide an electrical output signal related to the intensity of the incident light signal. In this context the word "light" is used to denote electromagnetic radiation in the visible and the near-infrared range of the spectrum. For the purposes of the contemplated application, the wavelength limits may be set at 0.4 and 4 μ. Over this spectral range several physical mechanisms and devices are available for detection; the utility of any one device is confined to a part of this range. It is therefore necessary to discuss a variety of devices.

The general properties of photodetectors are discussed, their common basic characteristics identified, and the parameters which are descriptive of their capabilities as detectors or demodulators of light are defined. Specific detectors will then be discussed in detail.

It is assumed that information is conveyed by an amplitude modulated light beam. The function of the detector is to retrieve the modulating signal. It must therefore act as an integrating device; the period of integration must be long compared with one cycle of the carrier, and short compared to the period of the highest component of the modulating signal. In principle any body which absorbs the incident radiation and which changes some of its physical properties as a result of absorption may act as a detector, but vast practical differences exist among the variety of materials and configurations which may be employed as detectors.

In the infrared region considerable use has been made of thermal detectors. These detectors convert the incident radiation into heat and then the change in temperature of the detecting element is measured. The merit of such detectors is that they permit an absolute determination of the incident energy; their response is within wide limits independent of the wavelength of the radiation. Other radiation detecting devices are usually calibrated by means of thermal detectors. On the other hand, the integration time of thermal detectors is long; they could only be employed for the demodulation of signals modulated at an impractically slow rate. Because of their slow response and their low sensitivity, thermal detectors will not be considered.

The other group of radiation detectors is based on the photoelectric effect which implies the conversion of the energy of the incident radiation into energy of electrons contained in the detecting element without communicating this energy to the entire material. Photoelectric detectors are quantum detectors because the processes which take place in them preserve the quantum character of the radiation and absorption process. The basic law of every photoelectric effect is that the absorption of energy from the radiation field proceeds in quanta of size $h\nu$, where h is Planck's constant and ν the frequency of the radiation. Moreover, each quantum of energy absorbed from the radiation field is imparted to a single electron.

In the visible part of the spectrum one quantum is generally sufficient to impart enough energy to an electron enabling it to leave a suitable solid. In other words, an external photoelectric effect may take place. The emitted electrons may be collected directly; the current collected is proportional to the intensity of the incident radiation. In the infrared region the energy absorbed from the radiation field is generally insufficient to free the electron entirely, but it may be sufficient to impart to the electron such freedom of motion that it can then be detected by sensing the conductivity of a suitable solid or by sensing the potential difference developed between different points in the solid. Detectors of this type are said to be based on the internal photoelectric effect.

The practice and terminology in the visible and infrared region is somewhat different, but there are common features. In all photoelectric devices operating in their proper range, the voltage or the current output of the device is proportional to the intensity of the input signal. The power output of a photoelectric device operating into a proper load is then proportional to the square of the input radiation intensity. Because of this square law property, photoelectric devices are capable not only of demodulation but of mixing functions as well. However, it must be kept in mind that the output of a photoelectric detector is subject to frequency limitations and that in the case of an extended photodetector the output will be averaged over the variable illumination of the photosurface. Therefore, if two light beams of constant intensity and frequencies ν_1 and ν_2 should be incident on the photodetector, the difference frequency $|\nu_1 - \nu_2|$ will be detected only if the integration time of the photodetector is short compared with $|\nu_1 - \nu_2|^{-1}$ and if the phases of the incident beams do not vary in such an irregular manner over the photosurface that a cancellation of the difference signal will take place upon averaging over the entire surface.

It has already been stated that for light of a fixed wavelength (frequency) the ratio of output voltage (current) to input intensity is a constant. This ratio is called the "responsivity" (R); as a function of

wavelength it usually has one maximum. To characterize the spectral variation of the response of a detector, it is customary to provide graphs showing the relative responsivity, i.e., the responsivity for wavelength λ divided by the peak responsivity. The relative response curves are identical for detectors which utilize the identical physical processes and materials, while the peak responsivity may depend on technical characteristics of the instrument as well. When the responsivity R of an instrument is given without qualification in the visible region, it is understood that this is the value obtainable for the wavelength at which its response is the greatest. Responsivity is expressed in volts per watt or amperes per watt.

There are random fluctuations in every photodetector which cause the output signal to fluctuate even in the presence of a constant input signal. These fluctuations constitute the noise generated by the detector. This internal noise limits the capability of the detector for the detection of low-level signals. When the noise output is analyzed according to frequency, it is found that for frequencies that are low compared with the optical ones the noise power output of a detector is proportional to the bandwidth. The noise of the photodetector is characterized by the noise equivalent power (NEP) for one cycle bandwidth. This is the input signal which produces the same output voltage as is present in a one cycle bandwidth due to noise alone.

The NEP is a function of the wavelength of the signal. In the visible range when a figure of NEP is quoted without further specification, it refers to the wavelength for which the responsivity is maximum; in the infrared range it refers to the 500°K black body source. In the former case the NEP can then be computed for another wavelength by means of the relative sensitivity curves according to the equation

$$\text{NEP}(\lambda)\, R(\lambda) = \text{NEP (peak)}\, R\ \text{(peak)} \ . \qquad \text{(I-1)}$$

Similar conversion may be made in the infrared for a source of a different temperature or for a monochromatic source. The noise power output of the detector which is proportional to the bandwidth is also proportional to the square of the noise output voltage. The NEP is proportional to the square root of the bandwidth; its proper unit is $W\text{-}sec^{-1/2}$, although frequently the $sec^{-1/2}$ is omitted.

A commonly used figure of merit of a photodetector is the reciprocal of NEP, called "detectivity" D. For most photodetectors the NEP is proportional to the square root of the area; therefore the quantity.

$$D^* = \frac{A^{1/2}}{\text{NEP}} \qquad \text{(I-2)}$$

is a better measure of the detectivity because it is independent of the size of the detector. Modern publications use D*, whose unit is $cm\text{-}sec^{-1/2}/W$.

The physical processes in every detector have a finite lifetime. Together they impose a limitation on the speed with which the output of the detector can be altered by altering its input. Each detector is characterized by a response time τ whose reciprocal is the highest angular frequency of modulation or variation the detector can follow accurately. This is essentially the integration time of the detector. When the modulation frequency is varied, the responsivity varies according to the formula (Ref. I-1)

$$R(f) = \frac{R_o}{(1 + 4\pi^2 f^2 \tau^2)^{1/2}} \qquad \text{(I-3)}$$

where f is the modulation frequency. When $2\pi f = \tau^{-1}$ the responsivity is down to $R_o/\sqrt{2}$, where R_o is its value for low modulation frequencies.

The figures of merit R, D, D*, and τ are not absolute constants of the material or the physical process. They may depend on the environmental conditions and on the average signal level. For example, the detectivity depends on the temperature of the detector and also on the average output current of the detector. The dependence of the figures of merit on these conditions is different for each kind of photodetector.

The role of the different figures of merit may be summarized as follows: the responsivity curves determine the usefulness of a detector as a function of the propagating field (carrier) wavelength. The peak responsivity determines the output voltage or current level of the instrument. The NEP or detectivity determines the least detectable signal, and the response time τ the highest modulation frequency.

2. PHOTOMULTIPLIERS

In the visible and near-infrared region of the spectrum the photomultiplier is the most efficient and convenient detector of radiation. It is based on the external photoelectric effect and the subsequent amplification of the electron current by means of a number of secondary emitting stages termed "dynodes." The amplification is simply a matter of convenience: it increases the responsivity of the instrument, but it does not increase its ability to detect weak signals. The basic and determining process in the photomultiplier is the external photoelectric effect, which consists of two steps: absorption of light by a solid and emission

of an electron. Light may be absorbed without an electron being emitted; this occurs every time an electron-hole pair is created by absorption of light in a semiconductor.

According to the basic law of the photoelectric effect already mentioned, the emission of each electron is caused by the absorption of a single photon. Electron emission will take place only when the photon possesses sufficient energy to overcome the work function of the solid, i.e., when

$$h\nu \geq e\Phi \tag{I-4}$$

where e is the electronic charge and Φ is the work function. This relation sets a long wavelength limit for every photoemissive detector; it may be put in the form

$$\lambda_L = \frac{12,400}{e\Phi} \tag{I-5}$$

where λ_L is the wavelength limit in angstroms and $e\Phi$ is the work function of the photocathode in electron volts.

The element with the lowest work function is cesium. For this element $e\Phi = 1.9$ eV; therefore, the wavelength limit of a cesium photocathode is about 6500 Å. Composite photocathodes consisting of combinations of metals and oxides have lower work functions; they are capable of functioning up to about $\lambda = 1.2\ \mu$. Naturally, as the limit is approached the efficiency of the detector decreases. The variation of detector efficiency with wavelength is apparent from the responsivity curves or the curves of quantum efficiency, which in the case of photoemissive detectors are simply related to the responsivity curves.

Quantum efficiency η is the number of emitted electrons divided by the number of incident photons. The frequency ν, quantum efficiency incident power P, and the photoelectric current i are related as ows: The number of incident quanta per second is $n = P/h\nu$, the tron current emitted from the photosurface is ηne; therefore

$$i = \eta e\, P/h\nu\ . \tag{I-6}$$

Responsivity $R(\nu)$ is proportional to i/P; therefore

$$R(\nu) = \frac{Ke\eta(\nu)}{h\nu} \tag{I-7}$$

where K is a suitable constant which depends on the amplification of the photomultiplier. For the purposes of this study the quantum efficiency is a more convenient variable than the responsivity. The quantum efficiencies of the red-sensitive photocathodes are shown in Fig. 31.

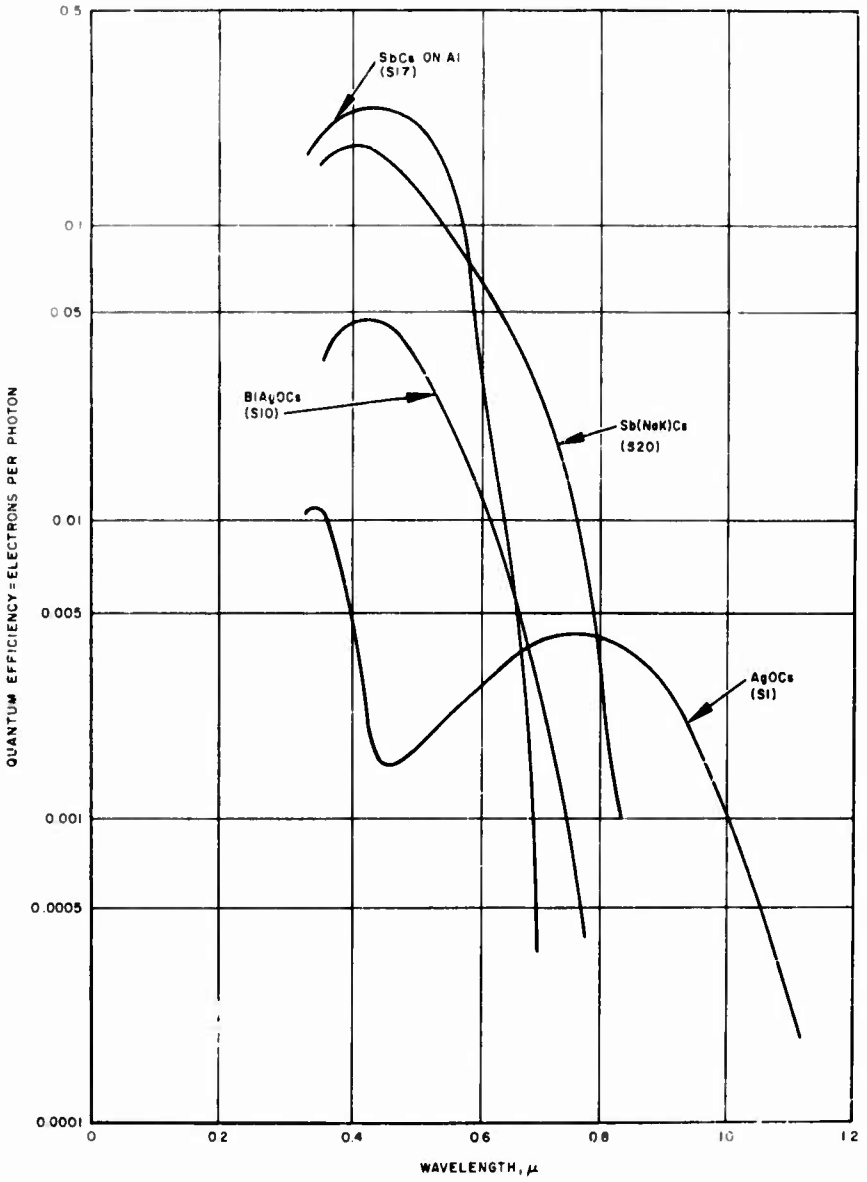

Fig. 31. Spectral Response of Various Photocathodes.

The following four wavelengths are particularly important in laser technology: 6328 Å, 6943 Å, 1.06 μ, and 1.13 μ. These are the wavelengths of neon, ruby, neodymium, and neon lasers, respectively. Table 3 contains quantum efficiencies and relative responsivities of the photosurfaces S-1, -10, -17, and -20 at these important frequencies. Clearly only the S-1 surface is suitable for 1.06 and 1.13 μ radiation, and the S-17 surface is inferior to the others at the two shorter wavelengths.

A number of photomultiplier tubes are available with these surfaces. The responsivity and the noise equivalent input of the photomultipliers are usually given in microamperes per lumen* and in lumen (Ref. I-2). A test lamp of color temperature 2870°K is employed in place of a monochromatic source to determine responsivity and NEP. The data found in the literature may be converted so that responsivity is expressed in microamperes per watt input and NEP in watt input where the input radiation is that of the peak response. The conversion is accomplished by making use of Engstrom's conversion factors k which take into account the entire spectral response of the photodetectors (Ref. I-3). These factors are listed in Table 4. The data in Table 5 are found in Ref. I-2 concerning photomultipliers with S-1, S-10, and S-20 spectral responses.

For tubes of S-10 and S-20 spectral response the figures of Table 5 may be converted to noise equivalent power at the peak of the response by means of Engstrom's factors. Then the noise equivalent power for the relevant radiation may be obtained by making use of the data of Table 3. In this manner the values of NEP were calculated and are given in Table 6.

In the course of defining noise equivalent power it has been assumed that the noise originates in an unilluminated photodetector; in short, the dark current noise has been dealt with. Consider now a detector which is already illuminated and ask what noise will interfere with the detection of an incremental signal. In addition to the noise due to the dark current, there will be noise attributable to the random fluctuations of the existing photocurrent. These fluctuations are the consequence of the atomic nature of electricity; the photocurrent consists of the flow of an integral number of electrons. The rms value of the shot noise current is given by the formula

$$i_s = \sqrt{2eI\Delta f} \qquad (I\text{-}8)$$

where e is the electronic charge (1.60×10^{-19}C), I is the total current in the photodetector, and Δf is the output bandwidth (Ref. I-4).

*1 lm = 1.496×10^{-3} W.

TABLE 3

QUANTUM EFFICIENCIES AND RESPONSIVITIES OF
RED-SENSITIVE PHOTOSURFACES

	6328 Å		6934 Å		1.06 μ		1.13 μ	
Photo-surface	Quantum Efficiency	Respon-sivity	Quantum Efficiency	Respon-sivity	Quantum Efficiency	Respon-sivity	Quantum Efficiency	Respon-sivity
S-1	0.0033	0.56	0.0040	0.80	0.0009	0.29	0.00016	0.03
S-10	0.0070	0.30	0.0028	0.10	0	0	0	0
S-17	0.0080	0.08	0.0004	0.017	0	0	0	0
S-20	0.045	0.41	0.028	0.22	0	0	0	0

TABLE 4

WAVELENGTHS OF PEAK RESPONSE
AND ENGSTROM'S FACTORS

Photosurface	Wavelength of Peak Response	Engstrom's Factor
S-1	8000	93.9
S-10	4500	508.0
S-20	4200	428.0

TABLE 5

NOISE IN PHOTOMULTIPLIER TUBES

Tube	Spectral Response	Noise Equivalent Illumination	Temperature, ^{o}C
6217	S-10	4.0×10^{-11} lm	25
7162	S-1	1.7×10^{-12} W	25
7265	S-20	7.5×10^{-13} lm	25
7265	S-2.	1.0×10^{-13} lm	-80
7326	S-20	1.9×10^{-12} lm	25
7326	S-20	3.0×10^{-13} lm	-80

TABLE 6

NEP IN ONE-CYCLE BAND AT 6328 Å AND 6943 Å
FOR SEVERAL PHOTOMULTIPLIERS

Tube	NEP, W-sec$^{-1/2}$		Temperature, °C
	6328 Å	6943 Å	
7102	3.0×10^{-12}	2.1×10^{-12}	25
6217	2.6×10^{-13}	7.9×10^{-13}	25
7265	4.3×10^{-15}	8.0×10^{-15}	25
7265	5.6×10^{-16}	$10.[illegible] \times 10^{-16}$	-80
7326	1.07×10^{-14}	2.0×10^{-14}	25
7326	1.6×10^{-15}	3.2×10^{-15}	-80
For $\lambda = 1.06\ \mu$ the NEP of the 7102 tube is 5.9×10^{-12} W-sec$^{-1/2}$. For $\lambda = 1.13\ \mu$ it is 5.7×10^{-11} W-sec$^{-1/2}$.			

The shot current is independent of the nature of the photodetector. It becomes significant when the photodetector is used to detect a small variable illumination in the presence of a constant one (background). Let this constant illumination be $P_.$. The corresponding photocurrent I is calculated by means of I-6. Therefore,

$$i_{sh} = \left(\frac{2e^2 \eta P_{\Delta} f}{h\nu} \right)^{1/2} \quad . \tag{I-9}$$

The shot noise equivalent input signal P_{sh} is calculated by making use of (I-6) again

$$P_{sh} = \left(\frac{2Ph\nu\Delta f}{\eta} \right)^{1/2} \quad . \tag{I-10}$$

Attention is called to the role of the quantum efficiency η. It does not enter into the calculation of the NEP which pertains to the dark current noise, but it does affect the value of the shot noise.

The absolute responsivity of a photomultiplier depends on the voltages applied to its dynodes. The manufacturers usually state the responsivity under specified conditions in microamperes per lumen, the source of irradiation being a black body at 2870°K temperature. To convert this responsivity into microamperes per watt illumination for a monochromatic radiation it is necessary to divide by Engstrom's k multiplied by the relative responsivity at the wavelength of the monochromatic radiation. The absolute responsivity is of no importance in the detecting capability of the photomultiplier; however, it does influence the design of the amplifier which follows the photomultiplier. The calculation of the signal-to-noise ratio is based on the NEP of Table 6 plus the shot noise calculated from (I-10) plus other noise that may be entering the detector with the signal, including the noise due to signal fluctuations.

The response times of ordinary photomultipliers are between 1 and 3 nsec. From (I-3) it is found that the responsivity is fairly uniform until the frequency $f = 1/2\pi\tau$ is reached. Thus the performance of the commercial photomultipliers begins to be degraded between 50 and 150 Mc modulation frequency. Actually, Herriott (Ref. I-5) obtained beat notes up to 300 Mc in modulation frequency using an ordinary 7102 multiplier phototube to mix modes of the 1.153-μ neon line. Special tubes are required for the detection or demodulation of signals varying at a faster rate.

3. MICROWAVE PHOTOTUBES

Siegman and McMurtry (Ref. I-6) have shown that a traveling-wave tube may be used as a phototube. They have obtained outputs up to 4200 Mc in modulation frequency when irradiating a Sylvania TW-530 traveling-wave tube with ruby radiation containing several axial modes. Such tubes could also be used to demodulate amplitude-modulated light with modulation frequency extending into the microwave range.

The traveling-wave phototube is an example of a microwave phototube which consists of a photoemissive surface followed by a microwave amplifier. Such a structure is shown schematically in Fig. 32. When amplitude-modulated light strikes the cathode it produces a corresponding amplitude-modulated electron beam. This beam is then accelerated and passed through a microwave tube element such as a traveling-wave amplifier. The latter amplifies the modulation of the electron beam and extracts the modulated signal which then emerges at the output.

Questions of transit time do not arise in connection with the operation of such a tube because the space-charge wave which represents the modulating signal travels down the tube element where the interaction with the microwave field takes place.

The cathode of the TW-530 tube is of the BaO:SrO thermionic type; it is not especially suitable for photoelectric emission for incident ruby light. Consequently, it is not surprising that McMurtry and Siegman obtained quantum efficiencies of only 10^{-5} to 10^{-6} with such a tube. The low quantum efficiency is offset by the 40-dB gain of the traveling-wave tube.

A photomixer image tube was constructed by Lucy (Ref. I-7). This tube contains an S-1 photosurface which is scanned in the manner of a conventional image tube. The emerging electron beam is directed into a traveling-wave amplifier. Detection of 3.4 Gc beats was reported with a quantum efficiency of 3×10^{-6} at 7000 Å.

An X-band microwave phototube was constructed by Petroff and associates (Ref. I-8). This tube had an S-1 photosurface; the amplification of the traveling-wave tube was 30 dB. Signals were obtained at 8.4 and 10.5 Gc. Quantum efficiency data were not published.

There are no published data concerning the noise and responsivity of microwave phototubes. In most instances no suitable amplitude-modulated light input was available for the testing of these tubes, and only semiquantitative data were obtained by means of mixing experiments with light of somewhat uncertain composition.

The distribution in electron transit times limits the frequency response of conventional electrostatic photomultipliers to less than a few hundred megacycles. Gaddy and Holshauser (Ref. I-9) have proposed a device called the dynamic crossed-field photomultiplier in which the electron transit time is rigidly controlled through the use of a microwave electric field to provide the energy for secondary electron emission. The maximum possible bandwidth of their device is half of the electric field frequency.

The high-frequency field is applied across a condenser, one plate of which has been treated to be an efficient secondary emitter as illustrated in Fig. 33. A photocathode is incorporated at one end of this plate. Electrons emitted when the field is positive will be accelerated toward the other plate. If a magnetic field B is applied perpendicular to the electric field E, the electrons will be bent into curved trajectories, and for appropriate values of the field E and B and the frequency ω of the electric field some of the electrons will be returned to the first plate and produce secondaries.

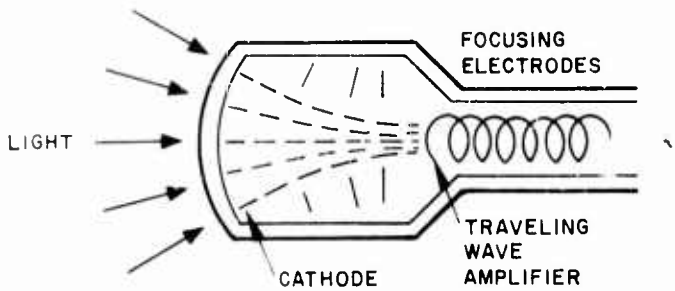

Fig. 32. Microwave Phototube.

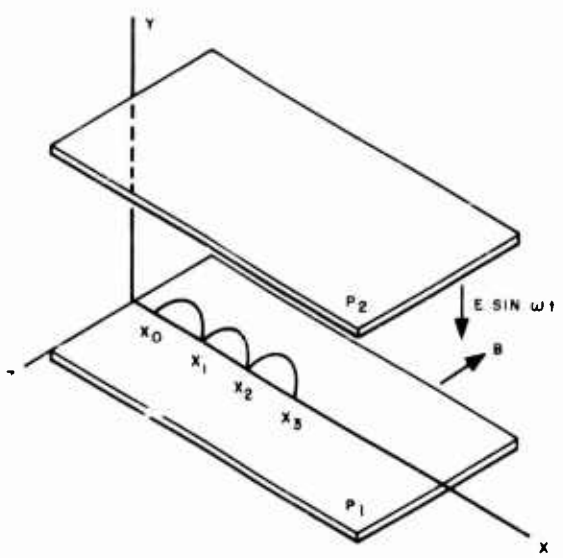

Fig. 33. Physical Configuration of Electron Multiplication System.

The analysis of Gaddy and Holshauser demonstrates that only those electrons emitted at the cathode during the first 60 degrees of a period of the electric field can satisfy the conditions necessary to proceed through a series of multiplications and be collected along with the generated secondaries. The electrons become even more tightly bunched in phase as they proceed through successive steps of multiplication. Signal frequencies in the range $\omega_s < \omega/2$, where ω is the frequency of the microwave electric field, are detected and amplified directly by the device, but frequencies in the range $\omega/2 \leq \omega_s \leq 3\omega/2$ beat with the driving field to produce outputs with frequencies from zero to $\omega/2$. The bandwidth for direct detection and amplification is $\omega/2$.

As with most fast photodetectors developed so far, noise data at high frequencies are not available. Incoherent light modulated at 3 Gc was successfully detected with an experimental device in its mixing mode of operation. A disadvantage of this detector lies in the fact that it samples the photon signal for only one-sixth of each period of the microwave electric field and so must operate at a lower signal-to-noise ratio than a "full-time" electrostatic photomultiplier. Like the other photoemissive devices, it suffers from poor quantum efficiency at the wavelengths of the most useful laser oscillators.

4. SOLID STATE DETECTORS UTILIZING INTERNAL PHOTOEFFECTS

Beyond 1.1μ, where photoemissive devices no longer have sufficient sensitivity, detectors utilizing internal photoeffects must be employed. Solid state detectors with detectivities approaching the theoretical photon noise limit in the wavelength range most likely to be used (0.4 μ to 4.0 μ) are available as a result of the considerable progress in infrared technology in the past decade. The objectives of this section are (1) to discuss the factors which limit the response time of these detectors, (2) to attempt to evaluate the lower limit to the response time as determined by material properties and the state of art in detector fabrication, and (3) to examine any possible change in detectivity that may result from design for rapid response.

A Near Infrared Detectors

There are two internal photoeffects which are the basis of solid state detectors operating in the near infrared range of interest. In both cases, absorption of photons leads to a change in the concentration of free, mobile charge carriers within the material. In the first class of detectors, called intrinsic, the energy of an absorbed photon creates

an electron-hole pair, i.e., the excitation process raises an electron from a valence band state to a conduction band state and only photons with energies greater than the intrinsic band gap are effective. The excitation process in the second class of detectors, called extrinsic, is the ionization of an impurity center to produce a free carrier and a charged defect site. The optical absorption constant in intrinsic materials is large, ranging up to 10^5 cm^{-1}, whereas in extrinsic materials it is rarely greater than 10^2 cm^{-1}. Photogenerated carriers are therefore confined to much smaller regions of intrinsic detectors.

Of the extrinsic detectors available, p-type gold-doped germanium is best suited to the near infrared since its long wavelength cutoff λ_o (defined as the wavelength at which the responsivity decreases to one-half its maximum value) is 7.0 μ. Since in extrinsic detectors majority carriers are generated by the absorbed light, only photoconductive operation is feasible. The time constant of these detectors, set by the recombination time for free carriers with ionized impurity sites, is of the order of 1 μsec. The low absorption cross section requires a geometrical configuration which would make the capacity of the detectors of the order of 20 μμF and the resistance 1 MΩ. Bandwidths greater than 1 Mc are therefore not attainable with this device without severely degrading performance. It should also be noted that this detector requires refrigeration and does not achieve optimum detectivity unless cooled to 60°K (below the temperature of liquid nitrogen). The same considerations concerning bandwidth are pertinent to all the extrinsic photoconductors, and those with longer wavelength cutoffs have the additional disadvantage of requiring even lower temperatures of operation.

The intrinsic detectors useful in the near infrared can be divided into single crystal and thin film classes for consideration. The latter includes the lead salt series of photoconductors which are available as chemically deposited or evaporated thin films in a variety of geometric configurations. Single crystals of these materials have proved difficult to prepare. The long wavelength cutoffs of these materials range from 2.5 μ for PbS to 4.5 μ for PbTe. However, their response times are very long, ranging from 10 to 1000 μsec; the shorter times are available only at the expense of detectivity. The bandwidths required for optical Doppler radars are therefore beyond the capability of this group of detectors.

There remain intrinsic single crystal detectors which do offer the possibility of meeting the requirements required of a laser receiver system. The long wavelength cut-offs of detectors that have been fabricated to operate over the spectral range of interest are listed in Table 7. Where more than one value appears in the table, each corresponds to a different temperature of operation. Operation of all the detector materials listed depends on the generation of electron-hole pairs which

TABLE 7

LONG WAVELENGTH CUTOFF FOR VARIOUS DETECTOR MATERIALS

	Si	GaAs	GaSb	Ge	InAs	InSb
λ_o [a]	0.8	0.9	1.5	1.8	3.7	7.3 (300°K) 5.6 (77°K)

[a] λ_o is the wavelength at which responsivity has decayed to one-half its peak value.

occurs when a photon with energy greater than the energy gap between valence and conduction bands is absorbed. Incident radiation can be monitored by "counting" the number of electron-hole pairs generated. The three techniques that have been utilized for the counting process are illustrated in Fig. 34. Figure 34 (a) represents a detector operated in the photoconductive mode. The dashed line represents the steady state electron-hole concentration in a uniform block of material. The current that flows in response to an electric field applied between the electrodes provides a measure of the free carrier concentration. When signal photons are incident on the detector, an additional concentration of carriers is set up which varies with position in the detector as shown by the solid curve in Fig. 34 (a). Because of the additional carriers a larger current flows in the external circuit.

The photoelectromagnetic (PEM) mode of operation is obtained if the electric field is removed from the photoconductor so that it is connected directly across a load and a magnetic field is applied perpendicular to the plane of the figure. Because of the concentration gradient of electron-hole pairs produced by the absorbed radiation in the material, carriers drift in the direction in which radiation is incident. The Lorentz force due to the magnetic field on the moving carriers deflects the electrons and holes to opposite electrodes and produces current in the external load (as illustrated in Fig. 34 (b)).

The third mode of operation is the photovoltaic mode in which a p-n junction is produced immediately behind the surface on which radiation is incident by diffusing a p-type dopant into n-type material (Fig. 34 (c)). The generated electron hole pairs diffuse to the junction under

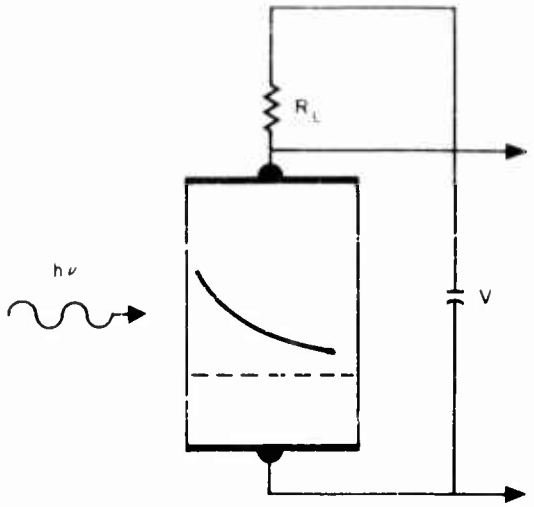

(a) Photoconductive mode

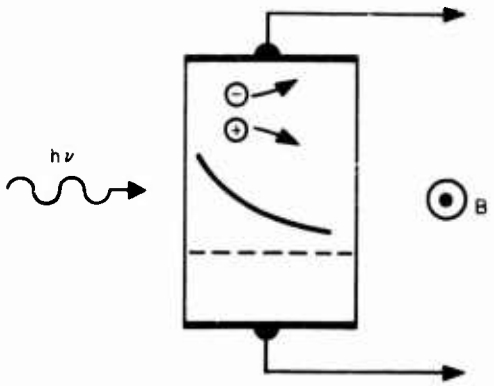

(b) Photoelectromagnetic mode

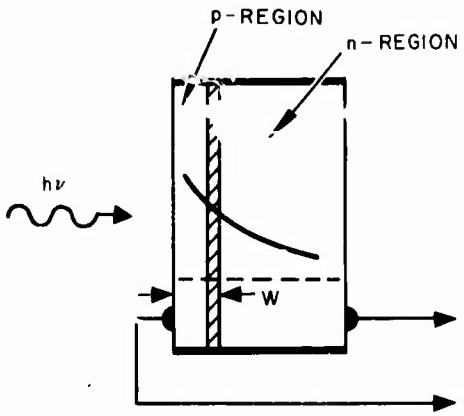

(c) Photovoltaic mode

Fig. 34. Three modes of Operation of Solid State Photodetectors.

the influence of the concentration gradients set up in response to the incident radiation. The electric fields in the junction drive the electrons to the n-side and holes to the p-side of the detector. With zero applied bias, an external photocurrent can be observed or the detector may be operated with reverse bias in what is essentially a photoconductive mode.

By appropriate control of the fabrication process, it is possible in some semiconductors to make the transition region between the n and p regions large or even to arrange that the detector consist of three regions: a thick n-type base region on which there is first a moderately thick intrinsic region, and then a very thin p region at the surface on which radiation is incident. Such a p-i-n structure has somewhat different response time characteristics when biased in the reverse direction and is particularly useful for weakly absorbed radiation. (For a more detailed analysis and review of the properties of infrared detectors see Refs. I-1 and I-10.)

B. Factors Determining Response Time of a Photodetector

The response time of a detector will depend on the mean time between the generation of excess carriers by light and either their recombination or their collection at the electrodes in PC and PEM cells. The requirement for fast response and maximum responsivity determines the geometry of the detectors. The response time of a detector depends on the mean lifetime of the photogenerated excess carriers. In sufficiently small structures this lifetime will be determined by the transit time of a carrier and so is dependent on the geometry of the detector. To achieve the short response times needed for optical Doppler radar applications requires very small structures and since these have been achieved most successfully in photovoltaic detectors, the preceding remarks will be illustrated by a more detailed consideration of such devices.

Consider first the p-n junction cell illustrated in Fig. 34 (c). A photon flux density F_o is incident on the front surface of the cell giving rise to an excess concentration of generated electron-hole pairs that varies with position inside the cell according to the relation

$$n = F_o (1-R) \alpha e^{-\alpha x} \qquad \text{(I-11)}$$

where R is the reflection coefficient of the semiconductor surface and α is the absorption constant for the wavelength of interest. The excess carriers will diffuse in the concentration gradient created and the resulting particle flux density will be given by the diffusion equation

$$\Phi_n = -D_n \frac{dn}{dx} \qquad \text{(I-12)}$$

D_n is the diffusion constant of the excess minority carriers and in the case of the p-n junction device illustrated it is the diffusion constant of electrons in the p-type layer adjacent to the surface. It is related to the electron mobility by the Einstein relation $D_n = \mu_n kT/e$; (k is Boltzmann's constant, T the absolute temperature, and e the magnitude of electronic change). Since particle flux density can also be written as the product of concentration and velocity, $\Phi_n = nv$, the velocity is found to be

$$v = -\frac{D_n}{n}\frac{dn}{dx} = +\frac{kT}{e}\mu_n \alpha \quad . \tag{I-13}$$

The response time of the detector may be estimated as the time it would take for a carrier generated at the surface to diffuse to the junction:

$$\tau = \frac{W}{v} = \frac{eW}{kT\mu_n \alpha} \quad . \tag{I-14}$$

W is the depth of the junction below the irradiated surface. For a germanium detector at room temperature looking at the 1.15 μ helium-neon gas laser line, the parameters have the following values

$$\alpha \sim 10^4 \text{ cm}^{-1}$$

$$\mu_n = 3900 \text{ cm}^2/\text{V-sec}$$

$$T = 300^\circ\text{K} .$$

If we substitute these values into (I-14) it is found that $\tau \sim 10^{-9}$ sec for a junction depth W of 10μ. It has been tacitly assumed in the above analysis that the diffusion length of minority carriers in the material is large compared to W, or, stated in another way, the mean lifetime against recombination is larger than the transit time τ. If this were not the case, a significant portion of the photogenerated carriers would recombine before reaching the junction and would not contribute to the electrical output of the detector. The electron-hole recombination time τ_o is a function of the impurity content of the material and it varies from a few milliseconds to 10^{-8} sec in most semiconductors. For materials used in detectors it can generally be assumed that $\tau_o > \tau$ and that the corresponding diffusion lengths are larger than the junction depths.

In the example cited, the absorption constant was so large ($\alpha = 10^4$ cm^{-1}) that most of the incident radiation was absorbed within a few microns of the surface. If technologically possible, the junction

could be brought to within 2 μ of the surface with no appreciable loss in signal but at a considerable improvement in response; τ would be reduced by a factor of 5 to 2 x 10^{-10} sec. Alternatively, a laser line (at such a wavelength that α is only 10^3 cm^{-1}) could be detected as effectively by the original detector with a response time of 10^{-9} sec.

The p-i-n form of the photovoltaic detector presents the possibility of more efficient utilization of the radiation for a more weakly absorbed line. Thus, suppose the i-region extends from 2 μ below the surface to 10 μ below the surface. When a large reverse bias is applied across the detector, essentially the complete voltage drop appears across the intrinsic region, and a line at wavelength $\alpha = 10^3$ cm^{-1} generates carriers throughout the intrinsic region (see Fig. 35). Because the i region is very narrow, the electric field intensity for several volts reverse bias will be of the order of 10^3 V/cm or larger. In such fields the average drift velocity of carriers in a semiconductor increases and eventually reaches a saturation velocity v_o which in germanium is 6 x 10^6 cm/sec. (Refs. I-11 to I-13.) Estimating the response time of the detector as the time required for a photogenerated carrier to drift across the junction gives $\tau \sim 1.3 \times 10^{-10}$ sec.

It may not be possible to realize the transit time response of the photovoltaic detector because of RC limitations encountered in the circuit in which it is incorporated. A reverse-biased junction has a capacity determined by the area and width of the junction and the dielectric constant of the material:

$$C = \frac{8.85 \times 10^{-12} \frac{\epsilon}{\epsilon_o} A}{W} \text{ F} \qquad \text{(I-15)}$$

where

ϵ = dielectric constant in farads per meter

A = area of junction in square meters

W = width of junction in meters .

The p-i-n junction used for illustrative purposes above would have a capacity of 1.75 x 10^3 pF/cm^2. Diffused junctions with areas of 2 x 10^{-4} cm^2 can be fabricated, at least in germanium (Ref. I-14), and such a junction would have a capacity of 0.35 pF. The series resistance of the n-type base region in such a detector is in the range of 1 to 10 Ω so that the characteristic RC time of the device is 3.5 x 10^{-12} sec. This will be degraded if larger load resistors are coupled to the detector.

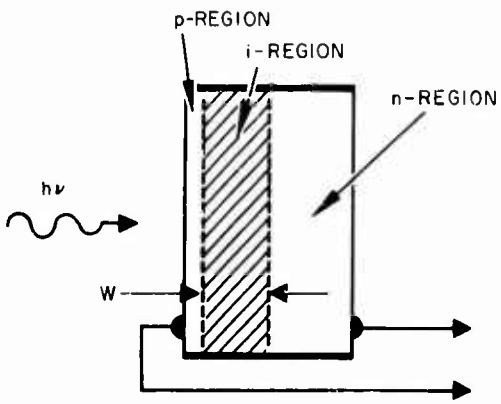

Fig. 35. p-i-n Junction Diode.

More detailed analyses of the operation of photovoltaic detectors are available in the literature (Refs. I-1, I-15). On the basis of such analyses and the current state of the art with respect to material preparation and device fabrication, Lucovsky, Lasser, and Emmons (Ref. I-16) have estimated the 3 dB cutoff frequencies of a variety of photovoltaic detectors for available laser lines ranging from the 6943 Å ruby line to the 2.49 μ U^{+3}: CaF_2 line. Their estimates place the frequency cutoffs between 4.6×10^9 cps and 7.3×10^{10} cps. They consider silicon, germanium and gallium arsenide operated at room temperature, indium arsenide at 196°K, and indium antimonide at 77°K (see Table 8).

Detailed reports of operating detectors are rather sparse. The most complete description of such a detector published (Ref. I-14) describes a germanium p-i-n junction with an i region 2.5 μ thick and 0.006 in. in diameter. This detector exhibited a pulse rise time of 0.6 nsec and detected beats up to 2 kMc in the output of a pulsed ruby laser.

A point contact p-π-n diode (Ref. I-17) with a π region 5 μ thick and 5 μ in diameter has been used to detect beats up to 936 Mc in a helium-neon laser operating at 1.15 μ (π indicates a lightly doped p region).

Saito, et al. (Ref. I-18), have used a standard germanium parametric diode to detect 4 kMc beats from ruby, and 11 kMc beats from such a source have been detected with a silicon p-i-n diode (Ref. I-19). Lucovsky, Lasser, and Emmons (Ref. I-16) reported beat measurements up to 1.46 kMc with germanium, silicon, gallium arsenide, and indium arsenide photodiodes.

C. Noise Considerations in Fast Photocells

As noted earlier, the photovoltaic mode of operation will generally be preferred for very fast detectors because of the relative ease of fabricating structures having the small dimensions required. The current voltage characteristic of such a detector has been found to be:

$$I = I_s \left[\exp \frac{eV}{kT} - 1\right] - I_{sc} + \frac{V}{R_{sh}} . \qquad \text{(I-16)}$$

The first term on the right is the I-V characteristic of a p-n junction in the dark, the second term is the additional reverse saturation current due to optically generated carriers, and the third term represents the current through the shunt conductance of the diode. When operating into the small loads required to achieve wide band performance, the small series resistance of the base region must also be taken into account. The constant current equivalent circuit of such a detector under reverse bias is shown in Fig. 36. The microwave receiver is idealized as a series L, R circuit to provide the possibility of tuning. C is the diode capacity, r_p is the dynamic resistance of the diode $(\partial V/\partial I)$, and r_s is its series resistance.

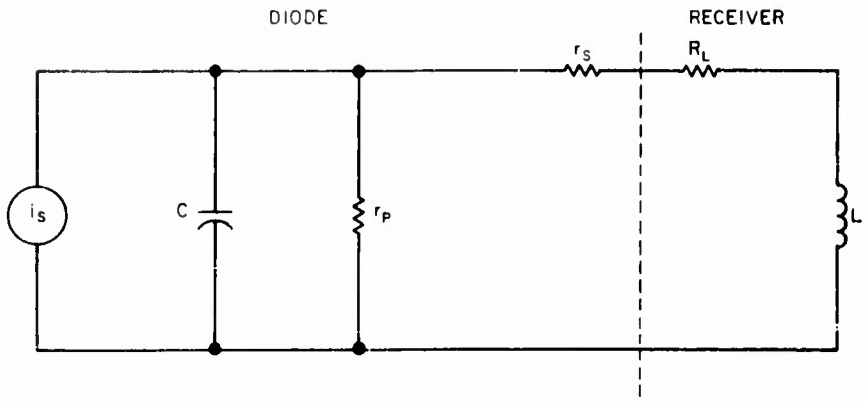

Fig. 36. Constant Current Signal Equivalent Circuit of Photodiode.

TABLE 8

DYNAMIC RESISTANCE AND DETECTIVITIES OF CANDIDATE PHOTODIODE MATERIALS

Laser System	Emission Line	Gallium Arsenide 300° K	Silicon 300° K	Germanium 300° K	Indium Arsenide 196° K	Indium Antimonide 77° K
Ion:Host	Microns	← Structure Critical Dimension 3 dB Frequency →				
$Cr^{+3}:Al_2O_2$ $Sm^{+3}:CaF_2$	0.6943 0.7083	P-N W 2 x 10^{-5} cm x.7 x 10^{10}	P-I-N W_I = 3 x 10^{-4} cm ω = 2.9 x 10^{10}	P-N W_p = 2.5 x 10^{-4} cm ω = 3.1 x 10^{1}	P-N W_p = 10^{-4} cm ω = 1.1 x 10^{11}	P-N W_p = 10^{-4} cm ω = 4.6 x 10^{11}
$Nd^{+3}:CaF_2$ $Nd^{+3}:CaWO_4$ $Nd^{+3}:SrMoO_4$ Ne:He	1.046 1.063 1.064 1.15			P-I-N W_I = 10^{-4} ω = 1.4 x 10^{11}	P-N W_p = 10^{-4} ω = 1.1 x 10^{11}	P-N W_p = 10^{-4} ω = 4.6 x 10^{11}
$Tm^{+3}:CaWO_4$ $Ho^{+3}:CaWO_4$	1.91 2.046				P-N W_p = 10^{-4} ω = 1.1 x 10^{11}	P-N W_p = 10^{-4} ω = 4.6 x 10^{11}
$U^{+3}:CaF_2$	2.49				P-N W_p = 10^{-4} ω = 1.1 x 10^{11}	P-N W_p = 10^{-4} ω = 4.6 x 10^{11}
λ_c (α = 10^3 cm^{-1}), microns	-	0.88	0.80	1.53	3.2	4.2
D^*_{peak}	-	2.9 x 10^{11}	3.4 x 10^{13}	10^{10}	5 x 10^9	1.5 x 10^{10}
NEP (A = 10^{-4} cm^2), watts	-	3.5 x 10^{-14}	3.0 x 10^{-16}	10^{-12}	2 x 10^{-12}	6.7 x 10^{-13}

NOTES:

1. The four upper rows are taken from Ref. I-16. Detectivity data as reported in various Photodetector Reports, Naval Ordnance Laboratory, Corona. D^* for Ge dates from 1955 and is probably not representative of best available today.

2. W_p = depth of function behind the irradiated surface; W_I = width of the intrinsic region.

The constant current generator has a magnitude

$$i_s = \frac{\partial I}{\partial F}\Delta F = -\frac{\partial I_{sc}}{\partial F}\Delta F$$

where F is the incident photon flux density.

The number of carriers created per second is ηAF, where η is the quantum efficiency, A is the area of the detector, and $I_{sc} = e\eta AF$ is the current produced by these carriers. The short circuit current is $i_s = e\eta A\Delta F$.

Reverse bias operation is preferred to photovoltaic operation when wide bandwidths are sought because r_p is higher and C is smaller than in the latter case. r_p is generally so large that it may be taken as infinite in a first approximation. The rms signal power developed in the R_L for a photon signal modulated at angular frequency ω is

$$S(\omega) = \frac{1}{2}(eA\eta)^2 \Delta F^2 \frac{R_L}{(1-\omega^2 LC) + \omega^2 C^2 (r_s + R_L)^2} \cdot \qquad \text{(I-17)}$$

When operated at resonance, R_{eq} for the photodiode is found from the above expression to be

$$R_{eq} = \frac{R_L}{\omega_o^2 C^2 (r_s + R_L)^2} \qquad \text{(I-18)}$$

and evidently decreases rapidly with frequency.

Three types of noise must be taken into account in treating photodiodes. At low frequencies, current noise having a power spectrum given by

$$\overline{i_I^2} \propto \frac{I^2}{f} \Delta f \qquad \text{(I-19)}$$

usually predominates. However, for most photodiodes fabricated with sufficient care this noise is negligible above a few kilocycles and so may generally be disregarded in discussing wideband laser receivers.

The most important source of noise in a photovoltaic detector is shot noise due to the particle nature of the current. It has a flat power spectrum (up to frequencies determined by transit time effects) given by

$$\overline{i_{sh}^2} = 2eI\Delta f \tag{I-20}$$

where, as before, I is the average diode current and e is the electronic charge.

The third source of noise which must be considered is thermal noise in the various resistive elements in the diode circuit. Since current noise can be neglected at the anticipated high frequencies of operation, the noise equivalent circuit of a photodiode can be drawn as in Fig. 37 with various current generators having the values

$$\begin{aligned} \overline{i_d^2} &= -2eI\Delta f \\ \overline{i_s^2} &= \frac{4kT}{r_s}\Delta f \\ i_L^2 &= \frac{4kT}{R_L}\Delta f \quad . \end{aligned} \tag{I-21}$$

The noise power developed in the load in this circuit is

$$N(\omega) = \frac{2eI\Delta f\, R_L + 4kT\Delta f\, \omega^2 C^2 (r_s + R_L)R_L}{(1-\omega^2 LC)^2 + \omega^2 C^2 (r_s + R_L)^2} + N' \tag{I-22}$$

where N' represents any noises arising from sources in the receiver other than R_L. The ratio of signal power to noise power is given by

$$\frac{S(\omega)}{N(\omega)} = \frac{\frac{1}{2}(eA\eta)^2 \Delta f^2 R_L}{2eIR_L + 4kT\,\omega^2 C^2 R_L (r_s + R_L) + N'\left\{(1-\omega^2 LC)^2 + \omega^2 C^2 (r_s + R_L)^2\right\}} \tag{I-23}$$

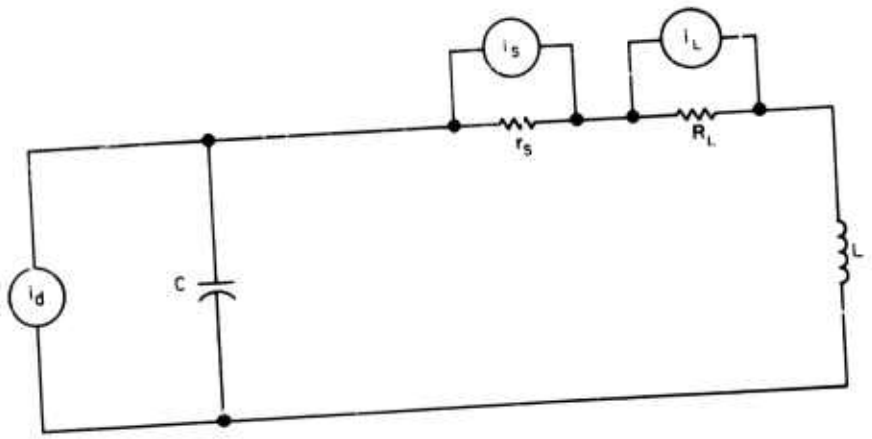

Fig. 37. Noise Equivalent Circuit for a Photodiode.

A minimum detectable signal photon flux density can be defined as that ΔF for which S/N = 1, and its rms value is given by

$$\Delta F^2_{rms} = \frac{1}{(eA\eta)^2} \left\{ 2eI + 4kT\omega^2C^2 (r_s + R_L) + \frac{N'}{R_L} \left[(1-\omega^2LC)^2 + \omega^2C^2 (r_s + R_L)^2 \right] \right\} . \quad \text{(I-24)}$$

The Q of the resonant circuit formed by the diode and its conjugate load in the receiver is given by $[\omega C (r_s + R_L)]^{-1}$ and for signals modulated at the resonance frequency ($\omega_o = (LC)^{-1/2}$) we get

$$\Delta F^2_{rms} = \frac{1}{(eA\eta)^2} \left\{ 2eI\Delta f + \frac{1}{Q^2} \frac{4kT\Delta f}{(r_s + R_L)} + \frac{1}{Q^2} \frac{N'}{R_L} \right\} . \quad \text{(I-25)}$$

The ideal mode of operation is one in which the diode current I is determined by the incident photon flux (i.e., $I = eA\eta\Delta F$) and is large enough so that the second and third terms in the braces are negligible.

Signal and noise power are then both determined by properties of the incident photon flux, and the detector will be either signal or background limited, depending on external conditions. In routine infrared application where extremely high frequency operation is not required, the cells can be operated with loads that match their dynamic resistance. Under these conditions the long wavelength detectors such as indium arsenide and indium antimonide should be thermal-background limited and the cells with shorter long wavelength cutoffs should be signal fluctuation limited. Actually only the best indium antimonide photovoltaic cells have been observed to attain this sort of ideal operation and then only when used in conjunction with specially designed amplifiers. Since for broad-band operation it is necessary to use a relatively low load impedance (R_L 50 Ω), the shot noise term will be negligible and the noise output will be dominated by thermal effects in the associated circuitry and amplifiers. This is evident from a comparison of the shot noise and thermal noise terms. The current I required to give a shot noise power equal to the thermal noise in the load at resonance is

$$I = 2\frac{kT}{e} \frac{1}{Q^2(r_s + R_L)} . \quad \text{(I-26)}$$

Taking a fairly typical value of 1Ω for r_s, assuming a matched load and a Q of 10, gives I = 1 mA. A photon flux ($\Delta F = I/\eta e$) of 1.3×10^{16} photon/sec is required to produce this much current in the diode. The minimum detectable photon flux, as set by thermal noise alone, is

$$A\Delta F_{rms} = \frac{1}{e\eta}\left\{\frac{4kT\Delta f}{Q^2(r_s + R_u)}\right\}^{1/2} = 1.2 \times 10^8 \text{ photon/sec} \qquad \text{(I-27)}$$

for a 1 cps bandwidth. Shot noise will thus be negligible for any signals less than approximately 10^{15} photon/sec.

The conclusion from the above is that photodiode performance as an envelope detector will always be limited by thermal noise in the load and amplifier. This limitation can be overcome in heterodyne operation if a local oscillator with the power outputs noted above is available. As shown by Forrester (Ref. I-20) and Oliver (Ref. I-21), both the shot noise power and the signal power increase in the same proportion as the local oscillator power is increased. It is therefore possible to achieve a condition where shot noise is dominant. The price that has to be paid for this improvement in performance is in the requirement for close alignment of signal beam and local oscillator beam. Constructive interference between the two beams can occur only if they are aligned within an angle $\Delta\theta \leq \alpha/d$, where λ is the wavelength of the light and d is the diameter of the collecting optics.

As an indication of what could be achieved with semiconductor photodiodes, the best currently available information concerning dynamic resistance and D* for the materials most likely to be used in the visible and near infrared has been added to Table 8. A word of caution is necessary in using these numbers. The data reported are from standard infrared detector evaluation procedures and so are with load resistors that approximately match the dynamic impedance. In broad-band envelope detection, thermal noise in the smaller loads required may severely degrade detectivity, as pointed out above. In heterodyne operation, the listed detectivities may well be achieved in practice.

Also included in Table 8 is an estimate of the longest wavelength λ_c at which a particular material may be used to produce fast photodetectors. This limit is chosen, on the basis of transit time considerations, as that wavelength for which the optical absorption constant is 1000 cm^{-1} at the operating temperature of the diode.

To assure optimum electrical characteristics, the material chosen should have a λ_c close to (and greater than) the laser wavelength being used. Fabrication of such a detector in an appropriate package may still be difficult; to date, no experimental performance limits (response time, detectivity in wide-band operation) have been reported.

5. SUMMARY

Of the various modes of operation of solid state photodetectors, p-n or p-i-n junction devices can probably achieve the highest speeds since it is now technologically possible to produce the small structures required. These devices are especially useful at wavelengths greater than 1.1 μ since they are the only devices with both fast response and high quantum efficiency in this region. The disadvantages to be considered are their limited capacity, which restricts the bandwidth over which they can be operated, and their small sensitive area. In addition, heterodyne operation is required to attain optimum sensitivity, and this imposes severe restrictions on the alignment of the signal radiation with respect to the local oscillator. Detectors operating at longer wavelengths (2 to 4 μ) also require cooling for maximum detectivity.

G. S. Picus

REFERENCES

I-1. P. W. Kruse, L. D. McGlauchlin, and R. B. McQuistan, Elements of Infrared Technology, (John Wiley and Sons, New York, 1962).

I-2. RCA Electron Tube Handbook

I-3. R. W. Engstrom, RCA Rev. 21, 184 (1960).

I-4. D. K. C. MacDonald, Phil. Mag. 40, 561 (1949).

I-5. D. R. Herriott, J. Opt. Soc. Am. 52, 31 (1962).

I-6. B. J. McMurtry and A. E. Siegman, Appl. Opt. 1, 51 (1962).

I-7. R. F. Lucy, Proc. IEEE 51, 162 (1963).

I-8. M. D. Petroff, H. A. Spetzler, and E. K. Bjornerud, Proc. IEEE 51, 614 (1963).

I-9. O. L. Gaddy and D. F. Holshauser, Proc. IEEE 51, 153 (1963).

I-10. "IRIA State of the Art Report on Infrared Quantum Detectors (U)," (CONFIDENTIAL) W. Wolfe and T. Limperis, Eds., published by the Institute of Science and Technology, University of Michigan, Ann Arbor, Mich. (Contract NOnr 1224 (12)) (July 1961).

I-11. E. J. Ryder, Phys. Rev. 90, 766 (1953).

I-12. J. B. Gunn, J. Electron. 2, 87 (1956).

I-13. J. B. Arthur, A. F. Gibson, J. W. Granville, J. Electron. 2, 145 (1956).

I-14. R. P. Riesz, Rev. Sci. Instr. 33, 994 (1962).

I-15. The p-n junction detector is covered in detail by D. E. Sawyer and R. H. Rediker, Proc. IRE 46, 1122 (1958). The basic work on the p-i-n structure was reported by W. W. Gartner, Phys. Rev. 116, 84 (1959). The graded junction diode which may be regarded as a cross between the two is described by A. G. Jordan and A. G. Milnes, IRE Trans. ED-7, 242 (1960).

I-16. G. Lucovsky, M. E. Lasser, and R. B. Emmons, Proc. IRE 51, 166 (1962).

I-17. L. U. Kibler, Proc. IRE 50, 1834 (1962).

I-18. S. Saito, K. Kurokawa, Y. Fujii, T. Kimura, Y. Uno, Proc. IRE 50, 2369 (1963).

I-19. H. Inaba and A. E. Siegman, Proc. IRE 50, 1823 (1962).

I-20. A. T. Forrester, J. Opt. Soc. Am. 51, 253 (1961).

I-21. B. M. Oliver, Proc. IRE 49, 1960 (1961).

APPENDIX II

SPONTANEOUS EMISSION POWER IN LASER AMPLIFIERS

The amplifying medium of a laser can be characterized by the simple energy level diagram in Fig. 38.

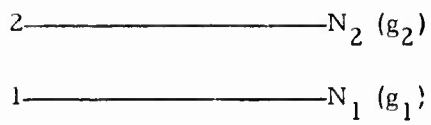

Fig. 38. Simplified Energy Level Diagram of Laser.

The method of calculating the spontaneous emission noise power is similar to that used by William H. Culver; however, we do not make the simplifying assumption $N_1 = 0$ and consider the general case where degeneracy may exist. The material gain is given by $G = I/I_o = e^{\alpha \ell}$ where

$$\alpha(\nu) = \frac{\lambda^2}{8\pi n^2 \tau_s} \left(N_2 - \frac{g_2}{g_1} N_1 \right) f(\nu); \qquad \text{(II-1)}$$

$f(\nu)$ is a line shape factor normalized such that

$$\int_0^\infty f(\nu)\, d\nu = 1 .$$

The peak absorption coefficient for a Lorentzian shaped line is

$$\alpha_L(\nu_o) = \alpha_{max} = \frac{\left(N_2 - \frac{g_2}{g_1} N_1 \right) \lambda_o^2}{4\pi^2 n^2 \Delta\nu \tau_s} \qquad \text{(II-2)}$$

and for a gaussian shaped line is

$$\alpha_G(\nu_o) = \alpha_{max} = \frac{\left(N_2 - \frac{g_2}{g_1} N_1\right) \lambda_o^2}{4\pi n^2 \Delta\nu \tau_s} \sqrt{\frac{\log 2}{\pi}}, \qquad \text{(II-3)}$$

where

N_1, N_2 ≡ respective population densities

g_1, g_2 ≡ respective degeneracy factors

$\Delta\nu$ ≡ linewidth in cps at 1/2 absorption

n ≡ index of refraction

λ_o ≡ free space center wavelength

τ_s ≡ radiative lifetime of level 2 .

We consider the case of a linear amplifier of gain g as in Fig. 39.

A = cross sectional area

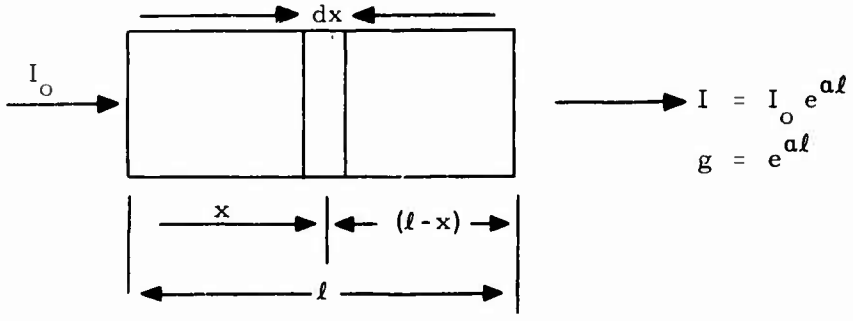

Fig. 39. Linear Amplifier.

At the same time that a beam is being amplified by passing through the active material, the active material is emitting spontaneous radiation causing a background noise. Some of this spontaneous emission is in turn amplified by passing through the amplifier. Each volume element (Adx) will radiate spontaneously at the rate of

$$\frac{N_2 f(\nu)\, Adx}{\tau 4\pi} \quad \text{photon/sec/solid angle/cps bandwidth.}$$

We obtain the total spontaneous emission by adding the emission in the various volume elements (Adx) multiplied by the gain appropriate to said volume element. Therefore,

$$\frac{P_{sp}}{h\nu} = \int_{x=0}^{\ell} \frac{N_2 f(\nu)\, A}{\tau 4\pi}\, e^{a(\ell - x)} dx \qquad \text{(II-4)}$$

$$= \frac{\left(N_2 - \frac{g_2}{g_1} N_1\right) \lambda^2 f(\nu)}{\tau\, 4\pi a} \left[e^{a\ell} - 1\right] . \qquad \text{(II-5)}$$

Substitution of

$$a = \frac{\left(N_2 - \frac{g_2}{g_1} N_1\right) \lambda^2 f(\nu)}{8\pi \tau n^2} \qquad \text{(II-6)}$$

yields

$$P_{sp} = \left(\frac{N_2}{N_2 - \frac{g_2}{g_1} N_1}\right) \frac{2h\nu^3}{c^2} n^2 \left[g - 1\right] \qquad \text{(II-7)}$$

where $g = e^{a\ell}$. We define $T_{noise} = T_n$ in the standard manner: it is the temperature of a black-body noise generator at the input terminal of the amplifier which gives the same noise power at the output terminal as that observed, i.e.,

$$P_{sp} = \left(\frac{N_2}{N_2 - \frac{g_2}{g_1} N_1}\right) \frac{2h\nu^3}{c^2} \left[g - 1\right] \equiv g \left[\frac{2h\nu^3}{c^2} \left(\frac{1}{e^{h\nu/kT_n} - 1}\right)\right] . \qquad \text{(II-8)}$$

(The factor n^2 drops out of the comparison, since if we refer the noise to the input, the solid angle is multiplied by $\approx 1/n^2$ due to refraction on entering the amplifying medium.) Solving for

$$T_n = h\nu/k \log \left[\frac{\left(2 - \frac{N_1 g_2}{N_2 g_1}\right) g - 1}{g - 1} \right] \qquad \text{(II-9)}$$

which for high gain and perfect inversion ($N_1 = 0$) reduces to the familiar limit

$$T_n = \frac{h\nu}{k \log 2} \quad .$$

If we wish to obtain the total spontaneous emission, we can integrate the previous result over frequency: i.e., $P_{tot} = \int P(\nu)\, d\nu$. The integrals, however, are difficult; therefore we approximate the integrals by the peak value of the integrand multiplied by the bandwidth at half gain

$$P_{tot} = \int_0^\infty P(\nu)\, d\nu \,\Big|_{\text{Lorentzian}} \approx P(\nu_o)\, \Delta\nu$$

$$= \left(\frac{N_2}{N_2 - \frac{g_2}{g_1} N_1} \right) \frac{2h\nu^3}{c^2} \quad (g - 1) \underbrace{\left(\frac{\log g_o}{\log \frac{g_o}{2}} - 1 \right)^{1/2} \Delta\nu}_{\delta\nu \;=\; \text{amplifier bandwidth (Ref. II-1)}} \qquad \text{(II-10)}$$

and similarly

$$P_{tot} = \int_0^\infty P(\nu)\, d\nu \Big|_{\text{Gaussian}} \approx P(\nu_o)\, \Delta\nu$$

$$= \left(\frac{N_2}{N_2 - \frac{g_2}{g_1} N_1} \right) \frac{2h\nu^3}{c^2} (g - 1) \left(\frac{\log \frac{\log g_o}{\log g_o/2}}{\log 2} \right)^{1/2} \Delta\nu \, . \tag{II-11}$$

The foregoing applies for single pass amplification. For helium-neon (6328 Å) the single pass gain is of the order of 1.1/m; therefore it is of interest to consider the noise properties of a laser regenerative amplifier.

The gain of a regenerative laser amplifier is given by (Ref. II-2)

$$G = \frac{(1 - R)^2 g_o}{(1 - R\, g_o)^2}$$

where R is the intensity reflection coefficient of the mirrors, and $g_o = e^{\alpha \ell}$.

For future reference we should note that

$$(G - 1) = \frac{(g_o - 1)\left(1 - R^2 g_o\right)}{\left(1 - R g_o\right)^2} \, . \tag{II-12}$$

A calculation of the spontaneous emission emitted from this regenerative amplifier yields the result that

$$P_{sp} = \left(\frac{N_2}{N_2 - \frac{g_2}{g_1} N_1} \right) \frac{2h\nu^3}{c^2} \quad \frac{n^2 (1 - R)}{(1 - R\, e^{\alpha \ell})^2} \quad (e^{\alpha \ell} - 1) \tag{II-13}$$

$$= \left(\frac{N_2}{N_2 - \frac{g_2}{g_1} N_1} \right) \frac{2h\nu^3}{c^2} n^2 \frac{(1 - R)}{(1 - R^2 g_o)} (G - 1)$$

for high gain $g_o R \approx 1$; therefore, the above reduces to

$$P_{sp} = \left(\frac{N_2}{N_2 - \frac{g_2}{g_1} N_1} \right) \frac{2h\nu^3}{c^2} n^2 (G - 1) \quad . \tag{II-14}$$

which we recognize as being identical to (II-7) with G, the regenerative gain, replacing the single pass gain $g_o = e^{\alpha \ell}$; hence this system has the noise temperature given by (II-9) with the regenerative gain replacing the single pass gain.

The relative merits of regenerative versus single pass amplification will not be argued at this time, but a limited comparison of the advantages of the separate approaches does seem in order.

Single pass amplification can utilize the bandwidth of the laser material to advantage, and as a preamplifier for a large shift Doppler receiver the advantages are obvious. Apertures would be necessary to spatially separate the various resolution elements of the system, and heterodyning could reduce the serious problem of noise in the unused portion of the amplifier frequency bandwidth (frequency mode selection performed at i.f. frequency).

Regenerative amplification provides an efficient method of combining mode (spatial and frequency) selection and amplification. Within a mode the amplifying bandwidth is given by (Ref. II-3)

$$\Delta\nu = \frac{(1-R)c}{2\pi n \ell \, R^{1/2} G^{1/2}} \tag{II-15}$$

and in certain applications this will be a disadvantage, viz., the large shift Doppler.

I. J. D'Haenens

REFERENCES

II-1. R. W. DeGrasse, E. O. Schultz-DuBois, and H. E. D. Scovil, "The three-level solid state traveling-wave maser," Bell System Tech. J., 38, 305 (1959).

II-2. V. N. Smiley, "An active interference filter as an optical amplifier," Proc. IEEE 51, 120-124 (1963).